

https://dspace.org/

The effect of rare earth elements corrosion inhibitors on the corrosion of titanium & aluminium in chloride containing media

Manjo, Julius Mbimbi-Ikoli

2022

https://hdl.handle.net/10539/34904

Downloaded from a DSpace repository. https://dspace.org/



THE EFFECT OF RARE EARTH ELEMENT CORROSION INHIBITORS ON THE CORROSION OF TITANIUM & ALUMINIUM IN CHLORIDE CONTAINING MEDIA

A research report submitted in partial fulfilment of the requirements for the degree of

Master of Science in Chemical Engineering

Prepared by:

Julius M. Manjo

881145

Supervisors:

Dr. David Whitefield

Prof. Herman Potgieter

School of Chemical and Metallurgical Engineering

Faculty of Engineering and the Built Environment

University of Witwatersrand

September 2022

PLAGIARISM DECLARATION

I declare that this research report is my own, unaided work. It is being submitted for the Degree of Master of Science, Chemical Engineering at the University of the Witwatersrand, Johannesburg. It has not been submitted before for any degree or examination at any other University.



(Signature of candidate) 24th day August of 2022 at 14:17

ABSTRACT

Titanium and aluminium both showed good resistance to corrosion in both the saline NaCl and acidic HCl chloride containing solutions. This is due to their ability to form a passive protective, self-regenerating metal oxide layer. Titanium samples showed greater corrosion resistance by two orders of magnitude compared to the aluminium samples in NaCl, HCl solutions with and without inhibitors.

The corrosion inhibitors used were lanthanum and cerium acetylacetone and these showed good corrosion inhibition effects, consistent through the weight loss tests and potentiodynamic scans. This was observed by examination through scanning electron microscopy and optical microscopy. The presence of inhibitors was observed to decrease the corrosion rate by one order of magnitude, when compared to the corrosion rate of corrosive media without inhibitor.

The weight loss tests revealed that pitting occurred as a result of chloride attack on both aluminium and titanium, especially after immersion for a period of six weeks. Deep surface cracks were observed throughout the aluminium samples and to a smaller degree on the titanium samples.

Lanthanum acetylacetone showed signs of acting as an anodic inhibitor in most of the potentiodynamic tests, by increasing E_{corr} and shifting it towards a more positive (anodic) direction. However, cerium acetylacetone did not significantly and consistently show shifts in E_{corr}, hence it was classified as a mixed inhibitor in this study for Al in NaCl and HCl systems.

DEDICATION

I would like to express my sincere gratitude to my supervisor and co-supervisor Doctor David Whitefield and Professor Herman Potgieter. Their exceptional guidance, knowledge, constructive criticism, and patience gave me confidence which led to the completion of this work.

I am thankful to my colleague Komla Atta for guiding and advising me throughout my postgraduate studies, at the University of Witwatersrand.

A special thanks to my mentor and guardian Husayn Tambe Arrah, who constantly advised and encouraged me from my first year of undergraduate studies till date.

I cannot fully express my gratitude to my entire MANJO family for their constant support, sacrifice, and encouragement throughout my entire academic journey.

- Julius Berdu Manjo
- Matilda Fon Manjo
- Persis Yefon Manjo
- Robert Fon Manjo
- Larissa Jila Manjo

CONTENTS

PLAGIARISM DECLARATION 2
ABSTRACT 3
DEDICATION 4
LIST OF FIGURES 8
LIST OF TABLES 11
LIST OF EQUATIONS 12
LIST OF ABBREVIATIONS & SYMBOLS 13
CHAPTER 1: INTRODUCTION 14
1.1 BACKGROUND 14
1.2 Problem Statement 15
1.3 Research Questions 15
1.4 Research Objectives 16
1.5 Hypothesis 16
CHAPTER 2: LITERATURE REVIEW 17
2.1 Corrosion 17
2.2 Corrosion Inhibition 17
2.2.1 Anodic Inhibitors 18
2.2.2 Cathodic Inhibitors 18
2.2.3 Mixed Inhibitors 18
2.3 Rare Earth Metals as Corrosion Inhibitors 18
2.4 The Case of Aluminium 19
2.4.1 Factors Affecting Corrosion of Aluminium 20
2.5 The Case of Titanium 21
2.5.1 Corrosion Resistance of Titanium 21
2.5.2 Corrosion in Seawater 22
2.5.3 Corrosion in Chloride Solutions 23
2.5.4 Corrosion in Nitric Acid 24
2.6 REM Inhibitors 24
2.7 Rare Earth Metal Beta - Diketonates 26
CHAPTER 3: MATERIALS & METHODS 28
3.1 REM-Beta-diketone complexes synthesis 28
3.2 Inhibitor Characterization 28
3.3 Chloride Corrosive Media Preparation 31

3.4 Weight Loss Tests 31
3.5 Potentiodynamic Polarization Tests 32
3.6 Metal Sample Analysis 35
CHAPTER 4: ALUMINIUM EXPERIMENTS 36
4.1 Aluminium Sample Material Analysis 36
4.2 Aluminium Sample Preparation 36
4.3 Aluminium Samples for Weight Loss Tests 37
4.4 Aluminium in NaCl Experiments 38
4.4.1 NaCl Solutions Weight Loss Tests 38
4.4.2 Corrosion Rate of NaCl Solutions Weight Loss Tests 39
4.4.3 Inhibition Efficiency of $La(acac)_3$ and $Ce(acac)_3$ in NaCl solutions 44
4.4.4 NaCl Solutions Potentiodynamic Tests 44
4.4.5 SEM Analysis of NaCl Potentiodynamic Samples 46
4.5 Aluminium in HCl Experiments 52
4.5.1 HCl Solutions Weight Loss Tests 52
4.5.2 Corrosion Rate of HCl Solutions Weight Loss Tests 52
4.5.2 Inhibition Efficiency of $La(acac)_3$ and $Ce(acac)_3$ in HCl solutions 58
4.5.3 HCl Solutions Potentiodynamic Tests 59
4.5.4 SEM Analysis of HCl Potentiodynamic Samples 61
CHAPTER 5: TITANIUM EXPERIMENTS 66
5.1 Titanium Sample Material Analysis 66
5.2 Titanium Sample Preparation 66
5.3 Titanium Samples for Weight Loss Tests 67
5.4 Titanium in NaCl Experiments 67
5.4.1 NaCl Solutions Weight Loss Tests 67
5.4.2 NaCl Solutions Potentiodynamic Tests 72
5.4.3 SEM Analysis of NaCl Potentiodynamic Samples 73
5.5 Titanium in HCl Experiments 80
5.5.1 HCl Solutions Weight Loss Tests 80
5.5.2 HCl Solutions Potentiodynamic Tests 84
5.5.3 SEM Analysis of HCl Potentiodynamic Samples 85
5.5.3.1 SEM of Titanium Sample in HCl Without Inhibitor 85
5.5.3.2 SEM of Titanium Sample in HCl With Inhibitor 87
CHAPTER 6: CONCLUSION AND RECOMMENDATION 91
6.1 Conclusion 91
6.2 Recommendation 92

APPENDICES 93
Appendix A: 93
Appendix B: 95
Appendix C: 96
REFERENCES 100

LIST OF FIGURES

Figure 1: Schematic of polarization curve to show corrosion, adapted from (McCafferty, 2009) 17
Figure 2: Polarization curve for aluminium & stainless steel, 0.5M H_2SO_4 (Reboul, 2005). 19
Figure 3: Pourbaix phase diagram 'E vs pH' for aluminium, from (Pourbaix & Deltombe, 1958). 20
Figure 4: Weight loss test of 99.99% aluminium, 1M solution, 96hrs, from (Chatalov, 1952). 20
Figure 5: Pourbaix diagram of titanium, (Pourbaix, 1979). 22
Figure 6: Graph showing inhibition properties of various lanthanide metals, (Forsberg, 1981). 25
Figure 7: Drawing of the empirical structure of beta-diketonates. 26
Figure 8: SEM image of $La(acac)_3$ (2000 X). 29
Figure 9: EDS analysis of La based Inhibitor. 29
Figure 10: SEM analysis of $Ce(acac)_3$ (1600 X). 30
Figure 11: EDS analysis of Ce based Inhibitor. 31
Figure 12: Potentiodynamic apparatus setup. 33
Figure 13: Mounted titanium sample in resin. 34
Figure 14: Image of aluminium sample Al 5050 provided. 36
Figure 15: Prepared aluminium samples for weight loss test. 37
Figure 16: Submerged aluminium coupons during weight loss test. 38
Figure 17: Normalized cumulative mass loss of Al coupons in various 0.6 M NaCl solutions over a period of six weeks at 39
Figure 18: Corrosion rate for Al coupons in 0.6M NaCl for six weeks. 40
Figure 19: SEM image of Al in 0.6M NaCl without inhibitor, after a six-week weight loss test (800 X). 41
Figure 20: SEM image of Al in 0.6M NaCl with $La(acac)_3$ after a six-week weight loss test (1200 X). 42
Figure 21: EDS of Al surface after a six-week weight loss test in 0.6M NaCl with $La(acac)_3$. 42
Figure 22: SEM image of Al in 0.6M NaCl with $Ce(acac)_3$ after a six-week weight loss test (800 X). 43
Figure 23: XDS analysis of Al in 0.6M NaCl with Ce(acac)3 after a six-week weight loss test. 43
Figure 24: Inhibition efficiency of $La(acac)_3$ and $Ce(acac)_3$ in 0.6M NaCl in weight loss test. 44
Figure 25: Potentiodynamic curves of Al in 0.6M NaCl at 25^0C. 45
Figure 26: SEM image of Al reference sample without potentiodynamic immersion (732 X). 47
Figure 27: EDX surface analysis of Al reference sample without potentiodynamic immersion. 47
Figure 28: SEM of Al in 0.6M NaCl without inhibitor after potentiodynamic immersion at 25^0C (400 X). 48
Figure 29: SEM of Al in 0.6M NaCl without inhibitor after potentiodynamic immersion at 25^0C (1610 X). 49
Figure 30: EDX analysis of Al surface after potentiodynamic immersion in 0.6M NaCl without inhibitor. 49
Figure 31: SEM of Al in 0.6M NaCl with $Ce(acac)_3$ after potentiodynamic immersion at 25^0C *(732 X).* 50
Figure 32: SEM of Al in 0.6M NaCl with $La(acac)_3$ after potentiodynamic immersion at 25^0C (800 X). 51

Figure 33: Normalized cumulative mass loss of Al coupons in various 0.1 M HCl solutions over a period of six weeks at 25^0C. 52
Figure 34: Corrosion rate for Al coupons in 0.1M NaCl for a six-week weight loss test. 54
Figure 35: SEM image of Al in 0.1M HCL without inhibitor after a six-week weight loss test (426 X). 55
Figure 36: SEM of Al in 0.1M HCl without inhibitor after a six-week weight loss test (300 X). 56
Figure 37: XDS of Al in 0.1M HCl without inhibitor after weight loss test. 56
Figure 38: SEM of Al in 0.1M HCl with $Ce(acac)_3$ after a six-week weight loss test (250 X). 57
Figure 39: SEM of Al in 0.1M HCl with $La(acac)_3$ after a six-week weight loss test (250 X). . 58
Figure 40: Inhibition efficiency of $La(acac)_3$ and $Ce(acac)_3$ in 0.1M HCl in weight loss test. . 59
Figure 41: Potentiodynamic test for Aluminium in 0.1 HCl at 25^0C. 60
Figure 42: SEM image of Al in 0.1M HCl without inhibitor after potentiodynamic immersion (426 X). 62
Figure 43: EDS analysis of Al in 0.1M HCl without inhibitor after potentiodynamic immersion. 63
Figure 44: SEM image of Al in 0.1M HCl with $La(acac)_3$ after potentiodynamic immersion (732 X). 64
Figure 45: SEM image of Al in 0.1M HCl with $La(acac)_3$ (LEFT) and without inhibitor (RIGHT) after potentiodynamic immersion (105 X). 64
Figure 46: SEM image of Al in 0.1M HCl with $Ce(acac)_3$ after potentiodynamic immersion (800 X). 65
Figure 47: SEM image of Al in 0.1M HCl with $Ce(acac)_3$ (LEFT) and without inhibitor (RIGHT) after potentiodynamic immersion (200 X). 65
Figure 48: Titanium sample coupons 67
Figure 49: SEM image of Ti, without immersion for weight loss test (500 X). 69
Figure 50: SEM secondary of Ti sample, without immersion for weight loss test (500 X). 69
Figure 51: SEM image of Ti in 0.6M NaCl without inhibitor after six weeks weight loss test (500 X). 70
Figure 52: SEM secondary image of Ti in 0.6M NaCl without inhibitor after six weeks weight loss test (500 X). 70
Figure 53: SEM of Ti immersed in 0.6M NaCl with $La(acac)_3$ for a six-week weight loss test (500 X). 71
Figure 54: SEM of Ti immersed in 0.6M NaCl with $Ce(acac)_3$ for a six-week weight loss test (500 X). 71
Figure 55: Potentiodynamic plot of Ti immersed in 0.6M NaCl at 25^0C. 72
Figure 56: SEM image of Ti reference sample without potentiodynamic test (732 X). 74
Figure 57: SEM image of Ti reference sample without potentiodynamic test (1140 X). 74
Figure 58: EDX of Ti reference sample without potentiodynamic test. 75
Figure 59: SEM of Ti surface after immersion in 0.6M NaCl without inhibitor, after potentiodynamic test at 25^0C (732 X). 75
Figure 60: SEM image of Ti surface after immersion in 0.6M NaCl without inhibitor, after potentiodynamic test at 25^0C (732 X). 76
Figure 61: SEM of Ti surface after immersion in 0.6M NaCl with $La(acac)_3$, after potentiodynamic test at 25^0C (732 X). 77
Figure 62: SEM secondary Ti surface after immersion in 0.6M NaCl with $La(acac)_3$, after potentiodynamic test at 25^0C (732 X). 77
Figure 63: EDX of Ti surface after immersion in in 0.6M NaCl with $La(acac)_3$, after potentiodynamic test at 25^0C. 78

Figure 64: SEM secondary Ti surface after immersion in 0.6M NaCl with Ce(acac)$_3$, after potentiodynamic test at 25^{0}C *(750 X).* 78
Figure 65: SEM secondary Ti surface after immersion in 0.6M NaCl with Ce(acac)$_3$, after potentiodynamic test at 25^{0}C *(400 X).* 79
Figure 66: EDX of Ti surface after immersion in in 0.6M NaCl with Ce(acac)$_3$, after potentiodynamic test at 25^{0}C. 79
Figure 67: SEM image of Ti in 0.1M HCl without inhibitor after six weeks weight loss test (600 X). 81
Figure 68: SEM secondary image of Ti in 0.1M HCl without inhibitor after six weeks weight loss test (600 X). 82
Figure 69: SEM image of Ti in 0.1M HCl with La(acac)$_3$ after six weeks weight loss test (500 X). 83
Figure 70: SEM image of Ti in 0.1M HCl with Ce(acac)$_3$ after six weeks weight loss test (500 X). 83
Figure 71: Potentiodynamic plot of Ti immersed in 0.1M HCl at 25^{0}C. 84
Figure 72: SEM of Ti surface after immersion in 0.1M HCl without inhibitor, after potentiodynamic test at 25^{0}C *(732 X).* 86
Figure 73: SEM secondary image of Ti surface after immersion in 0.1M HCl without inhibitor, after potentiodynamic test at 25^{0}C *(732 X).* 86
Figure 74: SEM of Ti surface after immersion in 0.1M HCl with La(acac)3, after potentiodynamic test at 25^{0}C *(732 X).* 87
Figure 75: SEM secondary of Ti surface after immersion in 0.1M HCl with La(acac)3, after potentiodynamic test at 25^{0}C *(426 X).* 88
Figure 76: EDX of Ti surface after immersion in in 0.1M HCl with La(acac)$_3$, after potentiodynamic test at 25^{0}C. 88
Figure 77: SEM of Ti surface after immersion in 0.1M HCl with Ce(acac)3, after potentiodynamic test at 25^{0}C *(400 X).* 89
Figure 78: SEM of Ti surface after immersion in 0.1M HCl with Ce(acac)3, after potentiodynamic test at 25^{0}C. 90
Figure 79: EDX of Ti surface after immersion in in 0.1M HCl with Ce(acac)$_3$, after potentiodynamic test at 25^{0}C. 90
Figure 80: 10X (left) and 20X (right) optical micrograph of Al reference (potentiodynamic test). 96
Figure 81: 10X (left) and 20X (right) optical micrograph of Al in 0.6M NaCl without inhibitor (potentiodynamic test). 96
Figure 82: 10X (left) and 20X (right) optical micrograph of Al in 0.6M NaCl with La(acac)$_3$ (potentiodynamic test) 97
Figure 83: 10X (left) and 20X (right) optical micrograph of Al in 0.1M HCl without inhibitor (potentiodynamic test) 97
Figure 84: 10X (left) and 20X (right) optical micrograph of Al in 0.1M HCl with La(acac)$_3$ (potentiodynamic test) 97
Figure 85: 20X (left) and 50X (right) optical micrograph of Ti in NaCl without inhibitor (potentiodynamic test) 98
Figure 86: 10X (left) and 20X (right) Optical micrograph of Ti in HCl without inhibitor. 99

LIST OF TABLES

Table 1: Summary of types and attributes of corrosion inhibitors, adapted from (Pourbaix, 1979). 19
Table 2: Corrosion rates of titanium in hydrochloric acid and other chloride media, (Toba & Kawano, 2014), (Blashchuk, et al., 1988). 23
Table 3: Semi-quantitative EDS results for $La(acac)_3$. 30
Table 4: Semi-quantitative EDS results for $Ce(acac)_3$. 31
Table 5: Summary of aluminium sample XRF analysis. 36
Table 6: Summary of potentiodynamic test for Al in 0.6M NaCl solutions at 25^0C. 46
Table 7: Summary of Potentiodynamic tests of Al in 0.1M HCl solutions at 25^0C. 61
Table 8:Summary of Titanium sample XRF analysis. 66
Table 9: Summary of weight loss measurements of titanium coupons in 0.6M NaCl solutions at 25^0*C.* 68
Table 10: Summary of potentiodynamic test for Ti in 0.6M NaCl solutions at 25^0*C.* 73
Table 11: Summary weight loss measurements of titanium coupons in 0.6M NaCl solutions at 25^0*C.* 80
Table 12: Summary of corrosion rate of Ti results for chloride solutions without inhibitor 80
Table 13: Summary of potentiodynamic test for Ti in 0.1M HCl solutions at 25^0C. 85
Table 14: Weekly weight measurements (in grams) of Al coupons in NaCl solutions 93
Table 15: Weekly weight measurements (in grams) of Al coupons in HCl solutions 94
Table 16: Summary of Aluminium Corrosion Rate results for weight loss and potentiodynamic tests. 95
Table 17: Summary of Titanium Corrosion Rate results for weight loss and potentiodynamic tests. 95

LIST OF EQUATIONS

Equation 1: Metathesis reaction to produce $Ce(acac)_3$ from Na(acac).....26
Equation 2: Metathesis reaction to produce $Ce(acac)_3$ from H(acac).....26
Equation 3: Direct synthesis reaction to produce $La(acac)_3$ from La and H(acac). 27
Equation 4: Corrosion rate equation from weight loss.....32
Equation 5: Inhibition Efficiency equation from Corrosion Rate.....32
Equation 6: Corrosion rate equation from tafel diagram. 34
Equation 7: Current density equation.....34
Equation 8: Equivalent weight equation. 35

LIST OF ABBREVIATIONS & SYMBOLS

$La(acac)_3$ – Lanthanum Acetylacetone

$Ce(acac)_3$ – Cerium Acetylacetone

E_{corr} – Corrosion Potential

i_{corr} – Corrosion Current

SEM – Scanning Electron Microscope

XRD – X-ray Diffraction

EDS – Energy Dispersive Spectroscopy

XRF – X-ray Fluorescence Spectrometer

CHAPTER 1: INTRODUCTION

1.1 BACKGROUND

Corrosion causes damage to infrastructure in a wide range of industries, including oil and gas, petrochemical, aviation, construction, marine, firearm, and water treatment. The global economic effect of corrosion is in the order of a trillion US dollars per year, which corresponds to about 3-4% of the global GDP (Janse van Rensburg, et al., 2019). In South Africa, corrosion costs amount to billions of Rands corresponding to about 3-4% of local domestic GDP (Janse van Rensburg, et al., 2019). Corrosion can be reduced in two main ways: by using corrosion inhibition substances and/or the use of corrosion resistant materials. The replacement with corrosion resistant materials is a more costly alternative, relative to the incorporation of inhibitors into the environment, as well as the use of coatings or protective films which preserve the state of the parent material. A corrosion inhibitor is a substance that when added in small concentrations to a corrosive system, reduces the rate of corrosion, without affecting the concentration of any reagents. Hexavalent chromium was earlier used as a corrosion inhibitor due to its high efficiency but was discontinued due to its toxicity. Since then, different classes of inhibitors have been investigated with emphasis on being environmentally friendly while considering cost and efficiency. The salts of Rare Earth Metals (REM) offer an efficient, green alternative due to their extremely low ecological and environmental toxicity (Forsyth & Hinton, 2014). Despite REM being as effective as chromate inhibitors, they are more expensive but worthy when considering health and environmental effects. The combination of REM salts and beta-diketonate provide room for interesting synergistic inhibitory properties. This study focuses on the use of saline and acidic chloride media and diketonate REM salts in corrosion inhibition of Ti and Al samples. Immersion experiments were conducted in chloride media which simulated seawater and corrosive HCl acidic environments for periods of up to sixty days. Various techniques were employed, e.g., weight loss tests, microscopy and diffractometry to investigate the propagation and inhibition of corrosion in these systems.

1.2 Problem Statement

The importance of corrosion prevention spans economic, infrastructural, engineering, material science, medical and maritime areas. There is a huge industrial driving force to mitigate the corrosion effects, hence corrosion inhibition studies are often undertaken. In addition, chromates which were previously used as corrosion inhibitors, are being discontinued because of their high toxicity to both humans and flora. However, a balance between efficiency, cost and ecotoxicity must be struck and most importantly without compromise on health and safety. Certain inhibitors such as carboxylates are very cheap but not as efficient, and inhibitors such as tannins are eco-friendly but not efficient. The research for greener, non-toxic and effective alternatives to chromates prompted the study of REM salts as inhibitors.

1.3 Research Questions

a) Can REM beta-diketone complexes of lanthanum [La] and cerium [Ce] be considered as good corrosion inhibitors in chloride corrosive media environments?

b) Are the inhibitors in (a) compatible with the Al and Ti metal samples?

c) Are there changes to the metal surfaces occurring during corrosion in the presence of these corrosion inhibitors?

d) What types of corrosion inhibitors are these compounds: anodic, cathodic or mixed corrosion inhibitors?

e) What is the maximum efficiency of corrosion inhibition with a selected concentration of these inhibitors?

f) What is the role of the metal atom and beta-diketone in the corrosion inhibition process, i.e., does the efficiency of inhibition depend on the type of beta-diketone and/or metal?

1.4 Research Objectives

a) Synthesize rare earth element-beta-diketonate salt of lanthanum and cerium, $La(acac)_3$ and $Ce(acac)_3$.

b) Examine the performance of $La(acac)_3$ and $Ce(acac)_3$ in chloride environments by evaluating the inhibitor efficiency i.e., NaCl to simulate saline seawater and HCl to simulate acidic chloride mining environments.

c) Examine the performance of titanium and aluminium alloy samples in the presence of the chloride environments in (2) and in the presence of the inhibitors in (1), by checking corrosion rates and SEM analysis.

1.5 Hypothesis

REM salts will show a high-level of corrosion inhibition in chloride media for both Ti and Al, with Lanthanum salts showing better inhibition than cerium salts.

CHAPTER 2: LITERATURE REVIEW

2.1 Corrosion

The verb *corrode* comes from the Latin word *rodere* which means to gnaw and later came to mean the progressive wearing of a solid by chemical effects. Corrosion refers to the electrochemical and physicochemical reactions which occur between a metal and its surrounding media, leading to changes in its structure, composition, and bulk physical properties (Gräfen, et al., 2002). Thermodynamically, the process of corrosion is irreversible as a corroded metal will not be able to return to its previous state. This is because a system will always move towards a state of minimum free enthalpy (Coupry & Develay, 1971).

Electrochemically, corrosion occurs on two distinct areas of the metal, which are the cathode and the anode. Oxidation reactions occur at the anode and reduction reactions occur at the cathode. These reactions occur due to the movement of electrons from the anode to the cathode, which generates a current (Pourbaix, 1990). The relationship between these reactions can be described using a polarization curve (*Figure 1*) on which electrochemical potential is plotted against current density. Point C indicates the current at which corrosion occurs and when the rates of anodic and cathodic reactions are equal (McCafferty, 2009).

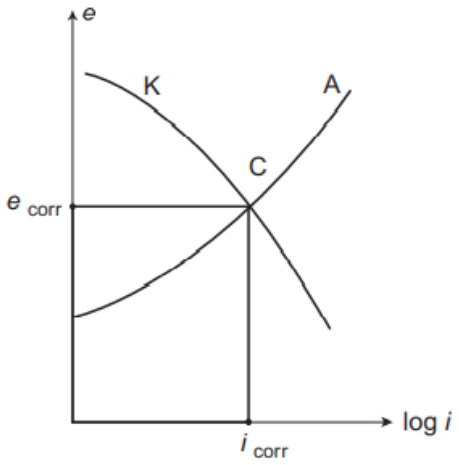


Figure 1: Schematic of polarization curve to show corrosion, adapted from (McCafferty, 2009)

2.2 Corrosion Inhibition

Inhibere is the Latin word from which inhibition stems, and it means “to stop or to retain”. A corrosion inhibitor is a substance than when added in small concentrations

to a corrosive system, reduces the rate of corrosion, without affecting the concentration of any reagents and corrosive agents. The development of corrosion inhibitors spans from medieval ages to this modern day, from the use of oils to prevent the rusting of swords, to the present day use complex coatings, as well as cathodic and anodic protection systems (Baroux, 2014).

In terms of electrochemistry, inhibitors can be classified as either anodic, cathodic, or mixed. As their name implies, anodic and cathodic inhibitors act to suppress the cathodic and anodic reactivities of metals. Mixed inhibitors combined the properties of both anodic and cathodic inhibitors. An inhibitor can be classified as an anodic or cathodic inhibitor when the change in E_{corr} is greater than 85mV in either the anodic or cathodic direction (Khaled & Amin, 2009). For anodic inhibitors, the potentiodynamic curve is shifted towards more positive potential values. Meanwhile for cathodic inhibitors, the potentiodynamic curve is shifted towards more negative potential values.

2.2.1 Anodic Inhibitors

Anodic inhibitors, also known as passivating inhibitors, are the most effective inhibitors because they cause a shift of the corrosion potential of the anode to the passivation range. Anodic inhibitors usually act by forming protective oxide layer which surrounds the metal (McCafferty, 2009) (Reboul, 2005).

2.2.2 Cathodic Inhibitors

Cathodic inhibitors function by either slowing the rate of cathodic reaction or by selective precipitation on the surface of the cathode to offer mass transfer resistance to the diffusion of oxidizing species (McCafferty, 2009). (Reboul, 2005).

2.2.3 Mixed Inhibitors

These inhibitors adhere to the surface of the metal and then repel water molecules by the presence of hydrophobic agents. The efficiency of these inhibitors is dependent on the metal involved, its affinity for the hydrophobic agent, the temperature and pressure of the system (Pourbaix, 1957).

2.3 Rare Earth Metals as Corrosion Inhibitors

Nowadays, inhibitors should not only be efficient and economic, but environmentally acceptable with a minimum ecological impact as well. *Table 1* gives a summary of the

types of corrosion inhibitors and their classification as effective, economic, ecological, or environmentally friendly.

Table 1: Summary of types and attributes of corrosion inhibitors, adapted from (Pourbaix, 1979).

Need	**Typical Inhibitors**
Effectiveness	Chromates, Nitrates, Phosphates
Economic	Molybdates, Carboxylates, Cations
Ecologic	Tannins, surfactants, natural compounds
Environmentally friendly	REM, organic & inorganic REM combinations

2.4 The Case of Aluminium

The electrochemical activity of aluminium is very different from other base metals due to the ability of aluminium to react with atmospheric oxygen to create a protective oxide layer creating passivity (see Figure 2). This aluminium oxide (Al_2O_3) layer is continuous, uniform, and self-generating.

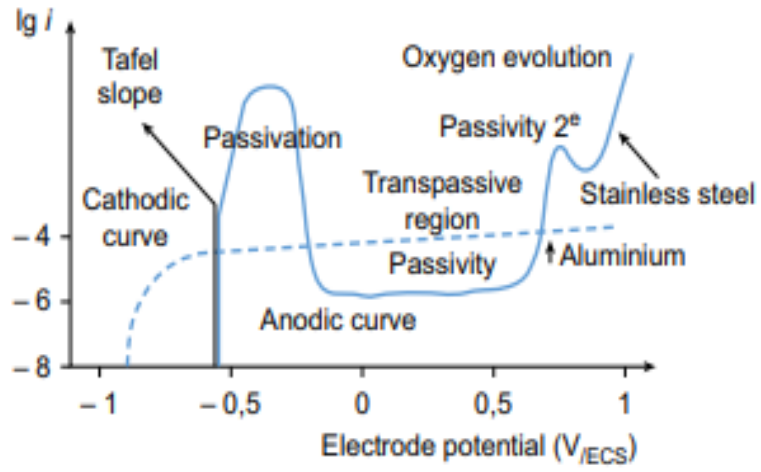


Figure 2: Polarization curve for aluminium & stainless steel, 0.5M H_2SO_4 (Reboul, 2005).

The Pourbaix diagram in Figure 3, shows the different zones of reaction between a metal and water. It highlights the zones of stability and vulnerability of the metal to corrosion and chemical attack. In the case for aluminium, three different zones exist, namely the corrosion, passivation, and immunity zones.

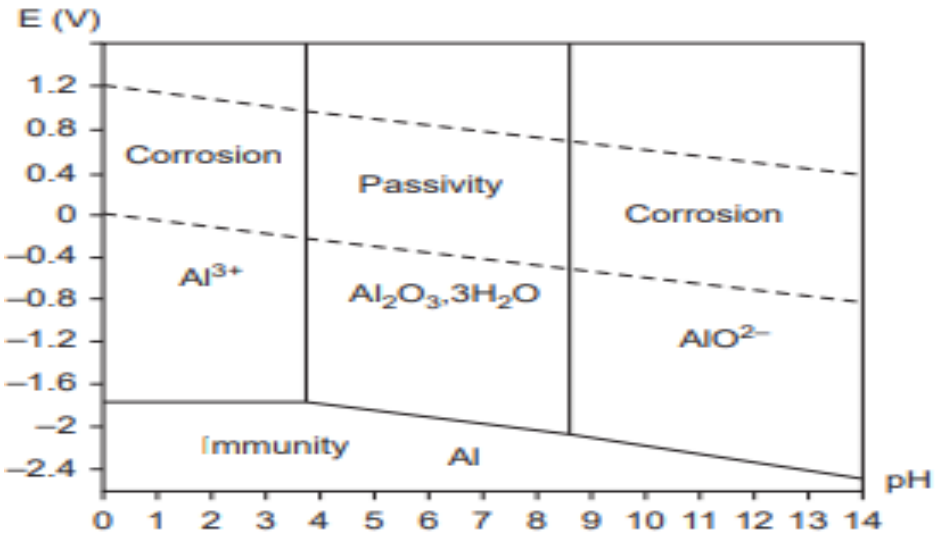


Figure 3: Pourbaix phase diagram 'E vs pH' for aluminium, from (Pourbaix & Deltombe, 1958).

2.4.1 Factors Affecting Corrosion of Aluminium

2.4.1.1 pH of Solution

The stability of the oxide film is directly affected by the pH. The pH optimal range for passivity is 5 – 8 (Figure 4) in line with the amphoteric nature of aluminium. (Chatalov, 1952).

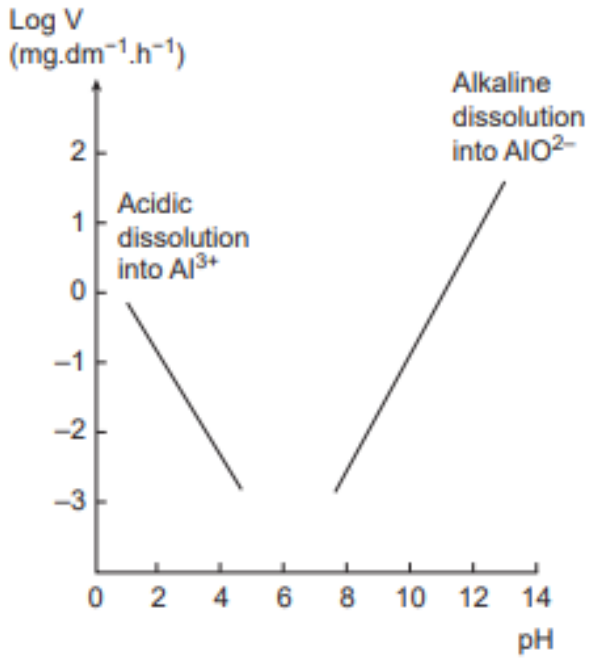


Figure 4: Weight loss test of 99.99% aluminium, 1M solution, 96hrs, from (Chatalov, 1952).

2.4.1.2 Corrosion in Mineral Acids

Mineral acids have a high rate of attack on aluminium, which increases with an increase in acid concentration. However, nitric acid has no effect on aluminium. This due to two things, the stable passivating oxide layer of Aluminium and the oxidizing nature of nitric acid which ensures the surface of the metal is always covered with its protective oxide layer (Patrie, 1952).

2.4.1.3 Corrosion in Alkaline Solutions

Potassium and sodium hydroxide cause metal attack of aluminium, even at small concentrations. (Chatalov, 1952).

2.5 The Case of Titanium

Titanium is one of the most abundant elements on earth, comprising about 0.6% of the earth's crust. Titanium has mechanical properties similar to mild steel, but a density of 4.51 g/cm^3 and high strength to weight ratio. These properties make titanium highly suitable for the aerospace industry (Greenwood & Earnshaw, 2007).

2.5.1 Corrosion Resistance of Titanium

Similar to aluminium, titanium is a very reactive metal and in aerated environments will form a protective, stable layer of titanium dioxide (TiO_2). This oxide layer is approximately 1.5 – 10 nm thick and strongly adheres to the metal surface (Zielinski & Sobieszczyk, 2008). This passivation and formation of the titanium dioxide layer is the reason for titanium's good corrosion resistance.

Despite such good corrosion resistance ability, titanium still suffers corrosion attacks from aggressive environments. Titanium may suffer different forms of localised and generalised corrosion such as crevice, pitting, erosion, fretting corrosion, stress corrosion cracking and hydrogen embrittlement (Fazel, et al., 2015).

The Pourbaix diagram of titanium in water, Figure 5, shows that shows that TiO_2 is stable over a wide range of potentials (Pourbaix, 1979).

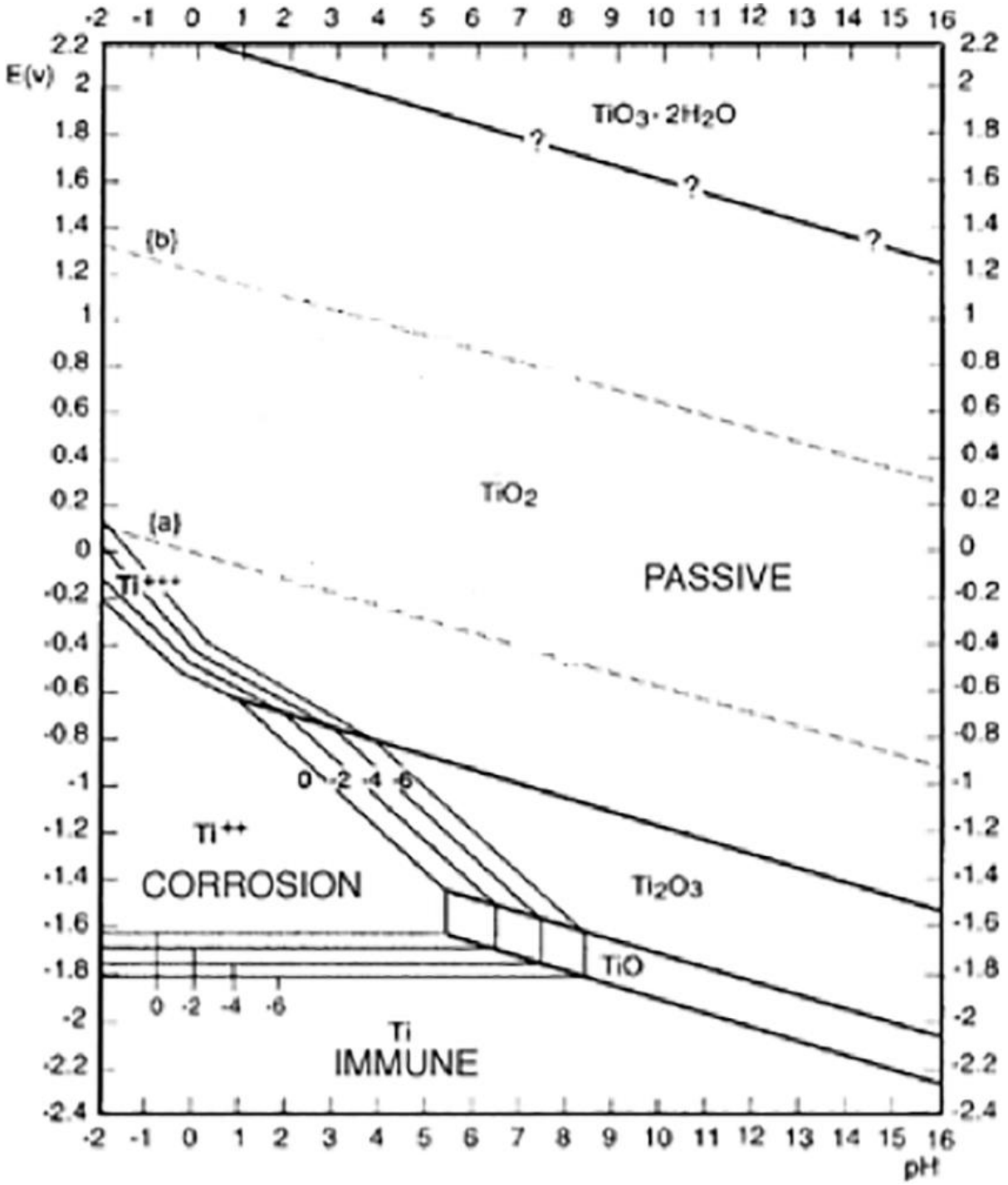


Figure 5: Pourbaix diagram of titanium, (Pourbaix, 1979).

2.5.2 Corrosion in Seawater

Titanium was observed to display good corrosion resistance in seawater and does not corrode at temperatures up to 180 ^{o}C (Greenwood & Earnshaw, 2007)

2.5.3 Corrosion in Chloride Solutions

Chloride containing solutions only moderately attack titanium. Acids such as hydrochloric acid does affect titanium metal. (Alfantazi, et al., 2016). The effect of HCl on the titanium corrosion rate generally increases with acid concentration and temperature of the solution. Table 2 shows the typical corrosion rates of a few corrosive media via weight loss test under different conditions. Ammonium chloride (NH_4Cl) attack titanium when it is present in high concentrations above 20% and elevated temperatures (Toba & Kawano, 2014).

Table 2: Corrosion rates of titanium in hydrochloric acid and other chloride media, (Toba & Kawano, 2014), (Blashchuk, et al., 1988).

Compound	**Concentration (%)**	**Temperature (ºC)**	**Corrosion rate (mm/yr)**
HCl (de-aerated)	1	35	0.003
	1	Boiling	2
	3	35	0.13
	3	Boiling	6.1
HCl (aerated)	1	35	0.003
	1	Boiling	1.83
	6	25	0.07
Aluminium Chloride	10	100	0.002
	10	150	0.033
	25	Room	0.001
	25	Boiling	50
Calcium Chloride	5	100	0.0005
	55	105	0.005
Magnesium Chloride	5	100	0.0008
	50	200	0.005
Potassium Chloride	30	110	0.013

2.5.4 Corrosion in Nitric Acid

The effect of nitric acid on titanium is similar in its effect on aluminium. The strong oxidizing nature of nitric acid encourages the passivation of titanium metal surface by the formation of stable oxides. At room temperature, titanium resist corrosion in nitric acid for concentrations up to 65% (Greenwood & Earnshaw, 2007).

2.6 REM Inhibitors

The salts of REM have been purported to be more environmentally friendly alternatives with similar levels of efficiency to the extensively used and very effective chromium ion inhibitors. Experiments conducted with the lanthanide series metal salts as corrosion inhibitors proved to be effective (Arnott, et al., 1985). The experiments used 1000 ppm REM chlorides ($NdCl_3$, $CeCl_3$, $LaCl_3$, YCl_3, $PrCl_3$) in a 1 M NaCl solution with aluminium alloy AA7075 and showed considerable corrosion inhibition. It was also observed that Ce^{3+} ions showed the best anti-corrosion properties with an almost 100% corrosion efficiency, Figure 6 (Salnikow & Zhitkovich, 2008). This was due to the formation of stable and very compact layers of cerium oxides and hydroxides on the aluminium surface (Kalman, 1994).

(Arnott, et al., 1987) conducted further experiments with a variety of cerium salts to determine which one has the best inhibiting properties. In this investigation cerium chloride, molybdate, fluoride and sulphate were used with total immersion of the Al alloy in a 0.6 M NaCl solution. The results showed that $CeCl_3$ had the best inhibition, followed by the sulphate, with both having over 95% efficiency. Cerium fluoride had the least inhibiting effect with less than 45% efficiency (Arnott, et al., 1989). These experiments highlighted the inhibitor capabilities of standard REM salts under a range of conditions, and it was important to understand which REM and salt works best under a particular condition.

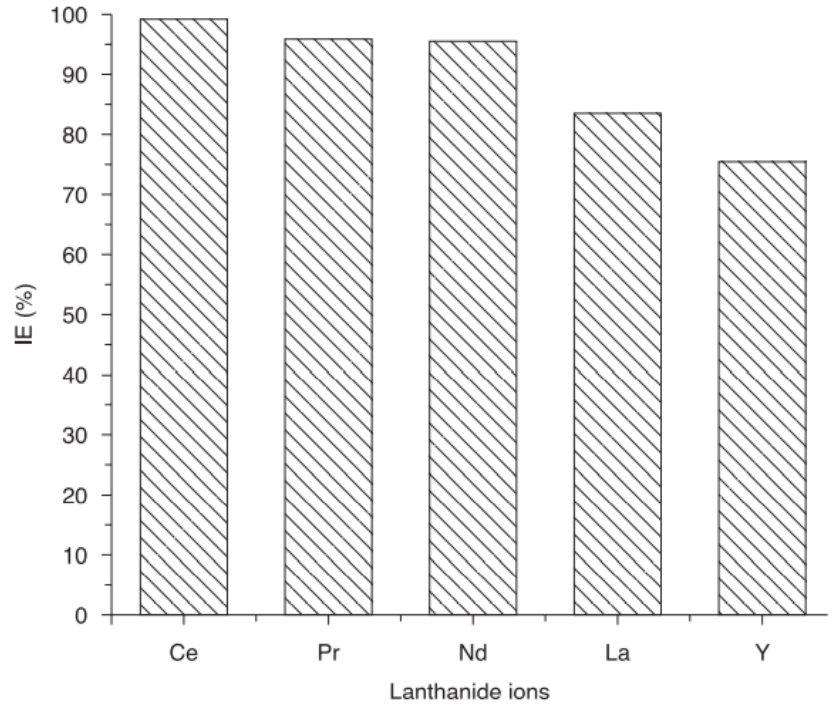


Figure 6: Graph showing inhibition properties of various lanthanide metals, (Forsberg, 1981).

Similar experiments were conducted with aluminium alloy and Al alloy composites. AA6061, AA6061-SiC, AA7075T6 and AA6061-Graphite were immersed in 1000ppm $CeCl_3$ solution for a week before being transferred into a NaCl solution. It was observed that the treated alloys performed significantly better than the untreated ones against corrosion (Forsberg, 1981). In the testing and research on REM salts, it was concluded that $CeCl_3$ was the most effective due to its good passivation and protection ability.

A more recent study by (Yasakau, et al., 2006), highlighted the mechanism of inhibition of lanthanum and cerium nitrates on AA2024 in 0.005M NaCl, where the respective REM hydroxides precipitate on S-phase regions and slow down cathodic and anodic reactions. It was observed that Ce had a slightly better inhibition efficiency relative to La due to the higher insolubility of cerium hydroxide relative to lanthanum hydroxide.

Another study by (Yasakau, et al., 2008), showed similar inhibition mechanism of lanthanum and cerium nitrates on AA5083 in a 0.05M NaCl solution, whereby respective hydroxides precipitated on cathodic regions of the metal and slowed the rate of corrosion.

2.7 Rare Earth Metal Beta - Diketonates

In the 1950s, beta - diketonates were used as extractants in solvent – solvent extraction processes, with various other uses. The neutral tri complexes have three beta – ketone ligands attached to a rare earth metal atom and can be represented by the general formula [R(β-diketonate)$_3$] (Brown, et al., 1969).

Structurally β-diketonate are composed of two carbonyl groups on the first and third carbon atom, hence the name 1,3-diketonate (Figure 7). The substituent groups can bond at either end of the β-diketonate, which gives it distinct properties. For example, alkyl substituent groups increase solubility. The simplest β-diketonate is acetylacetone which is composed of two methyl substituent groups, Figure 7 (Monticelli, 2018).

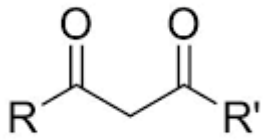


Figure 7: Drawing of the empirical structure of beta-diketonates.

There are two main methods of rare earth metal β-diketonate synthesis, which are by the metathesis reaction and direct synthesis reaction. Metathesis reaction constitutes more than 95% of the quoted literature production method whereby a reaction between a sodium or ammonium β-diketonate and rare earth metal chloride or nitrate reacts in water or ethanol as solvent (Hackerman & Snaveley, 1984).

$3\ Na(acac)_3 + CeCl_3 \text{ -----> } Ce(acac)_3 + 3\ NaCl$ Equation 1

Equation 1: Metathesis reaction to produce $Ce(acac)_3$ from Na(acac).

$3\ H(acac) + CeCl_3 \text{ -------> } Ce(acac)_3 + 3\ HCl$ Equation 2

Equation 2: Metathesis reaction to produce $Ce(acac)_3$ from H(acac).

The direct synthesis method comprises of reacting the rare earth metal directly with β-diketonate, in a 1:3 stochiometric ratio using toluene/an alcohol as an inert solvent. This leads to the production of hydrogen gas. The direct synthesis method ensures that the product is free from contamination of cations, anions, and water.

$La + 3\ H(acac) \text{ --------> } La(acac)_3 + 1.5\ H_2$ Equation 3

Equation 3: Direct synthesis reaction to produce $La(acac)_3$ from La and H(acac).

The combination of REM such as Lanthanum and Cerium cations to organic molecules, aim to improve on the moderate efficiency of the parent inhibitors, as well as to increase the function (mixed, anodic and cathodic) and range of environment which they act (Ivusic, et al., 2015). These environments could include acidic, chloride, alkaline, high temperature and high saline concentration environments. In another investigative study by (Xianghong, et al., 2010), sodium oleate and cerium were used individually and synergistically on the corrosion of cold rolled steel immersed in 3M phosphoric acid solution. This investigation was done by means of Electrochemical Impedance Spectroscopy (EIS), SEM, weight loss and potentiodynamic analysis. It was observed that individually Ce (IV) showed very poor inhibition efficiency and sodium oleate performed averagely well. Surprisingly, the combination of both inhibitors yielded a maximum inhibition efficiency of 97%.

A similar investigation conducted by (Fragoza-Mar, et al., 2012) with 1,3-diketone malonates for mild steel in 1M HCl solution, revealed that at 100 mg/l concentration the inhibitor efficiency ranged from 75% to as high as 96%.

(Ghanbari, et al., 2009) investigated the action of Cu, Zn, Mn and Co based beta-diketonate on mild steel in 1M phosphoric acid, 1M NaCl and 1M HCl solutions. It was observed that these beta-diketonate inhibitors showed very good inhibitor efficiencies over a wide range of pH solutions. This gives the promise of the wide range of environments in which beta-diketonate inhibitors can act through. In addition, it was also discovered that the inhibition efficiency in HCl was better than in the NaCl solution, which was attributed to the possible neutralisation of the surface charge by Na^+.

Despite the evidence of great inhibition efficiency from the synergy of metals, REMs and beta-diketonates, it is not yet exactly known which component is responsible for the majority surge in inhibition efficiency (Lawal, et al., 2022).

CHAPTER 3: MATERIALS & METHODS

3.1 REM-Beta-diketone complexes synthesis

A 10 g mass of REM halide salt was weighed out and placed in a conical flask. Two millilitres of methanol were added to the flask, just enough to dissolve the salt. After dissolution, the diketone solution was gradually added to the flask, in a total salt to diketone ratio of 1:3. The flask was stirred and then left to stand for a couple of hours to ensure reaction and crystallisation.

After settling for 2 hours, several drops of ammonium chloride were added to the flask to fully crystallize any remaining solids. The solution was then filtered through a filter paper and funnel to recover the solids. The flask and filter paper were washed with methanol to remove any leftover crystals and unreacted salts. The recovered crystals were placed in an oven at 40^{o}C and left to dry for 8 hours. The dried crystals were then recovered and placed in vials. This process was repeated for the preparation of all the REM beta-diketone inhibitors for this study.

3.2 Inhibitor Characterization

The prepared inhibitors were examined by EDS using a scanning electron microscope to determine the composition of the inhibitor. The EDS confirms the elements which gives an indication of the composition of the sample.

The image in Figure 8 shows the sample area used for the EDS analysis. The computed confirmed elements from this scan were chlorine, oxygen, lanthanum, and carbon (Figure 9). These elements confirm the presence of $La(acac)_3$ and some unreacted $LaCl_3$.

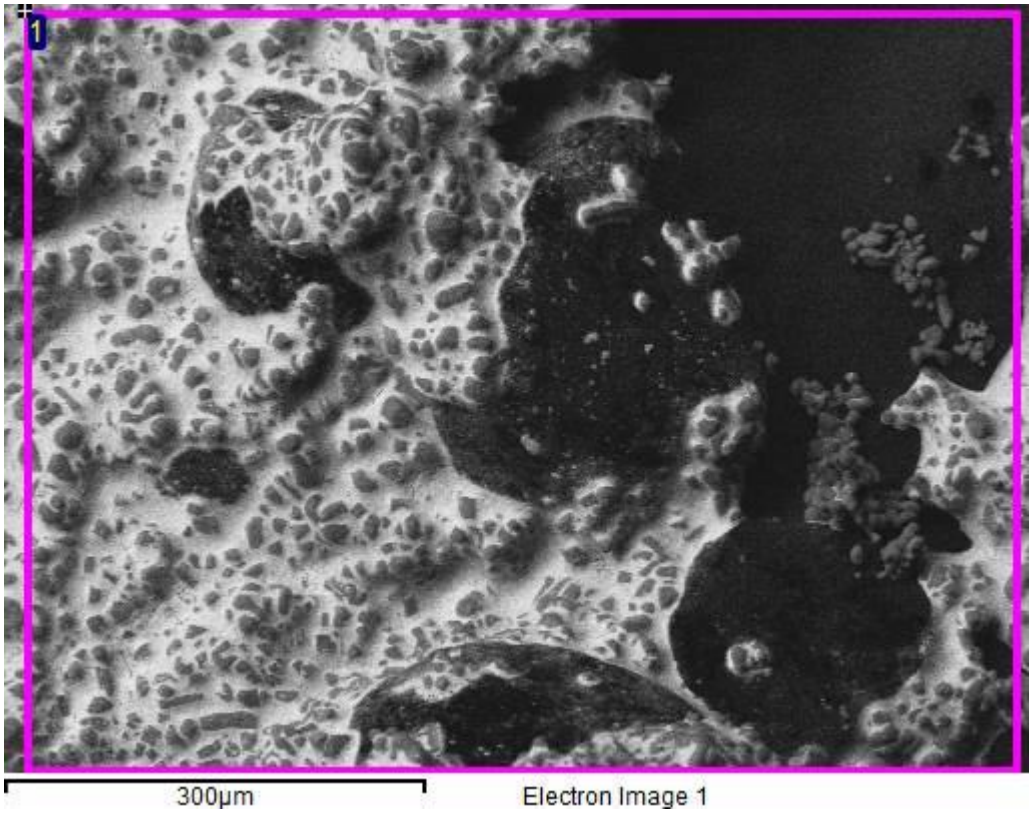


Figure 8: SEM image of La(acac)$_3$ (2000 X).

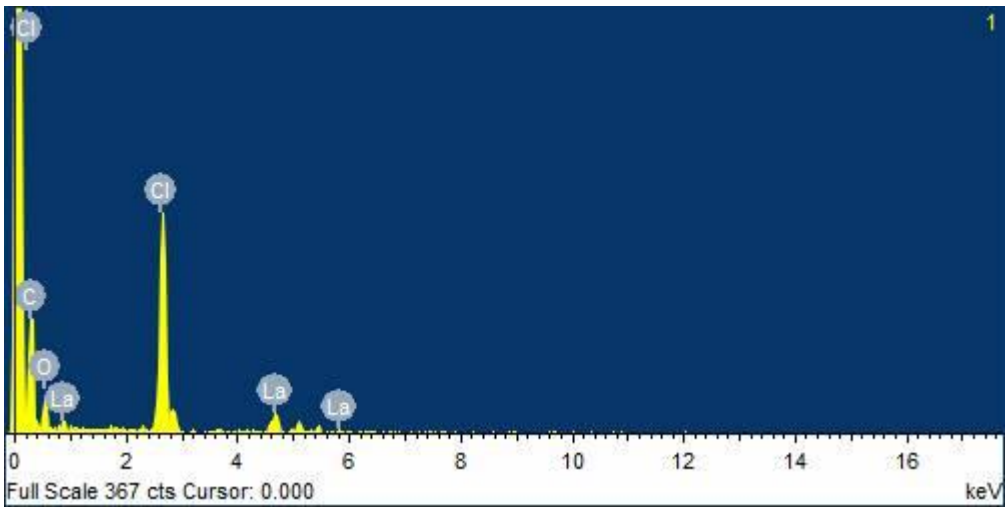


Figure 9: EDS analysis of La based Inhibitor.

Table 3: Semi-quantitative EDS results for $La(acac)_3$.

Element	Weight%	Atomic%
C K	56.05	76.33
O K	12.68	12.95
Cl K	20.47	9.45
La L	10.80	1.27
Totals	100.00	100.00

Figure 10 shows the area of interest for the Ce – based inhibitor sample. The EDS analysis indicated the presence of cerium, oxygen, carbon, and chlorine (Figure 11).

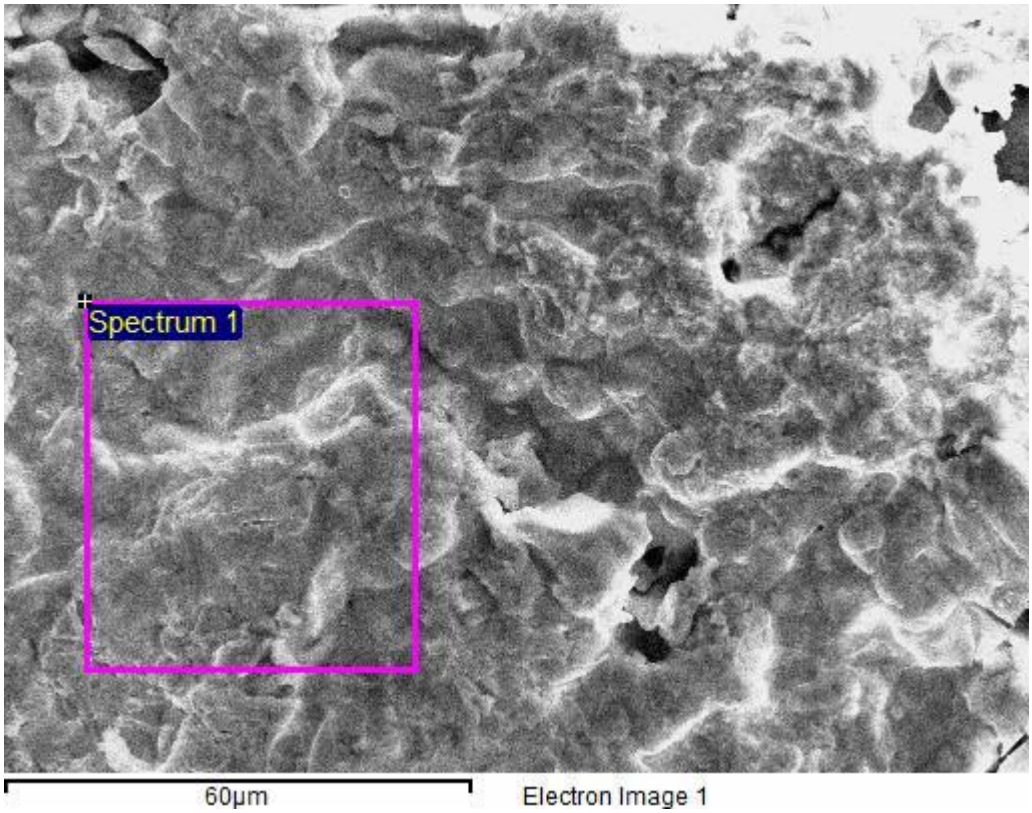


Figure 10: SEM analysis of $Ce(acac)_3$ (1600 X).

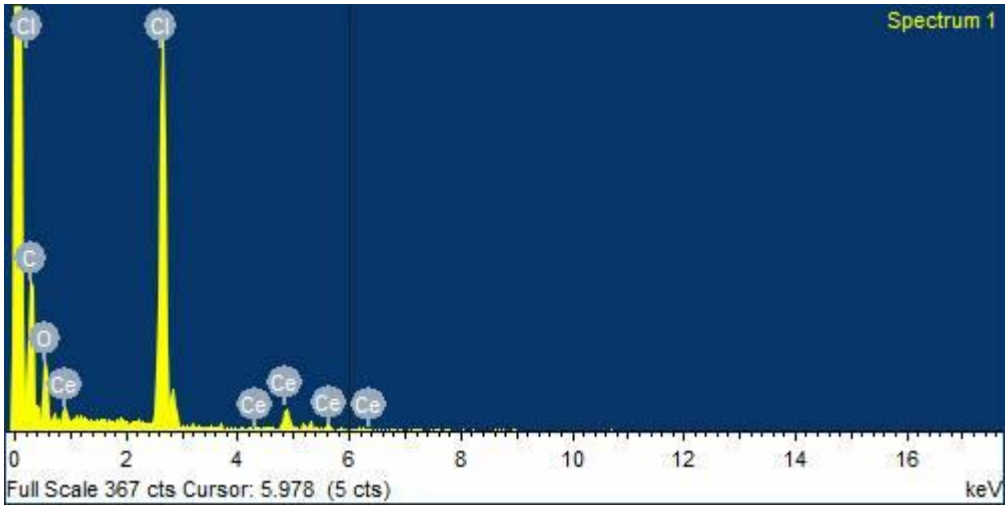


Figure 11: EDS analysis of Ce based Inhibitor.

Table 4: Semi-quantitative EDS results for $Ce(acac)_3$.

Element	Weight%	Atomic%
C K	53.37	72.94
O K	14.72	15.11
Cl K	23.73	10.99
Ce L	8.18	0.96
Totals	100.00	100.00

3.3 Chloride Corrosive Media Preparation

Seawater was simulated by the preparing a 0.6M NaCl solution which corresponds to 3.54 wt% NaCl (Hugel, 1960). The acidic chloride environment was simulated by using 0.1M HCl solution (Oakes, 1981). Hence two chloride environments were used in this study.

3.4 Weight Loss Tests

The weight loss tests were conducted to give an idea of how the different metal samples (Ti and Al) will react to long-term exposure in the chloride solutions (NaCl and HCl) with inhibitors ($La(acac)_3$ and $Ce(acac)_3$). The metal alloys were cut to a particular shape in immersed into the respective corrosive solutions and their mass

were recorded at time intervals to obtain a weight loss data over time, at room temperature and pressure.

The corrosion rate (CR) (in micrometres per year) was subsequently calculated from the weight loss data using Equation 4:

$$(\mathrm{CR}) = \mathrm{K} \times \frac{W_i - W_f}{\mathrm{DAT}} \qquad \text{Equation 4}$$

Equation 4: Corrosion rate equation from weight loss.

Where:
CR is the corrosion rate in micrometres per year
K is a factor which varies with unit of time used
W_i and W_f are recorded masses before and after immersion respectively (grams).
D is the density of the metal (g/cm^3)
A is the exposed area of the coupon in the chloride media (cm^2) and
T is the time of immersion (hours).

In addition to the above, the inhibitor efficiency (ε) was also calculated from the corrosion rate using the Equation 2:

$$\varepsilon = \frac{100\,\% \times (\mathrm{CR_{w/i}} - \mathrm{CR_i})}{\mathrm{CR_{w/i}}} \qquad \text{Equation 5}$$

Equation 5: Inhibition Efficiency equation from Corrosion Rate.

Where:
$CR_{w/I}$ is corrosion rate without inhibitor
CR_i is corrosion rate with inhibitor

3.5 Potentiodynamic Polarization Tests

Potentiodynamic polarization is a technique used to study the corrosion nature of metals when a potential is applied to an electrode and varied, at a set rate, while measuring the current through the electrolytic solution.

The potentiodynamic polarization tests was carried out in a three-electrode system contained in a 50ml corrosion glass cell, Figure 12. The setup included a counter, reference, and test electrode, connected to a potentiometer.

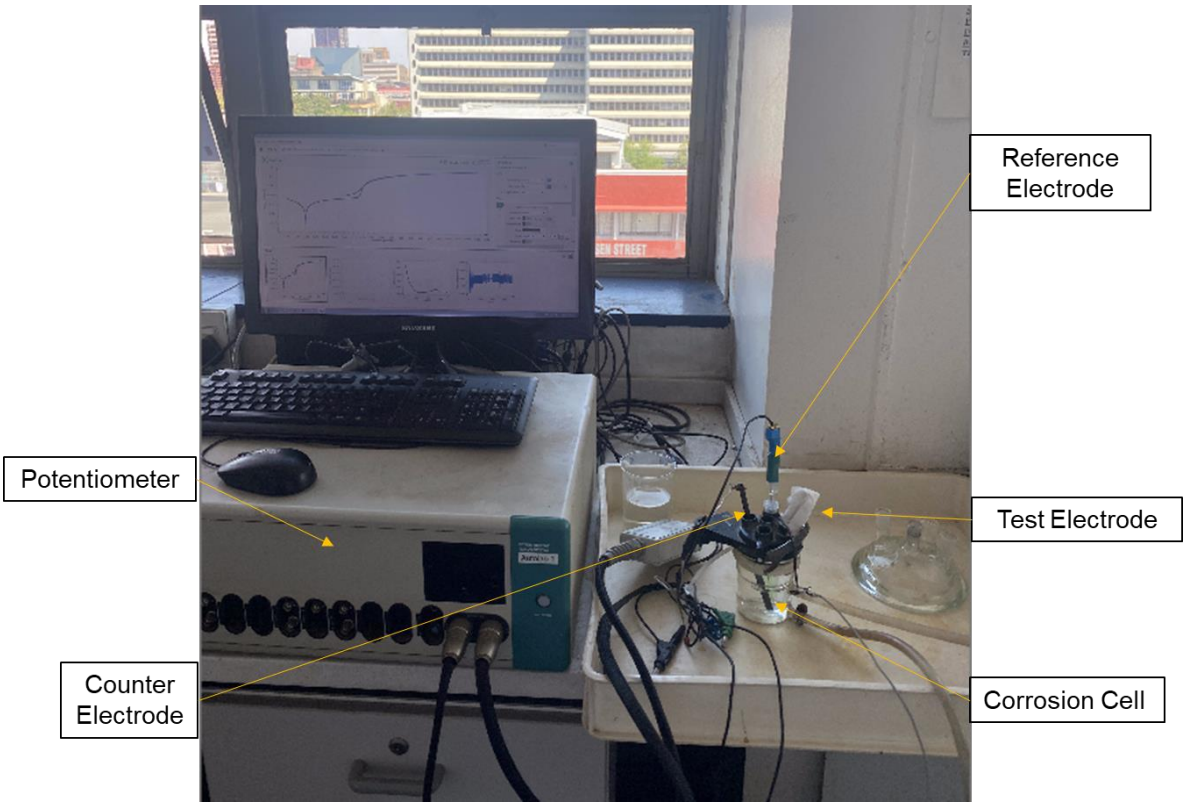


Figure 12: Potentiodynamic apparatus setup.

The polished and cut metal sample was cold mounted in a resin mould, Figure 13. The sample was wrapped with copper wires to ensure electrical connectivity, then a resin mix was poured into the mould with the wrapped sample. The mould was allowed to cure for 24 hours. After curing, the moulded sample was removed and tested for conductivity. The counter and reference electrodes were immersed in the solution in the cell, followed by the test electrode which was electrically connected by crocodile clips.



Figure 13: Mounted titanium sample in resin.

The AUTOLAB computer and potentiometer were set to run at a specified temperature, area of sample, and concentration. The current density and corrosion potential were obtained from the software. The corrosion rate of the overall system was calculated using the equation:

$$C_R = K\left(\frac{I_{CD} E_{EQ}}{D}\right) \qquad \text{Equation 6}$$

Equation 6: Corrosion rate equation from tafel diagram.

The corrosion rate was calculated as follows:

$$i_{CR} = \frac{I_{corr}}{A} \qquad \text{Equation 7}$$

Equation 7: Current density equation.

Where:

C_R is the rate of corrosion

K is a constant which depends on units used

I_{CD} is the corrosion current density (μA/cm^2)

E_{EQ} is the equivalent weight of the metal sample

D is the density of the metal sample (g/cm^3)

A is the exposed area of the metal sample (cm^2) and

I_{Corr} is the corrosion current in µA.

The metal samples have different corresponding metal compositions, hence the equivalent weight (E_{EQ}) of the sample with respect to metal compositions (Section 3.1), was calculated using Equation 8.

$$E_{EQ} = 1 \div \sum \left(\frac{f_i z_i}{M_i}\right) \qquad \text{Equation 8}$$

Equation 8: Equivalent weight equation.

Where:

f_i is the mass fraction of the elements present in the sample

z_i is the number of electrons exchanged by the elements present in the sample

M_i is the atomic weight of the element present in the sample.

3.6 Metal Sample Analysis

The provided Al and Ti metal samples for the experiments were initially analysed using an XRF. This provided the composition of the metal samples by element weight percentage and enabled the verification of the metal sample before any immersion began.

CHAPTER 4: ALUMINIUM EXPERIMENTS

4.1 Aluminium Sample Material Analysis

An XRF spectrometer analysis of the Al metal sample was conducted to assess its composition. The nominal composition of the sample is shown in the Table 5. The aluminium sample was initially thought to be Al 6201, but the XRF analysis showed it is similar in composition to Al 5050 (Figure 14).

Table 5: Summary of aluminium sample XRF analysis.

Element (wt %)	Al	Mg	S	Ca	Mn	Fe	Si
Al XRF	98.58	1.2	0.083	0.007	0.031	0.099	-
Al 6201	98.6	0.8	-	-	-	-	0.7
Al 5050	98.6	1.4	-	-	-	-	-

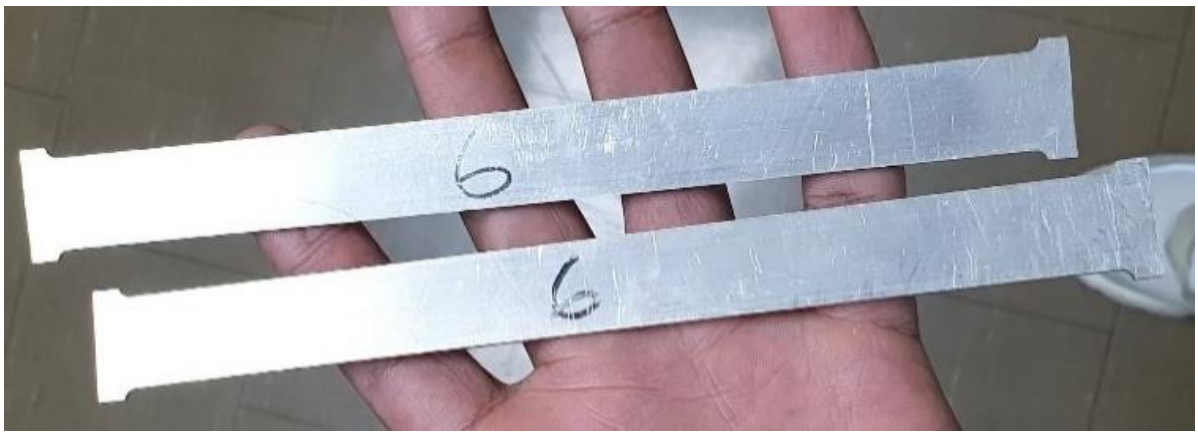


Figure 14: Image of aluminium sample Al 5050 provided.

4.2 Aluminium Sample Preparation

Smaller sample sizes were cut from the bulk sample using a laser cutting machine. For the immersion tests, the Al sample was cut to dimensions of 1cm × 0.9cm × 1.9 mm with a 1mm hole through the centre to allow for suspension in the solutions.

For the potentiodynamic tests, the samples were cut to dimensions of 1cm× 1cm × 1.9 mm to produce an exposed surface area of $1cm^2$. The surface of the cut samples was ground using silicon carbide papers of 80, 320, 600 and 800 grits. This was followed by diamond polishing after which the surfaces were rinsed with deionised water and

then degreased with acetone to remove any impurities. This procedure was done to ensure a smooth, clean, and mirror-like surface. The polished samples were examined under an optical and scanning electron microscope (SEM), to characterise the surface and to check for porosity prior to any type of corrosion testing.

4.3 Aluminium Samples for Weight Loss Tests

The cut samples were drilled with a hole in the middle (1mm diameter). This was done to allow the sample to be suspended, freely floating, and fully submerged within the corrosive solutions. There were six solutions in total. Two solutions were HCl and NaCl without inhibitor, two other solutions were HCl and NaCl with $La(acac)_3$ inhibitor, and the final two solutions were HCl and NaCl with $Ce(acac)_3$.



Figure 15: Prepared aluminium samples for weight loss test.

The mass of the submerged strips was measured and recorded before immersion and after immersion at different time intervals (1 day, 1 week, 2 weeks, 3 weeks, 4 weeks, 5 weeks, and 6 weeks). The weight loss was calculated from the difference between the mass recorded during these time intervals and before immersion.

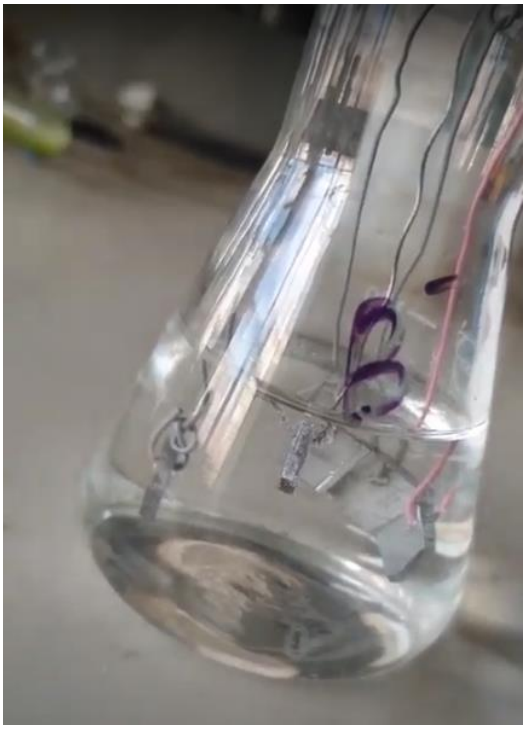


Figure 16: Submerged aluminium coupons during weight loss test.

4.4 Aluminium in NaCl Experiments

4.4.1 NaCl Solutions Weight Loss Tests

Five sets of six different immersion tests were conducted for aluminium. These solutions were NaCl without inhibitor, NaCl with lanthanum acetylacetone, NaCl with cerium acetylacetone These immersion tests were conducted for a period of six weeks and the weight of the samples were measured weekly (see Table 13 in appendix A). Figure 17 represents the normalized cumulative weight loss of the Al coupons immersed in the various solutions. It is observed that the weight loss in solutions without inhibitor is about five times higher than that of solution containing $La(aca)_3$ and $Ce(acac)_3$, and this ratio is fairly maintained for the duration of the experiment. This is a first confirmation that indeed the inhibitors work as expected by reducing the rate of weight loss.

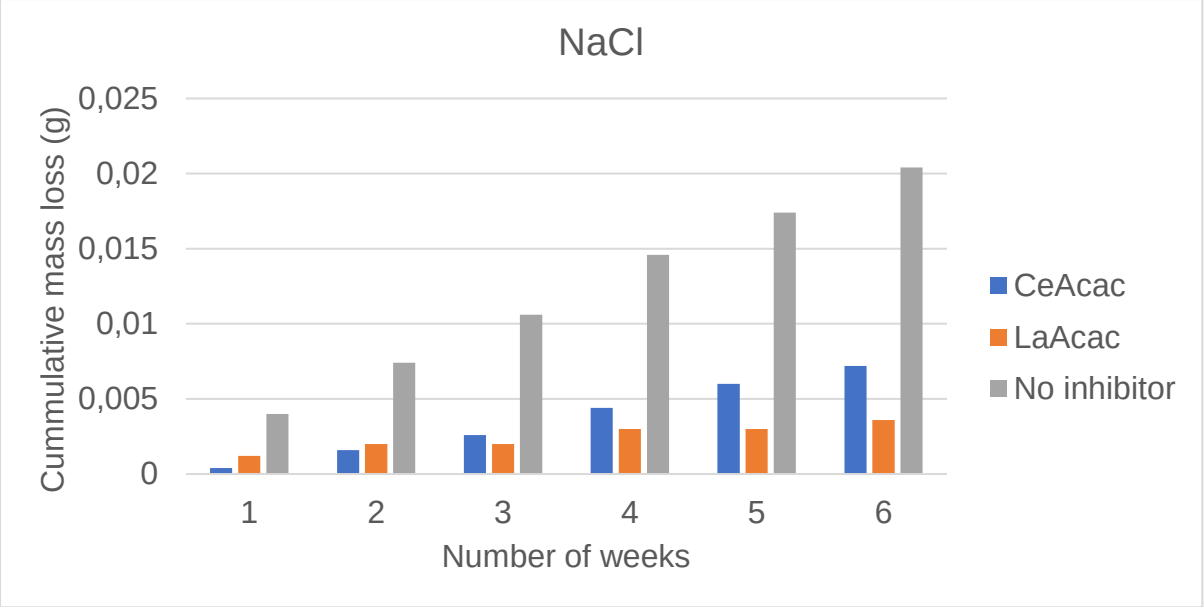


Figure 17: Normalized cumulative mass loss of Al coupons in various 0.6 M NaCl solutions over a period of six weeks at .

4.4.2 Corrosion Rate of NaCl Solutions Weight Loss Tests

The curves in Figure 18, were modelled with a linear fit to describe the corrosion rate data, with corresponding R^2 correlation values. In NaCl solution, the corrosion rate without inhibitor was about three times the corrosion rate of the samples in the presence of inhibitors. Lanthanum acetylacetone showed a general decrease in corrosion rate over time. Cerium acetylacetone showed an opposite trend and displays a slight increase in corrosion rate over time (see figure 18). Over the period of 6 weeks the $La(acac)_3$ inhibitor was more effective than the $Ce(acac)_3$ to lower the corrosion rate of the aluminium base alloy. The organic component of the inhibitor can adsorb onto the surface of the metal to provide a blanketing or blocking effect (Aejitha, et al., 2018). The resistance to mass transfer is a factor of the passivation layer, inhibitor adsorption and some of corroded material which reduces the influx of the chloride species (French, et al., 1993). The mass loss tests imply that the surface coverage of these different components is effective in decreasing the corrosion rate over time when $La(acac)_3$ is the inhibitor of choice, while no such effective and lasting inhibition over time is observed in the case when $Ce(acac)_3$ is used as corrosion inhibitor.

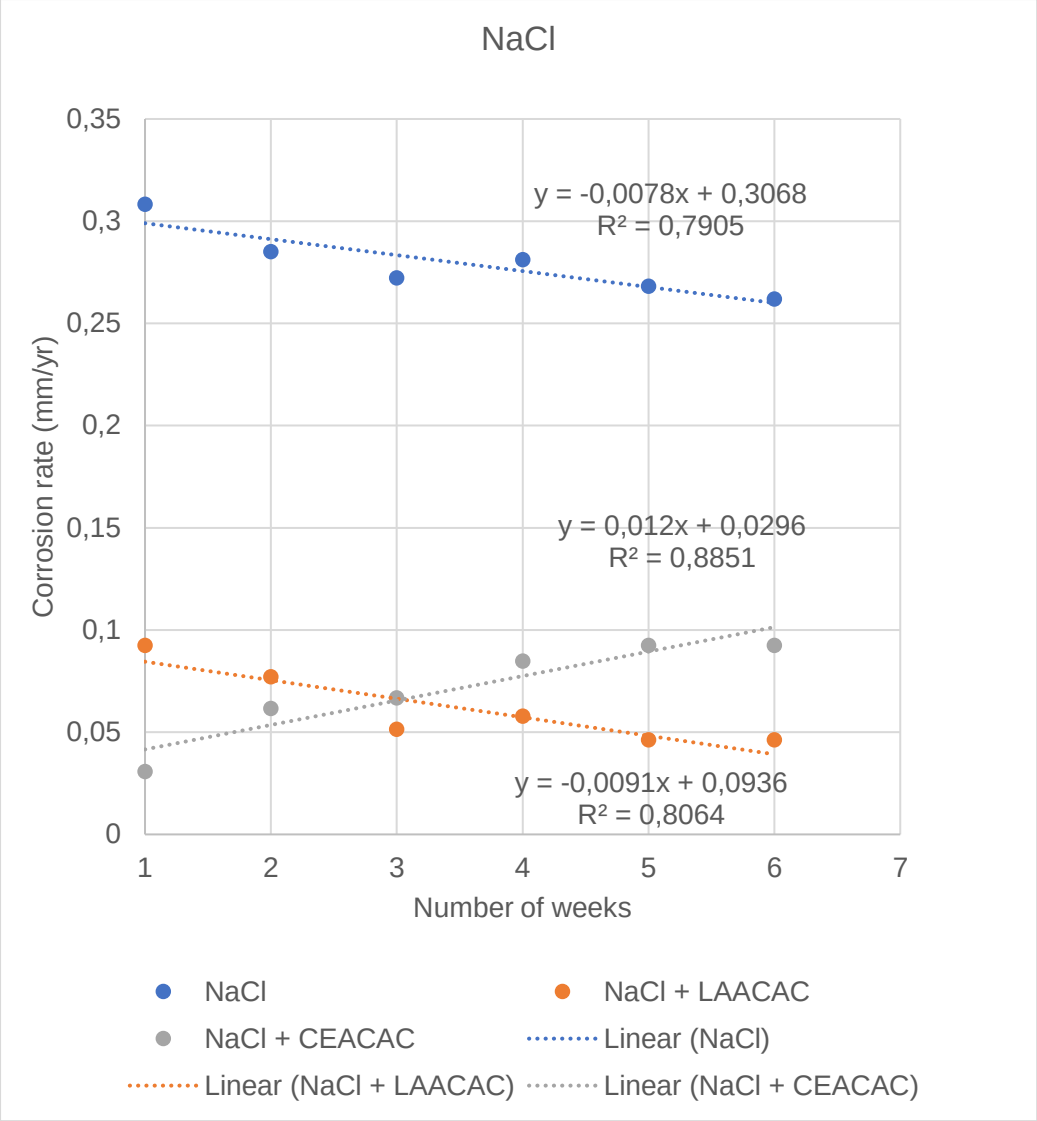


Figure 18: Corrosion rate for Al coupons in 0.6M NaCl for six weeks.

The mass loss coupons were observed under an optical and scanning electron microscope to investigate the corroded surfaces. The image shown in Figure 19 depicts the effect of NaCl solution on aluminium with no inhibitor present in the solution. An uneven layer and incomplete surface layer can be seen. Therefore, despite the good passivation ability of aluminium, attack by the aggressive chloride ions still occurs. This corresponds to previous results reported by (Reboul, 2005).

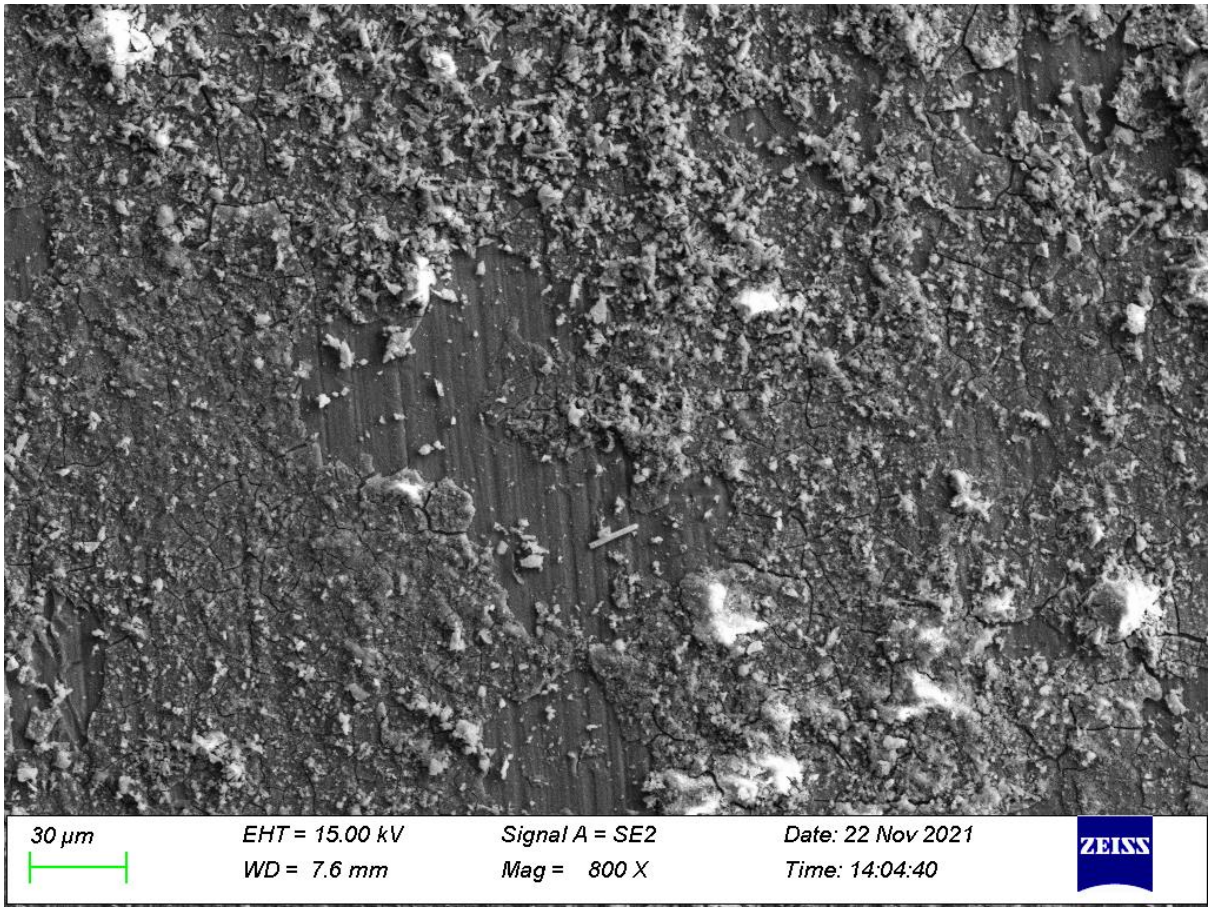


Figure 19: SEM image of Al in 0.6M NaCl without inhibitor, after a six-week weight loss test (800 X).

The SEM analysis of the coupon in the saline solution with $La(acac)_3$, which is displayed in figure 20, and again showed a damaged surface along with what appears to be $La(acac)_3$ and/or NaCl crystals.

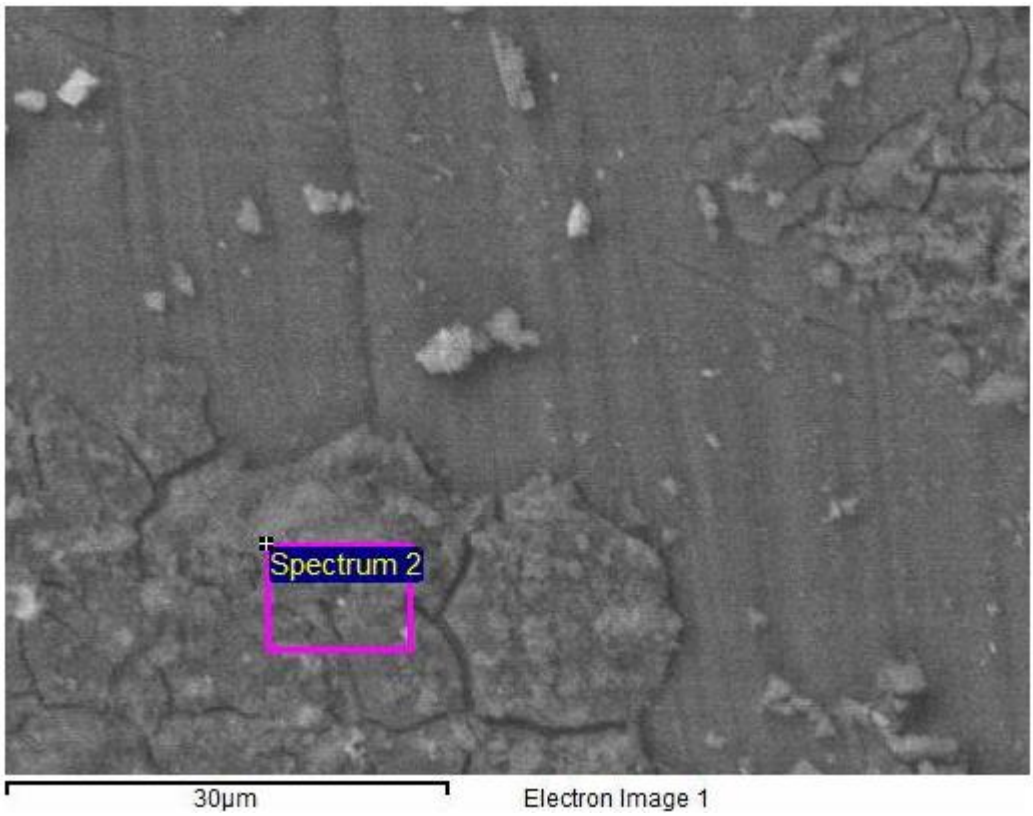


Figure 20: SEM image of Al in 0.6M NaCl with La(acac)$_3$ after a six-week weight loss test (1200 X).

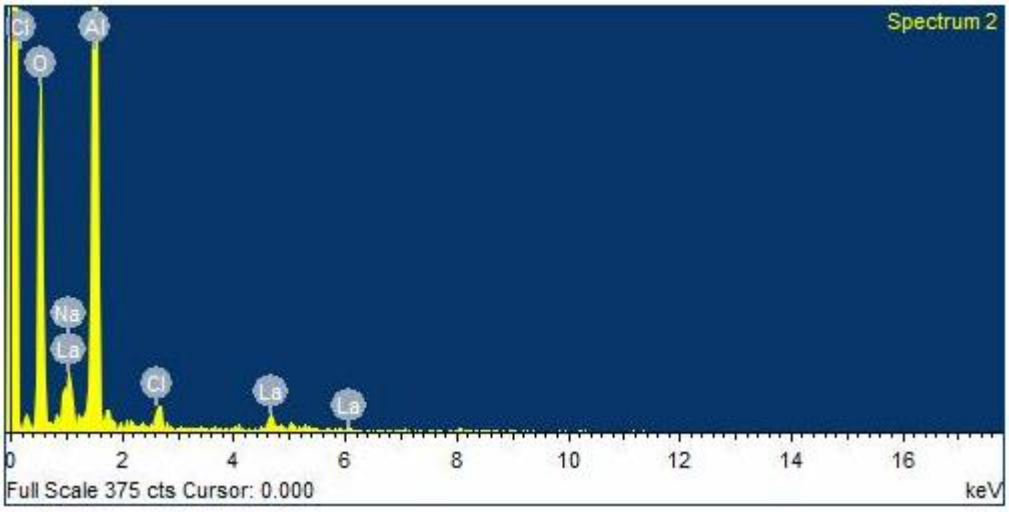


Figure 21: EDS of Al surface after a six-week weight loss test in 0.6M NaCl with La(acac)$_3$.

The SEM analysis of the coupon in NaCl with the Ce(acac)$_3$ inhibitor showed what appeared to be Ce(acac)$_3$ crystals on the surface (Figures 22 and 23).

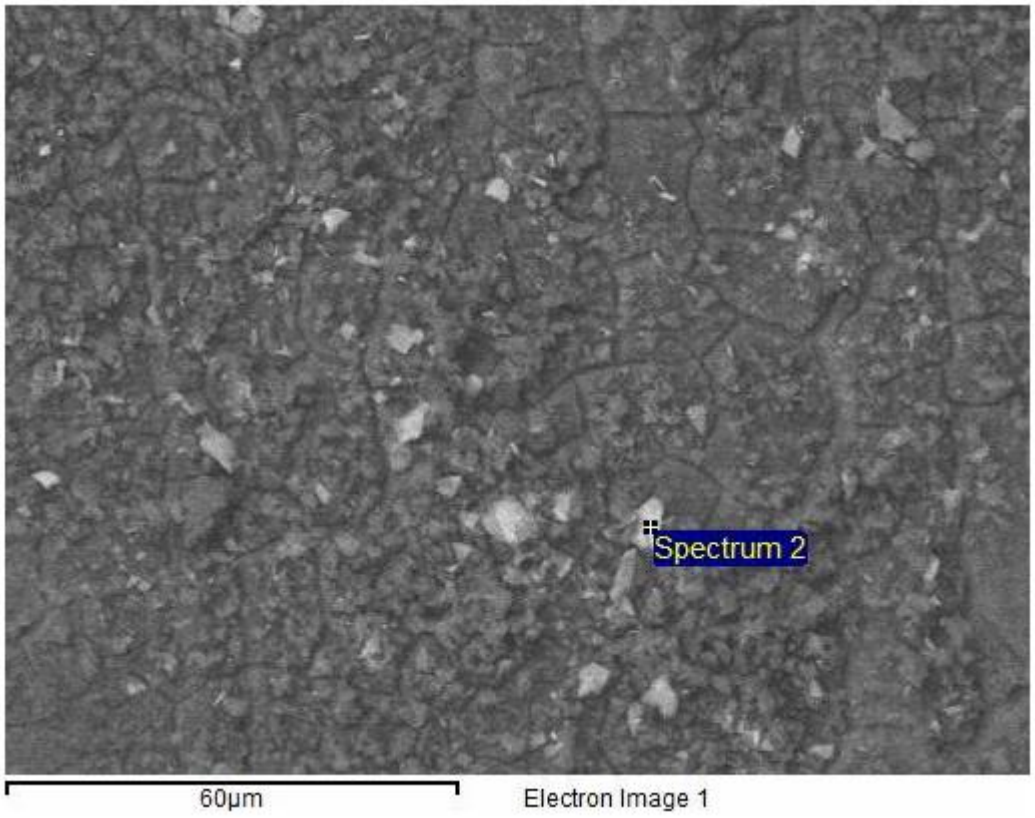


Figure 22: SEM image of Al in 0.6M NaCl with Ce(acac)$_3$ after a six-week weight loss test (800 X).

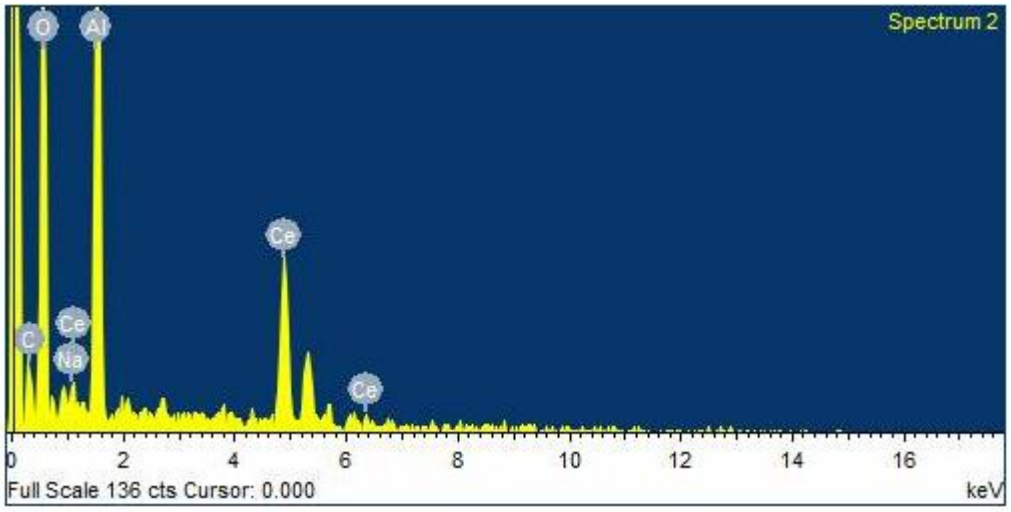


Figure 23: XDS analysis of Al in 0.6M NaCl with Ce(acac)3 after a six-week weight loss test.

4.4.3 Inhibition Efficiency of $La(acac)_3$ and $Ce(acac)_3$ in NaCl solutions

The inhibition efficiency was calculated from the corrosion rate of solutions with inhibitors relative to the solution without inhibitors. In NaCl, the efficiency of $Ce(acac)_3$ started off high at 90% but dropped consistently over time to a value of 65% after six weeks. The converse was true for $La(acac)_3$, where the inhibitor efficiency increased over time from a value of 70% to about 80% over the six-week immersion period (Figure 24). An increase in inhibition efficiency over time indicates the stability of the inhibitor specie in the corrosive media and the reverse is true for a decrease in inhibitor efficiency. This result shows that $La(acac)_3$ is more effective in preventing corrosion of long-term exposure to NaCl relative to $Ce(acac)_3$.

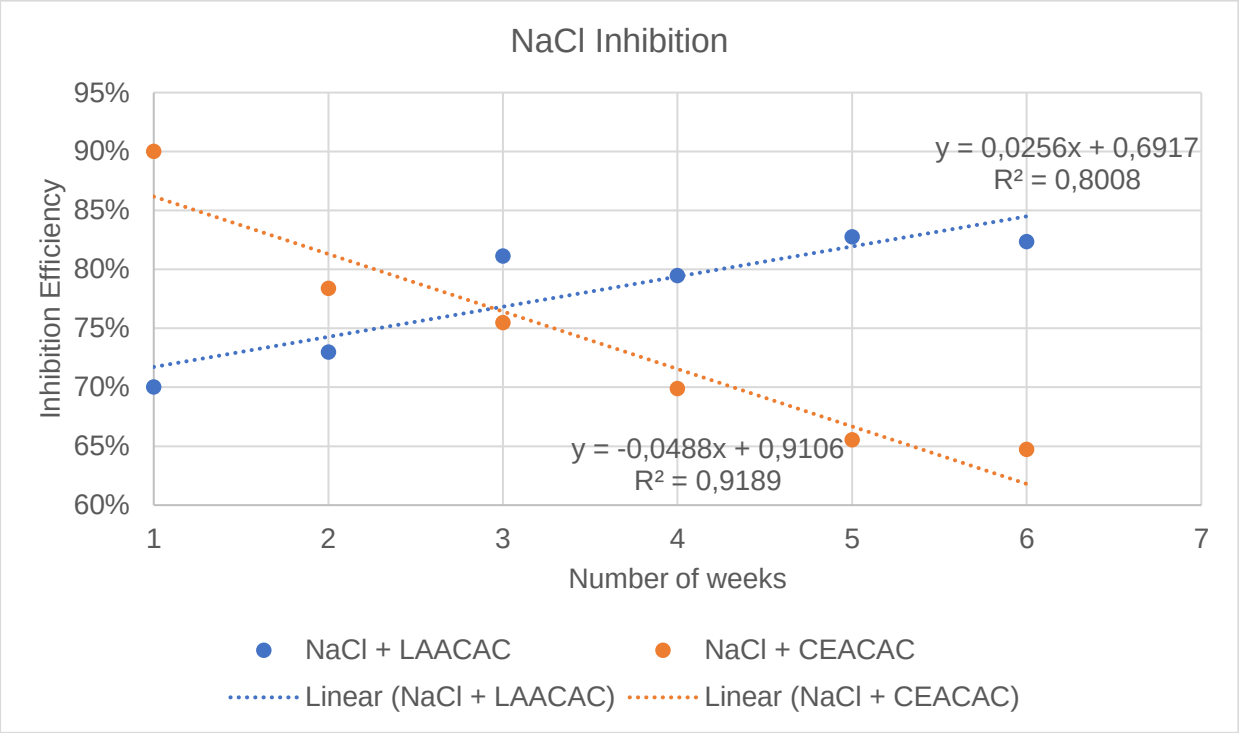


Figure 24: Inhibition efficiency of $La(acac)_3$ and $Ce(acac)_3$ in 0.6M NaCl in weight loss test.

4.4.4 NaCl Solutions Potentiodynamic Tests

The potentiodynamic tests on aluminium were conducted with three solutions: NaCl without inhibitor, NaCl with $La(acac)_3$ and NaCl with $Ce(acac)_3$. The potentiodynamic curves of the Al samples in the various NaCl solutions are shown in Figure 25.

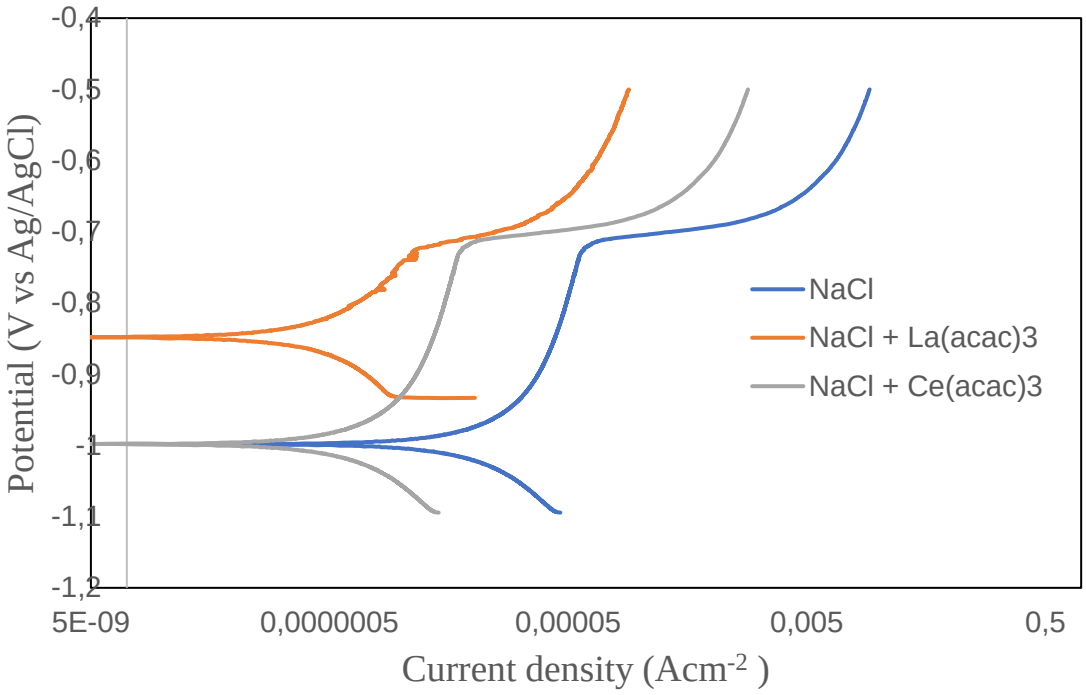


Figure 25: Potentiodynamic curves of Al in 0.6M NaCl at 25^{0}C.

The low current density values of order 10^{-6}, observed in the potentiodynamic curve for aluminium indicate relatively low corrosion rates and highlights the alloy as well as inhibitors' corrosion resistance effect under these conditions. The curves with the inhibitors $La(acac)_3$ and $Ce(acac)_3$ showed a decrease in corrosion current density and consequently a decrease in corrosion rate, as can be expected (Forsyth & Hinton, 2014).

The corrosion potential of NaCl and NaCl with $Ce(acac)_3$ are at approximately 1000 mV. In the case of NaCl with $La(acac)_3$, a 120mV shift in corrosion potential occurred in the positive (anodic) direction. An inhibitor can be classified as an anodic or cathodic inhibitor when the change in E_{corr} is greater than 85mV (Khaled & Amin, 2009). This positive shift, together with the reduction in i_{corr}, suggests that $La(acac)_3$ acts as an anodic inhibitor in the NaCl system. (Sastri, 2011). In the case of the $Ce(acac)_3$ curve (Figure 25), there is a decrease in corrosion current density relative to the NaCl solution without inhibitor. However, since there is little or no shift in the corrosion potential, one can deduce that $Ce(acac)_3$ acts as a mixed inhibitor in this system.

The i_{corr} parameters were used to calculate the corrosion rates and inhibition efficiencies for the various solutions (table 6). The corrosion rate in the presence of the two corrosion inhibitors are at least an order of magnitude smaller than in their absence, which quantifies and confirms the trend observed in the mass loss tests. Despite the different trends observed in the mass loss tests between the $La(acac)_3$ and $Ce(acac)_3$ inhibitors over time, the electrochemical evaluation shows that their final efficiencies are similar. In both the mass loss tests as well as electrochemical measurement, the $La(acac)_3$ was the most effective of the two inhibitors under the tested conditions. In other work in the literature where Ce compounds and La compounds were tested on Al 2024 under similar conditions, it was found that Ce-based were slightly more effective inhibitors than La-based inhibitors, and that inhibitor efficiencies as high as 99% % and 89% respectively could be achieved (Yasakau, et al., 2006). This difference could be due to the difference between the sample for this study Al 5050 and the sample Al 2024 used in (Yasakau, et al., 2006).

Table 6: Summary of potentiodynamic test for Al in 0.6M NaCl solutions at 25^0C.

	$-E_{corr}$ (mV)	i_{corr} ($\mu A/cm^2$)	Ba	Bc	CR (mm/yr)	IE (%)
NaCl	1000	7.68	76	42	5.12E-02	---
$La(acac)_3$	840	0.27	82	42	2.01E-03	96.1%
$Ce(acac)_3$	999	0.48	90	44	5.20E-03	89.8%

4.4.5 SEM Analysis of NaCl Potentiodynamic Samples

4.4.5.1 SEM of Aluminium Control Sample

An EDX analysis of the Aluminium reference sample shows mostly Al and some oxygen, thus confirming the presence of the Al_2O_3 passive layer. (Figure 26).

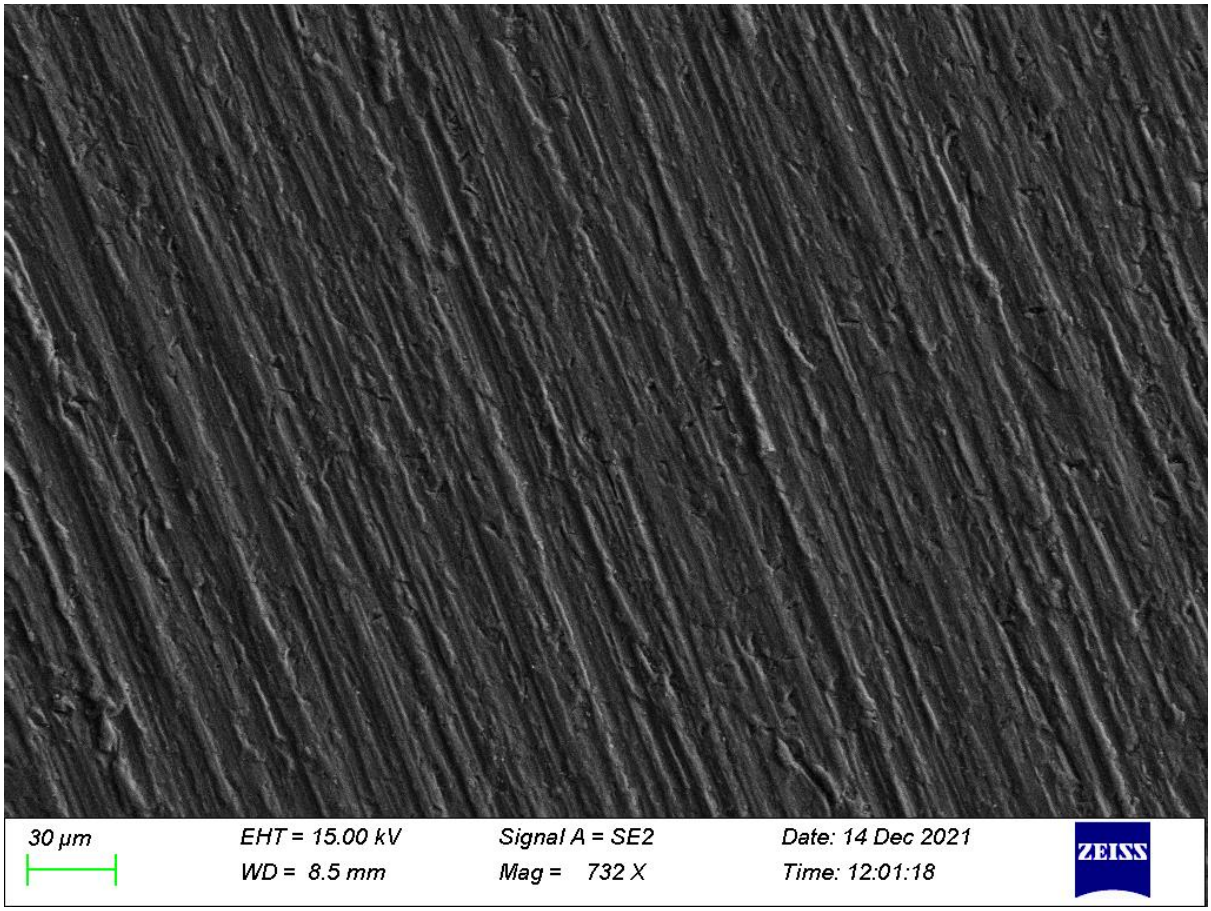


Figure 26: SEM image of Al reference sample without potentiodynamic immersion (732 X).

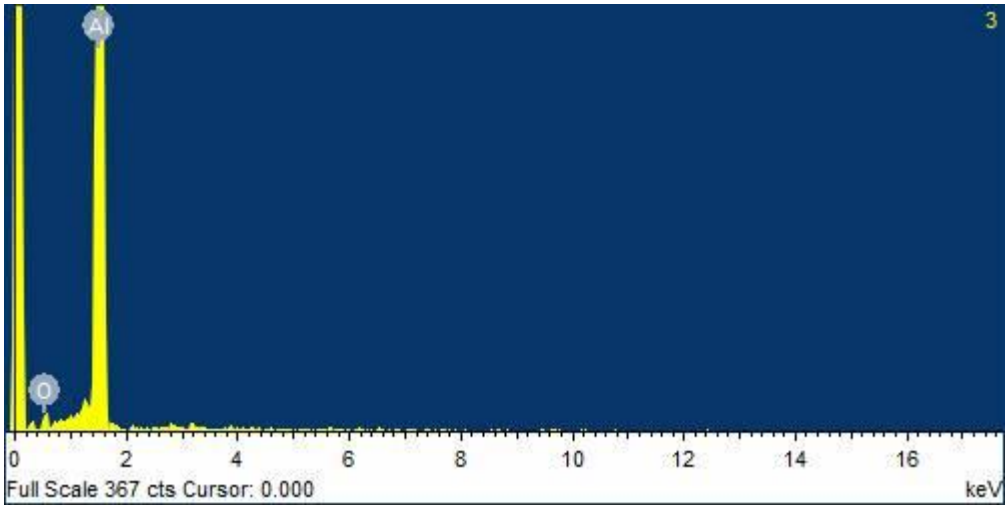


Figure 27: EDX surface analysis of Al reference sample without potentiodynamic immersion.

4.4.5.2 *SEM of Aluminium in NaCl Without Inhibitor*

The Al sample in NaCl without inhibitor showed pitting across the entire sample surface after exposure to the sodium chloride solution (Figure 28 & 29). The EDX analysis of these pits revealed the presence of Al, Na, O and Cl, which likely correspond to the presence of Al, Al_2O_3 and NaCl (figure 30).

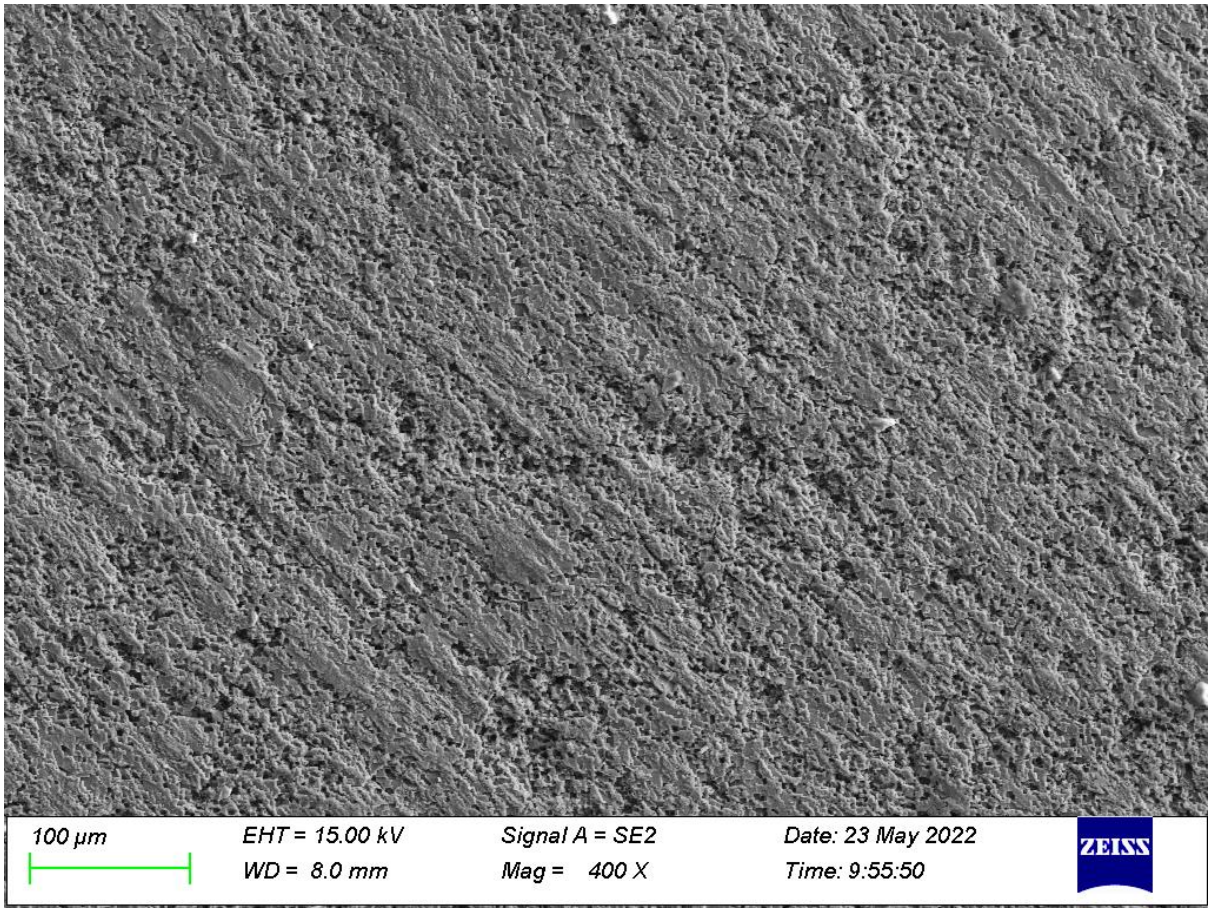


Figure 28: SEM of Al in 0.6M NaCl without inhibitor after potentiodynamic immersion at 25^0C (400 X).

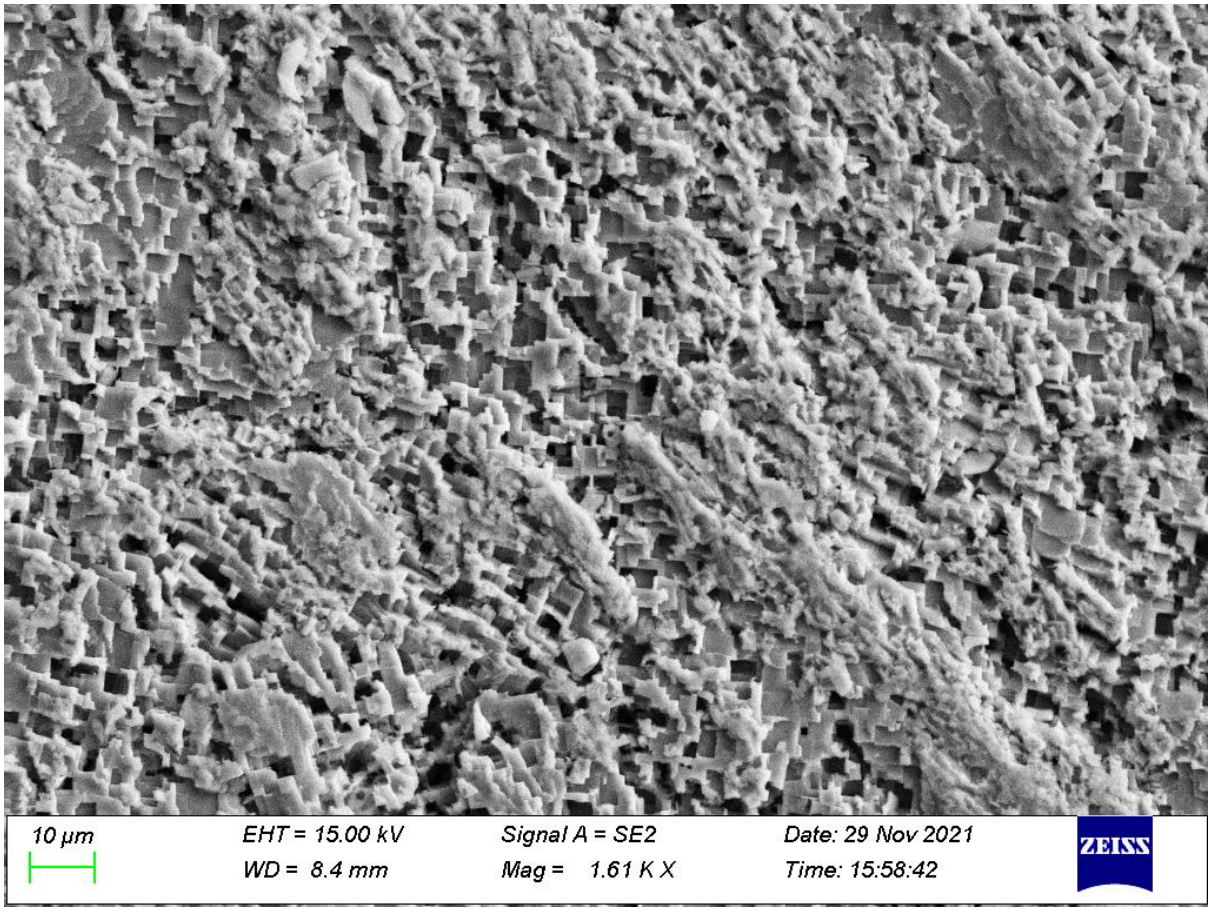


Figure 29: SEM of Al in 0.6M NaCl without inhibitor after potentiodynamic immersion at 25^0C (1610 X).

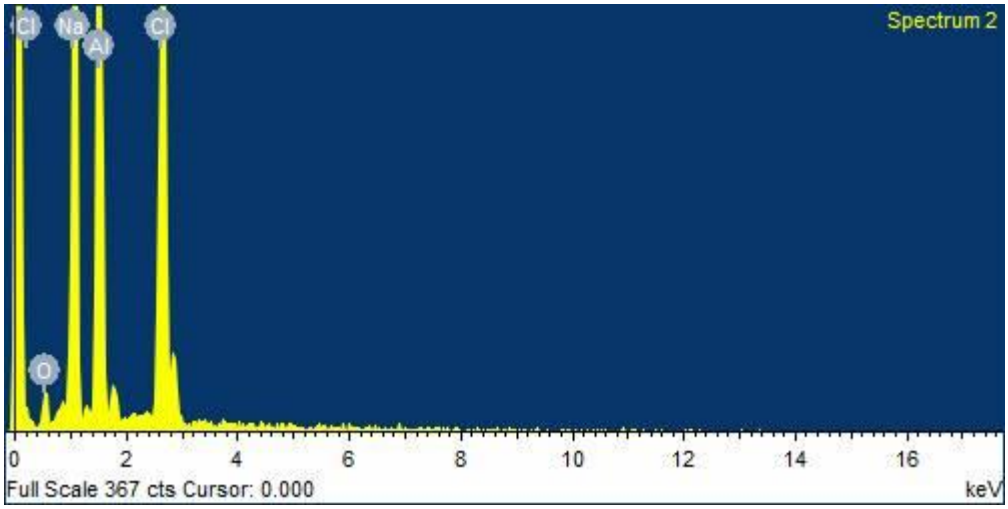


Figure 30: EDX analysis of Al surface after potentiodynamic immersion in 0.6M NaCl without inhibitor.

4.4.5.3 *SEM of Aluminium in NaCl with Inhibitors*

The aluminium coupons in the solutions containing inhibitors, showed relatively good resistance to surface degradation compared to the test without any inhibitor. The observed pitting spots were reduced to smaller, sporadic clusters of corrosion attack holes (Figure 31 and 32). This reduction of the surface attack shows the efficiency of the inhibitors to prevent corrosion and corresponds to the high level of inhibitor efficiency calculated for $La(acac)_3$ and $Ce(acac)_3$ inhibitors (96% and 90%, respectively) from the electrochemical measurements.

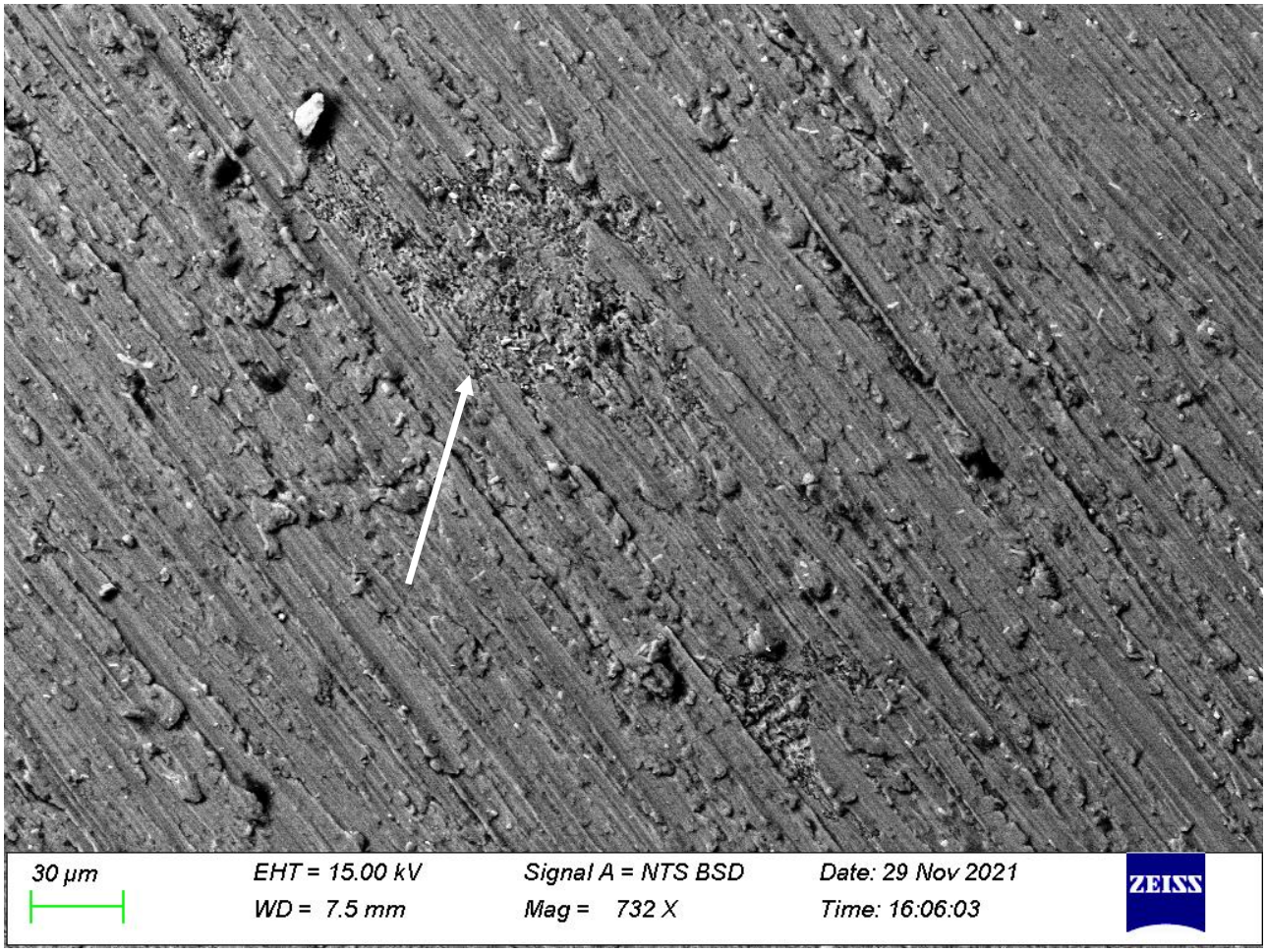


Figure 31: SEM of Al in 0.6M NaCl with $Ce(acac)_3$ after potentiodynamic immersion at 25^{0}C (732 X).

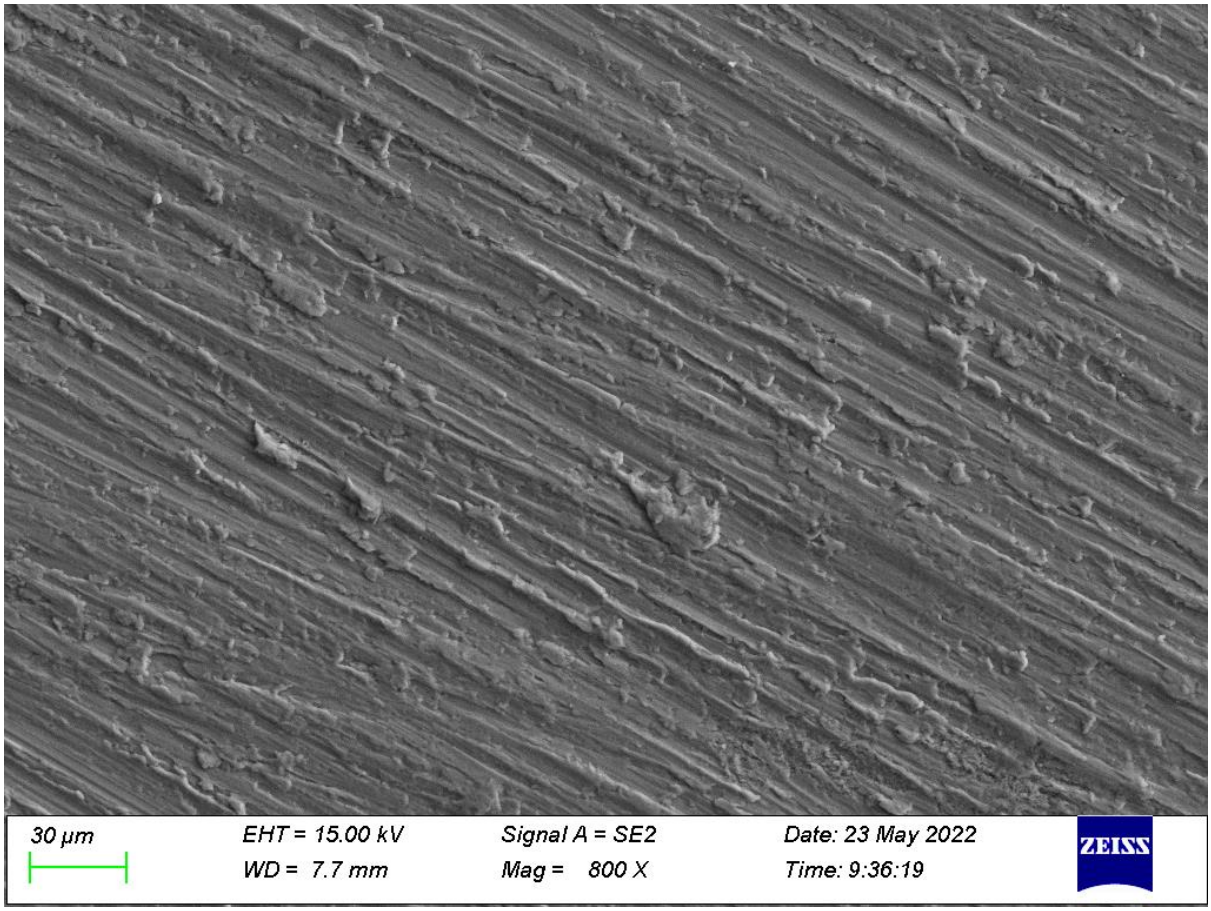


Figure 32: SEM of Al in 0.6M NaCl with $La(acac)_3$ after potentiodynamic immersion at 25^0C (800 X).

4.5 Aluminium in HCl Experiments

4.5.1 HCl Solutions Weight Loss Tests

Five sets of six different immersion tests were conducted for aluminium. These solutions were HCl without inhibitor, HCl with lanthanum acetylacetone, and HCl with cerium acetylacetone These immersion tests were conducted for a period of six weeks and the weight of the samples were measured weekly (see Table 14 in appendix A). Figures 33 represents the normalized cumulative weight loss of the Al coupons immersed in the various solutions. It is observed that the weight loss in solutions without inhibitor is about five times higher than that of solution containing $La(aca)_3$ and $Ce(acac)_3$, and this ratio is fairly maintained for the duration of the experiment. This is a first confirmation that indeed the inhibitors work as expected by reducing the rate of weight loss. It is also important to note that the weight loss results in HCl are an order of magnitude higher than observed in NaCl, which highlights the stronger corrosion attack of HCl.

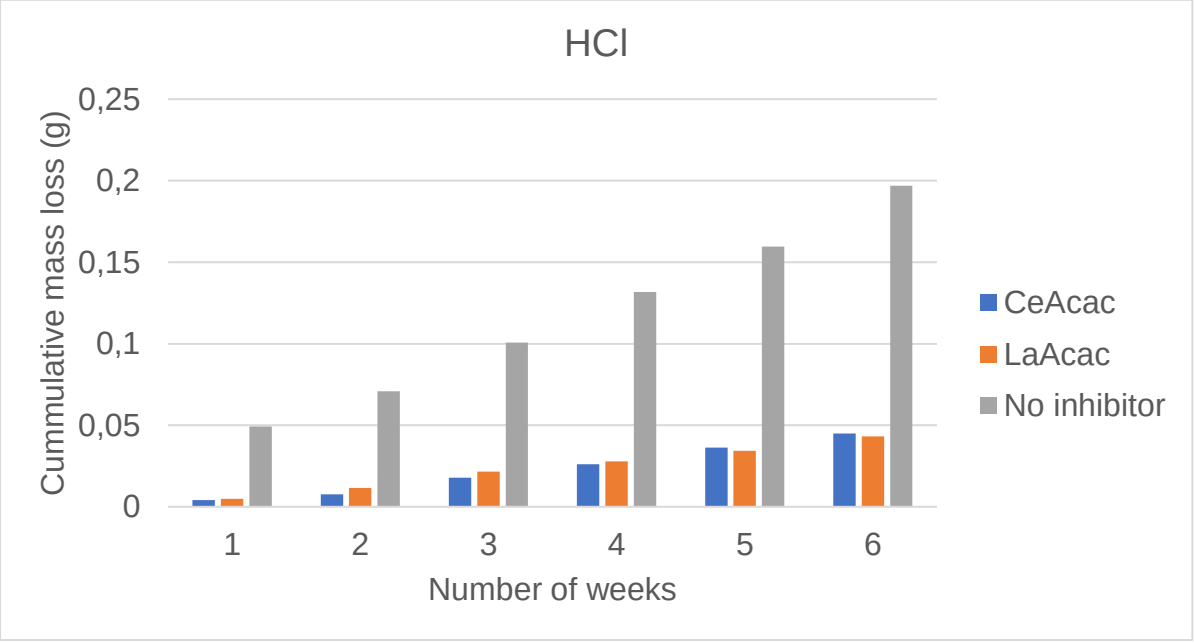


Figure 33: Normalized cumulative mass loss of Al coupons in various 0.1 M HCl solutions over a period of six weeks at 25^0C.

4.5.2 Corrosion Rate of HCl Solutions Weight Loss Tests

The curves were modelled with a linear and polynomial fit to describe the corrosion rate data, with corresponding R^2 correlation values. In HCl, the corrosion rate in the solution without inhibitor was more than five times that of solutions with inhibitors

present. This is in line with the principle of inhibition, as the effect of inhibitors can be appreciated in terms of significantly reducing the corrosion rate (Forsyth & Hinton, 2014). Despite the overall reduction in corrosion rate as explained, both $La(acac)_3$ and $Ce(acac)_3$ in this case showed an increase in corrosion rate of over time (figure 34). This can be attributed to the highly aggressive and acidic environment created by HCl, which continuously destroyed the passivation layer and inhibitor adsorption layer as it attacked the alloy thereby decreasing the inhibition ability of the inhibitors (Aejitha, et al., 2018).

In addition, over the period of 6 weeks, it was observed that the inhibitors had very similar results in terms of reduction in corrosion rate. The organic component of the inhibitor can adsorb onto the surface of the alloy to provide a blanketing or blocking effect, by preventing the diffusion, interaction and mass transfer of the metal and external species (Aejitha, et al., 2018). The resistance to mass transfer is a factor of the passivation layer, inhibitor adsorption and some of corroded material which reduces the influx of the chloride species (French, et al., 1993). The mass loss tests imply that the surface coverage of these different components is effective in decreasing the corrosion rate over time with both $La(acac)_3$ and $Ce(acac)_3$ proving to be suitable inhibitors in this system.

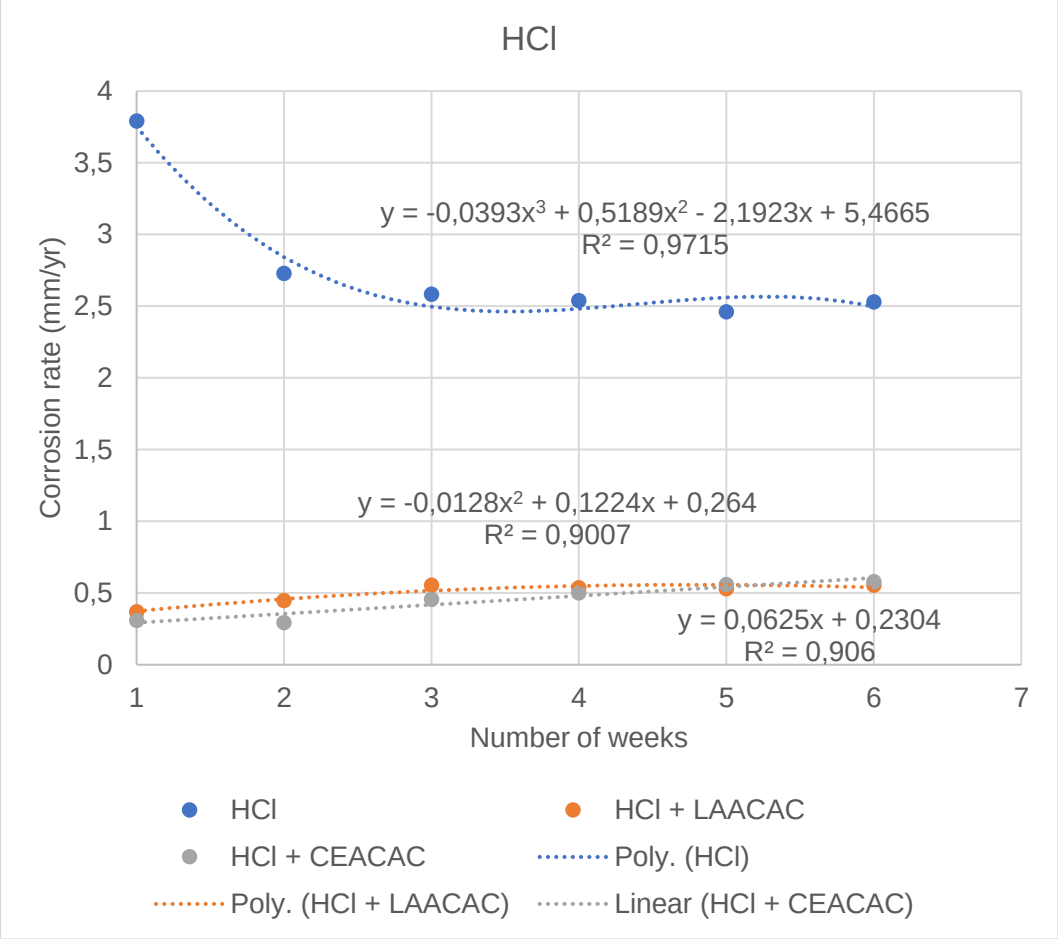


Figure 34: Corrosion rate for Al coupons in 0.1M NaCl for a six-week weight loss test.

HCl solutions were observed to have a high denaturing effect on the alloy's surface. The aluminium alloy after immersion into the various HCl solutions showed very intense signs of attack, pitting and crevices as seen in figures 35 and 36 without inhibitor. This highlights the high level of aggresion of chloride ions in acidic media (Mustafa, et al., 2022).

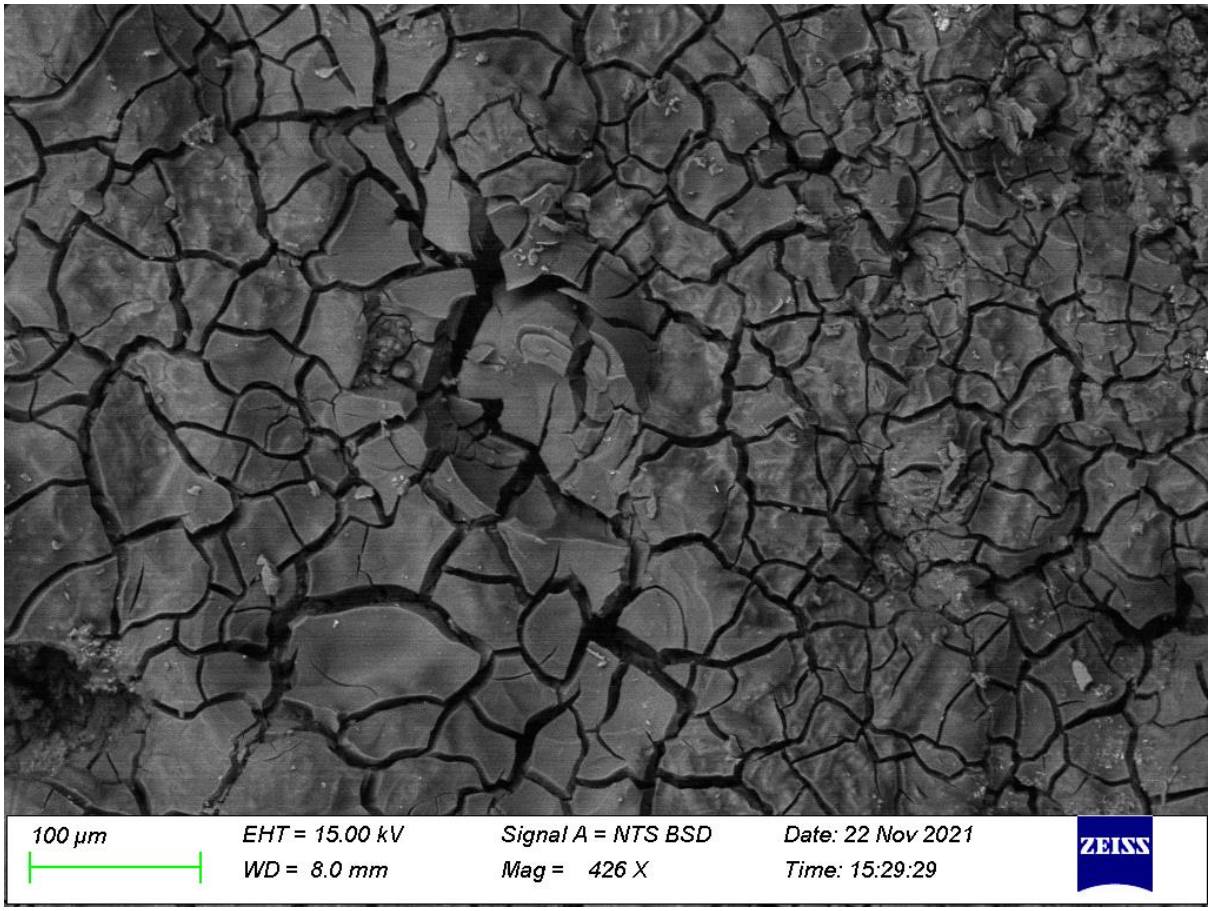


Figure 35: SEM image of Al in 0.1M HCL without inhibitor after a six-week weight loss test (426 X).

The images of the scanning and backscatter detectors showed the intensity of surface attacks by the HCl acid solution. The cracks were observed to cover the entire metal surface (Figures 35 and 36). This means that the HCl ruptured the passivation layer of the sample, initiated cracks, and continuously corroded the metal, by crevice corrosion, through the cracks as it seeped inside (Reboul, 2005).

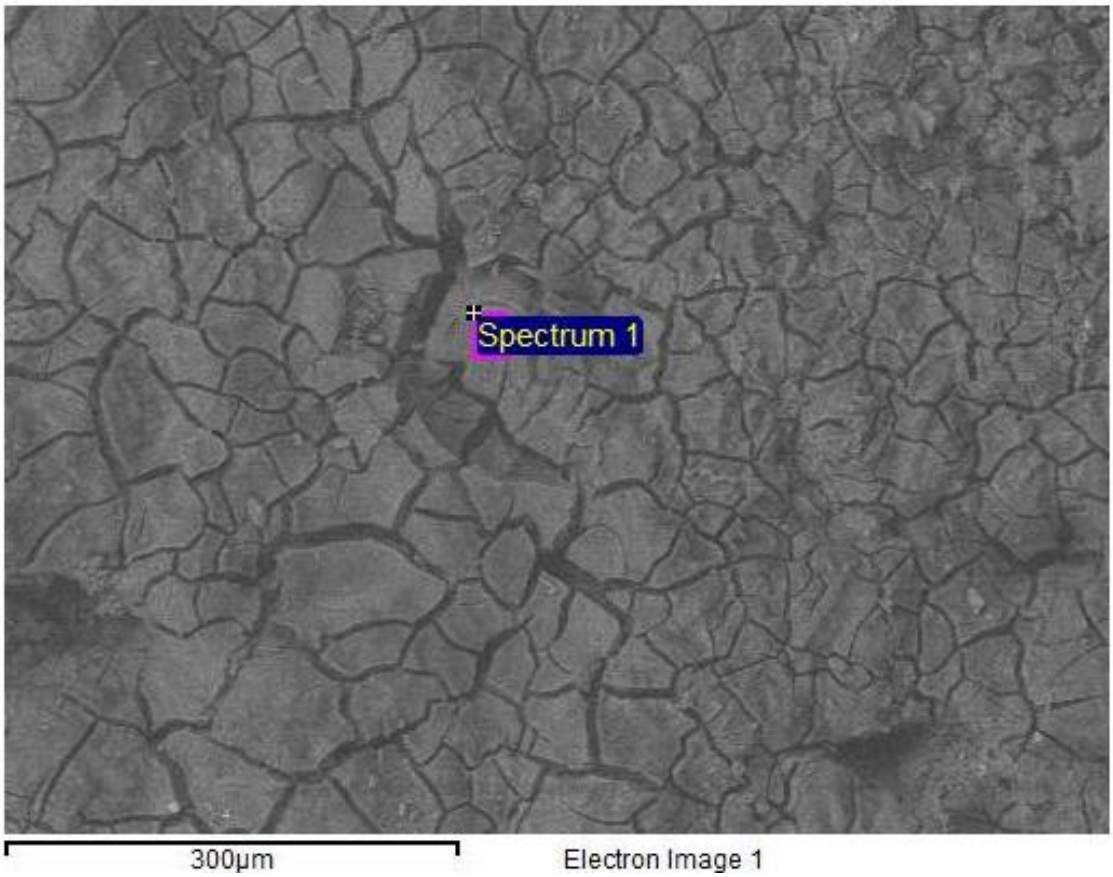


Figure 36: SEM of Al in 0.1M HCl without inhibitor after a six-week weight loss test (300 X).

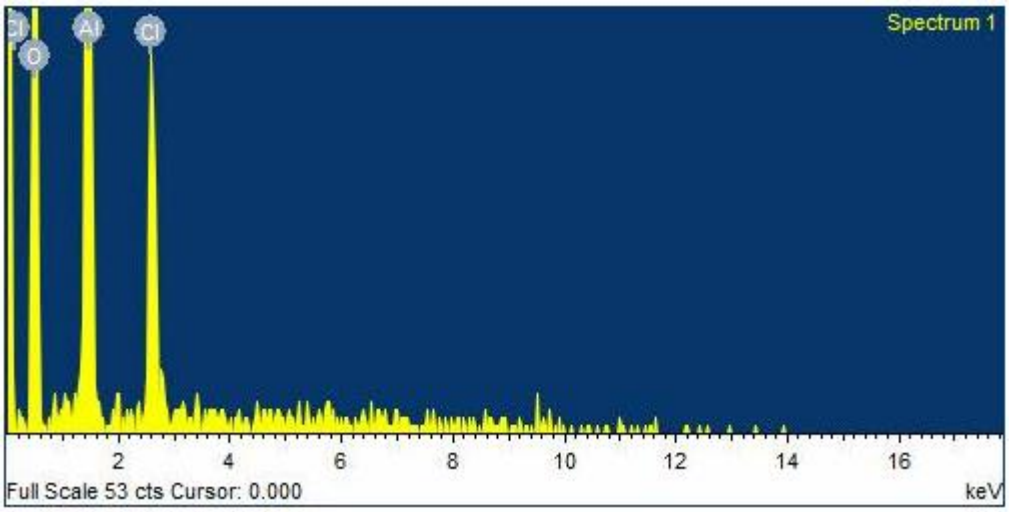


Figure 37: XDS of Al in 0.1M HCl without inhibitor after weight loss test.

The XDS analysis of the Al coupon in HCl (Figure 37) revealed the presence of Al, Al_2O_3 and Cl^-. This is consistent with literature as the acidic Cl^- ions attack the passivation oxide layer as, well as the metal surface (Reboul, 2005).

In the solutions containing La and Ce acetylacetone, the surface corrosion was not as severe as the case without inhibitor. Even though there was surface denaturing on the sample, the depth of the pit was shallower and pitting not as intense. (Figures 38 & 39). This means that the attack by HCl was very intense, as the large cracks and pits on the surface indicate the destruction of the passivation layer and crevice corrosion as the solution sipped into the cracks.

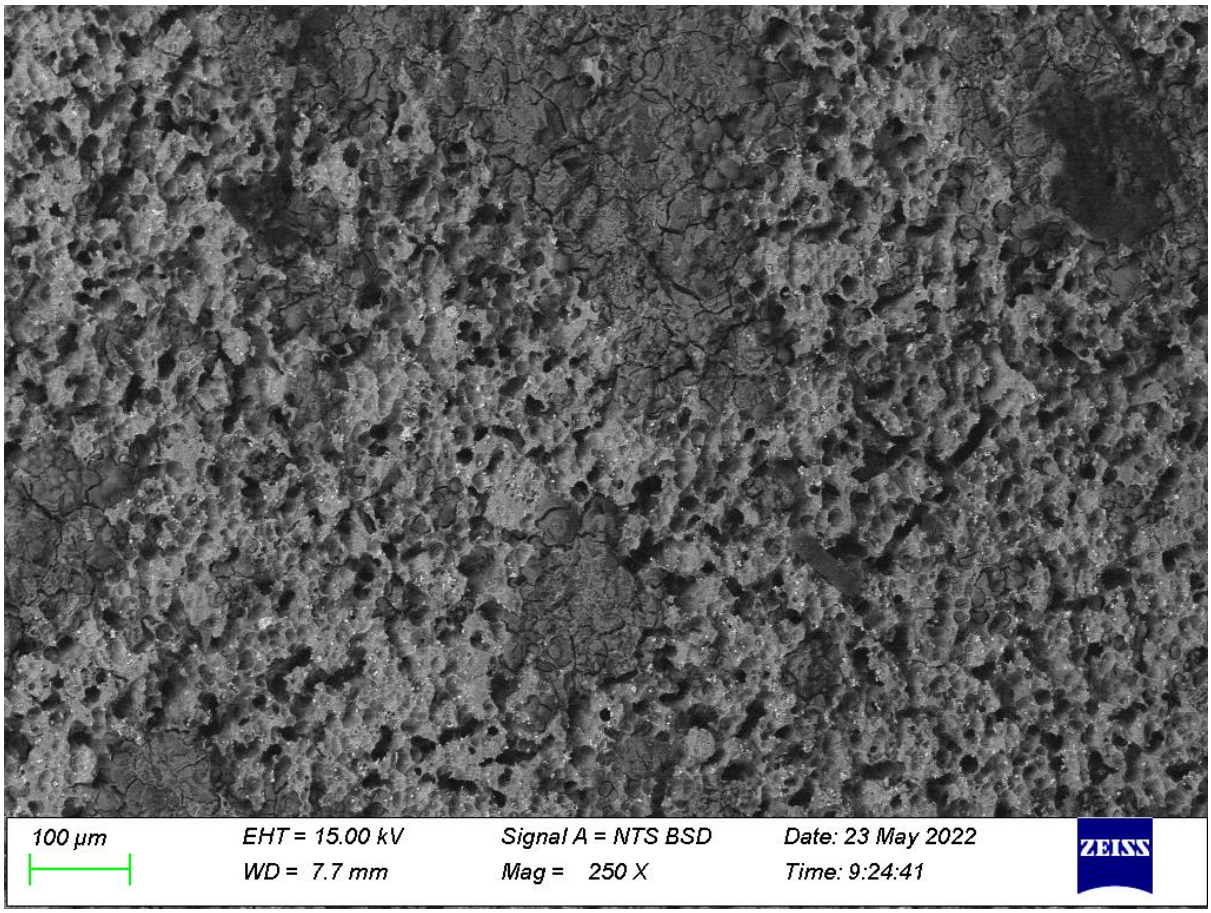


Figure 38: SEM of Al in 0.1M HCl with $Ce(acac)_3$ after a six-week weight loss test (250 X).

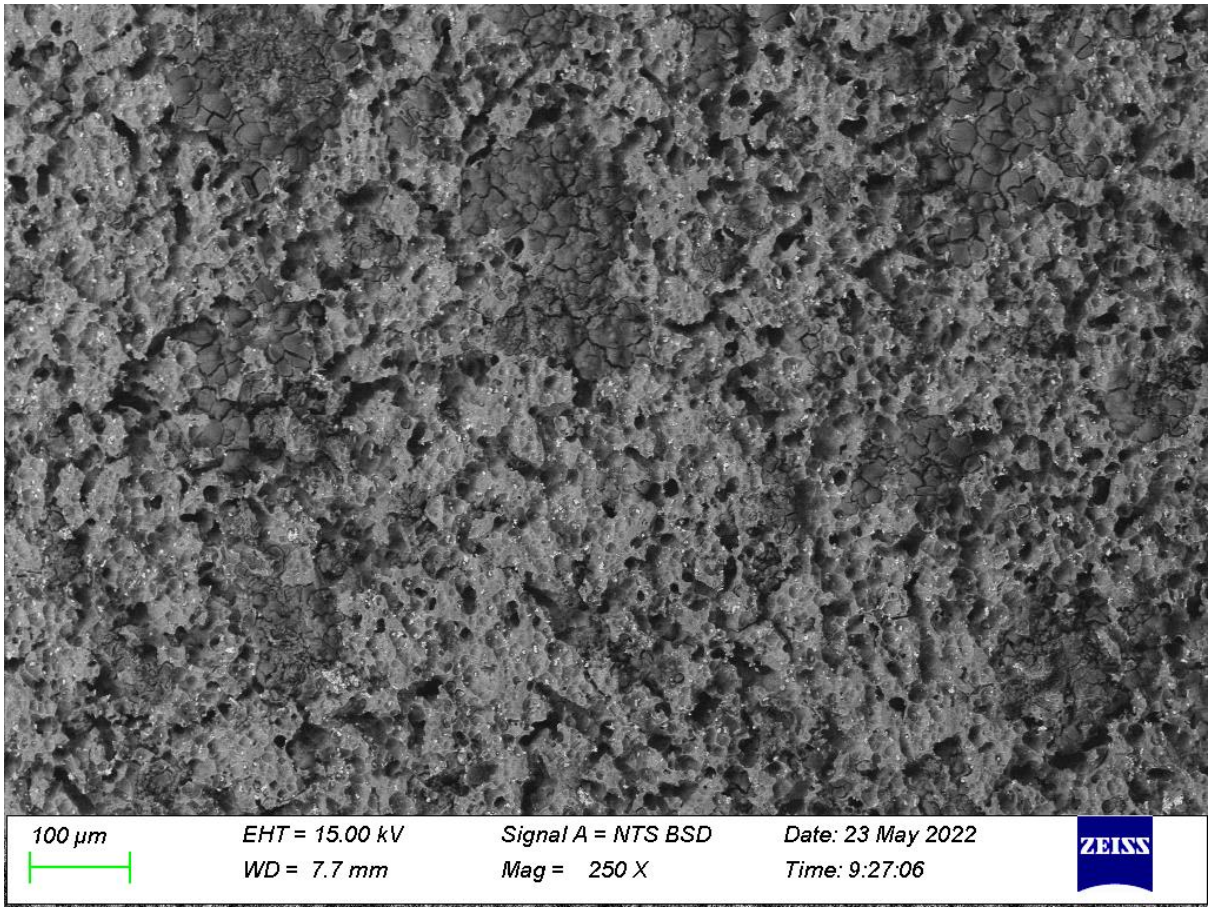


Figure 39: SEM of Al in 0.1M HCl with $La(acac)_3$ after a six-week weight loss test (250 X).

4.5.2 Inhibition Efficiency of $La(acac)_3$ and $Ce(acac)_3$ in HCl solutions

The inhibition efficiency was calculated from the corrosion rate of solutions with inhibitors relative to the solution without inhibitors. In HCl, the efficiency of $La(acac)_3$ and $Ce(acac)_3$ started off high at about 93% but dropped slowly over time to a value of 78% after six weeks (Figure 40).

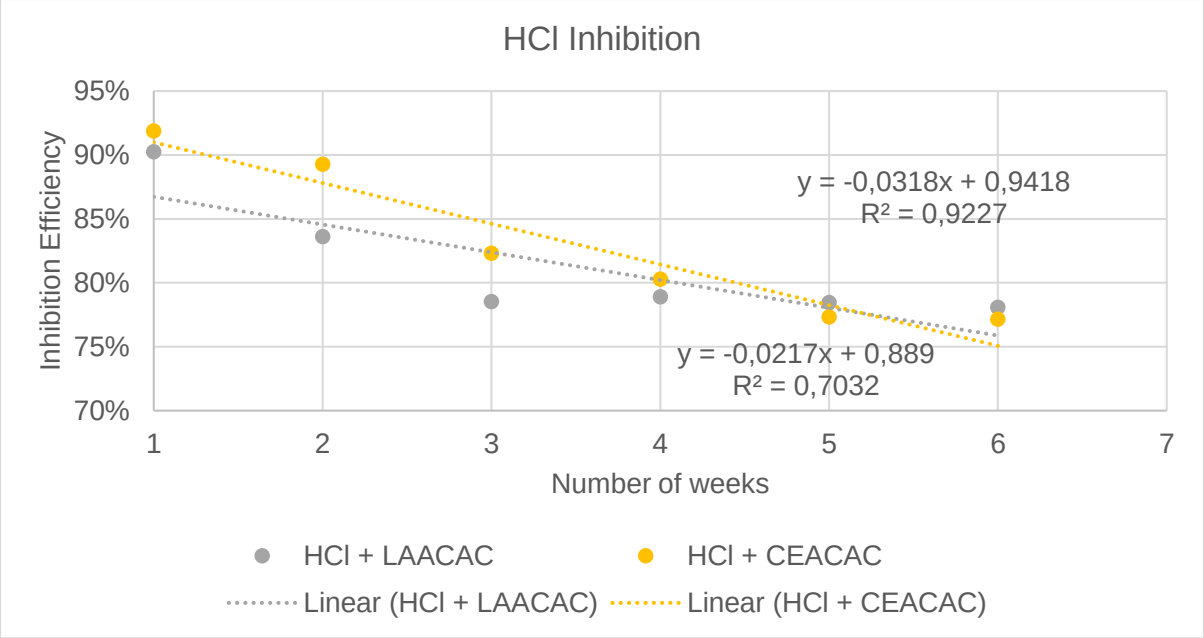


Figure 40: Inhibition efficiency of $La(acac)_3$ and $Ce(acac)_3$ in 0.1M HCl in weight loss test.

4.5.3 HCl Solutions Potentiodynamic Tests

The potentiodynamic tests on aluminium were conducted with three solutions: HCl without inhibitor, HCl with $La(acac)_3$ and HCl with $Ce(acac)_3$. The potentiodynamic curves of the Al samples in the various HCl solutions are shown in Figure 41.

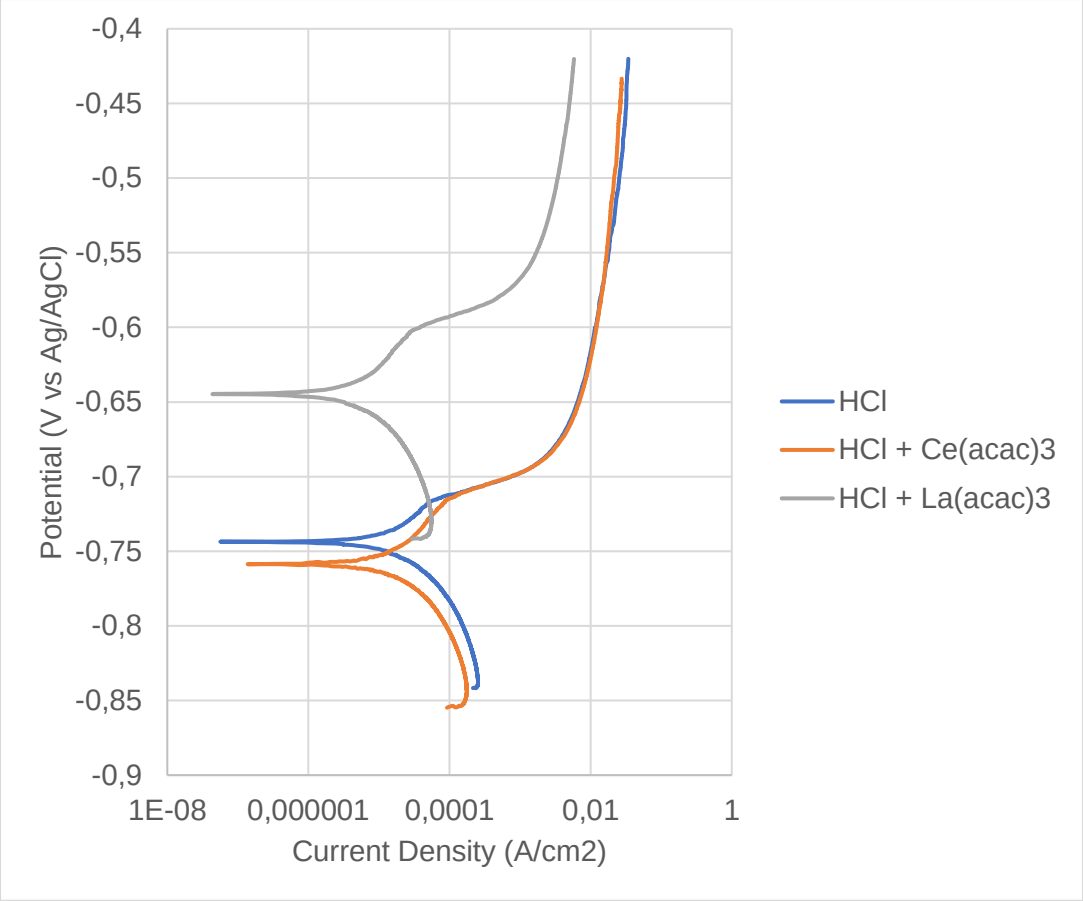


Figure 41: Potentiodynamic test for Aluminium in 0.1 HCl at 25^0C.

As observed in the case with NaCl, HCl solutions showed low current density values of order 10^{-6}, observed in the potentiodynamic curves for aluminium indicate relatively slow corrosion rates and highlights the metal as well as inhibitors' effect in resistance to corrosion, under these conditions as expected in (Forsyth & Hinton, 2014). The $La(acac)_3$ curve is observed to have a 103mV positive shift in E_{corr} and a decrease in I_{corr} relative to the HCl curve, indicates that $La(acac)_3$ acts as an anodic inhibitor in this system. The $Ce(acac)_3$ curve is observed to have a 15mV negative shift in E_{corr} and a decrease in I_{corr} relative to the HCl curve (Figure 41). Since the decrease in Ecorr is less than 85 mV, it can be said that Ce(acac)3 acts as a mixed inhibitor with predominantly cathodic inhibition properties (Khaled & Amin, 2009).

Table 7: Summary of Potentiodynamic tests of Al in 0.1M HCl solutions at 25^{0}C.

	-E_{corr} (mV)	I_{corr} (µA/cm2)	Ba	Bc	CR (mm/yr)	IE (%)
HCl	743	18.7	100	40	0.296	
$La(acac)_3$	640	3.97	120	51	0.0231	92.2%
$Ce(acac)_3$	758	9.63	110	45	0.0562	81.0%

The i_{corr} parameters were used to calculate the corrosion rates and inhibition efficiencies for the various solutions (table 7). The corrosion rate in the presence of the two corrosion inhibitors are at least an order of magnitude smaller than in their absence, which quantifies and confirms the trend observed in the mass loss tests. Despite the different trends observed in the mass loss tests between the $La(acac)_3$ and $Ce(acac)_3$ inhibitors over time, the electrochemical evaluation shows that they both work similarly in HCl systems. In both the mass loss tests as well as electrochemical measurement, the $La(acac)_3$ was the most effective of the two inhibitors under the tested conditions.

In addition, the results of the potentiodynamic tests show that the inhibitor efficiency of $La(acac)_3$ and $Ce(acac)_3$ are higher in 0.6M NaCl than 0.1 M HCl, contrary to what was experienced in a similar case in (Ghanbari, et al., 2009). The inhibitor efficiency was higher in NaCl relative to HCl due to the lesser aggressive nature of NaCl relative HCl which correlates to a stronger inhibition/adsorption effect of $La(acac)_3$ and $Ce(acac)_3$ (Yasakau, et al., 2008).

4.5.4 SEM Analysis of HCl Potentiodynamic Samples

4.5.4.1 SEM of Aluminium in HCl Without Inhibitor

Similarly, to NaCl, HCl without inhibitor showed small surface-wide pits which are due to the corrosion attack of HCl as seen in Figure 42. These holes are more widespread and deeper after immersion in HCl relative to NaCl due to the acidity and aggressive nature of the HCl. Contrary to what observed in the NaCl case, there were black deposits on the surface of the coupon (Figure 42). The EDS analysis of these black

deposits revealed the presence of Al, O and Cl, which should indicate the presence of Al_2O_3 and a chloride (Figure 43). The EDS does not show the presence of H, but it would be safe to assume that the Cl peak was due to the presence of HCl, and maybe $AlCl_3$.

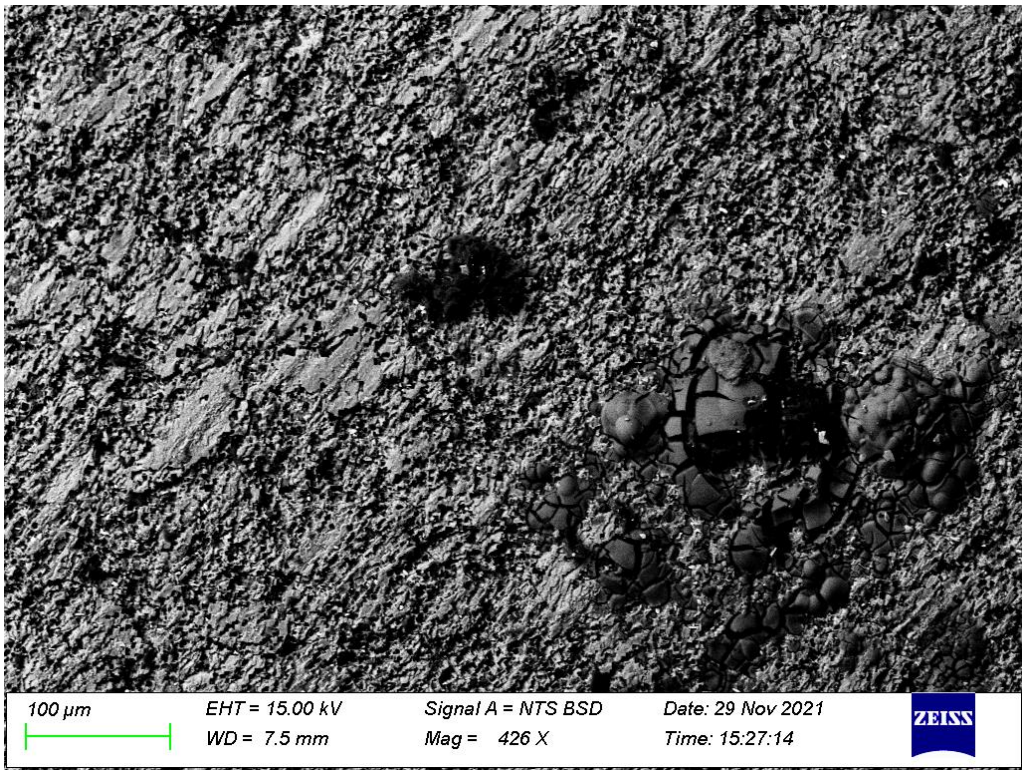


Figure 42: SEM image of Al in 0.1M HCl without inhibitor after potentiodynamic immersion (426 X).

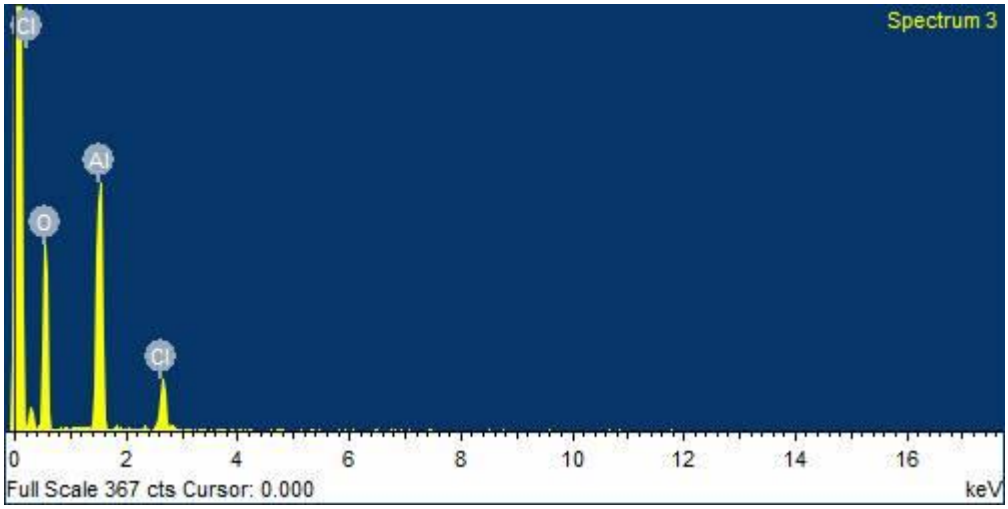


Figure 43: EDS analysis of Al in 0.1M HCl without inhibitor after potentiodynamic immersion.

4.5.4.2 SEM of Aluminium in HCl with Inhibitors

The aluminium coupons in the solutions containing inhibitors, showed relatively good resistance to surface degradation compared to the test without any inhibitor. The observed intensity of pitting spots were reduced (Figures 44 to 47). This reduction of the surface attack shows the efficiency of the inhibitors to prevent corrosion and corresponds to the high level of inhibitor efficiency calculated for $La(acac)_3$ and $Ce(acac)_3$ (92% and 81%, respectively) from the electrochemical measurements.

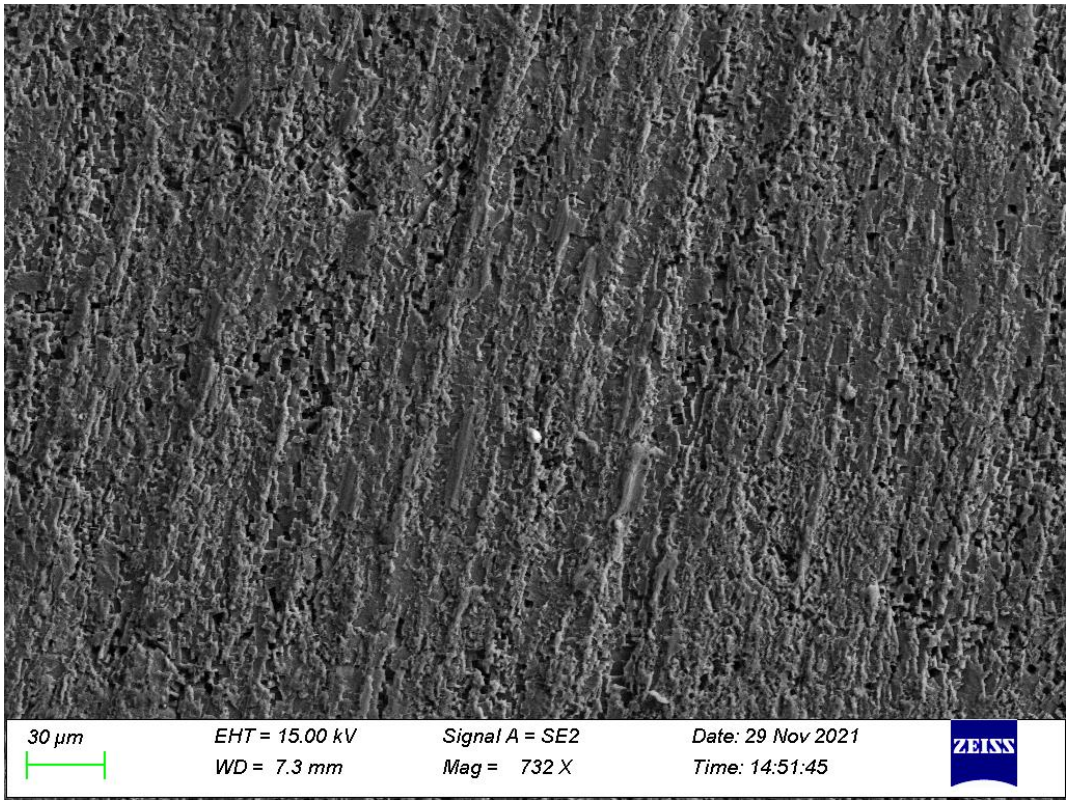


Figure 44: SEM image of Al in 0.1M HCl with $La(acac)_3$ after potentiodynamic immersion (732 X).

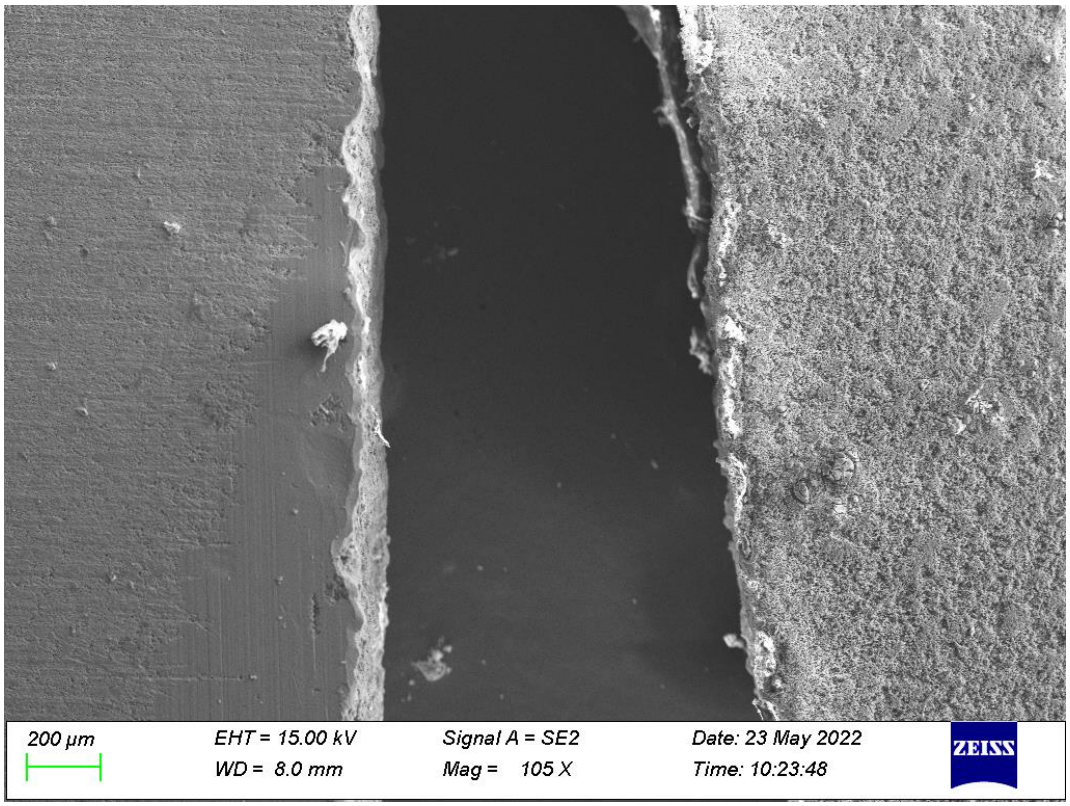


Figure 45: SEM image of Al in 0.1M HCl with $La(acac)_3$ (LEFT) and without inhibitor (RIGHT) after potentiodynamic immersion (105 X).

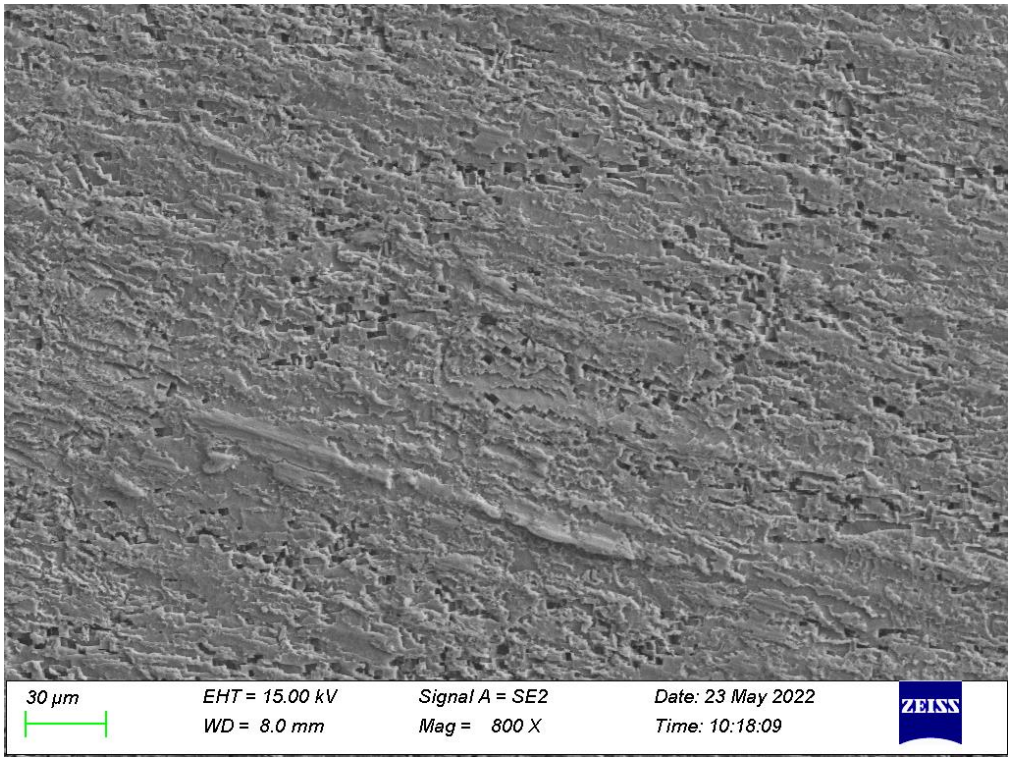


Figure 46: SEM image of Al in 0.1M HCl with $Ce(acac)_3$ after potentiodynamic immersion (800 X).

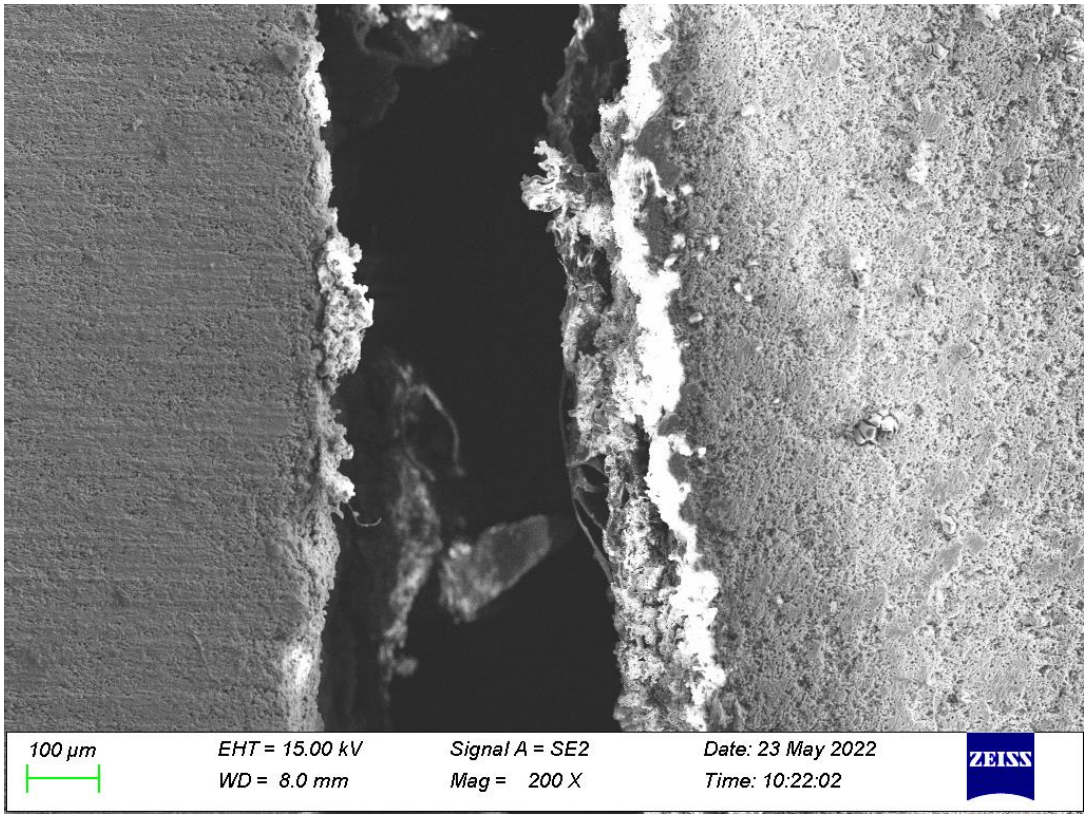


Figure 47: SEM image of Al in 0.1M HCl with $Ce(acac)_3$ (LEFT) and without inhibitor (RIGHT) after potentiodynamic immersion (200 X).

CHAPTER 5: TITANIUM EXPERIMENTS

5.1 Titanium Sample Material Analysis

An XRF spectrometer analysis of the Ti metal sample was conducted to assess its composition. The nominal composition of the sample is shown in the Table 8, the titanium sample provided was very similar in composition to Ti – 6Al – 4V and can therefore be assumed to be this grade of Ti.

Table 8:Summary of Titanium sample XRF analysis.

Element (wt %)	Ti	Al	V	Fe
Ti XRF	90.25	5.5	4.1	0.15
Ti – 6Al – 4V	90	6	4	-

5.2 Titanium Sample Preparation

Smaller sample sizes were cut from the bulk sample using a laser cutting machine. For the immersion tests, the Ti sample were cut to dimensions of 0.8cm × 0.4cm × 0.4mm. The titanium samples could not be cut thin or pierced with a metal cutter due to its hardness, hence a water pressure cutter was used to accurately cut the titanium.

The same cut sizes were used for the potentiodynamic tests which yielded an exposed surface area of 0.16 cm^2. The surface of the cut samples was ground using silicon carbide papers of 80, 320, 600 and 800 successive grits. This was followed by diamond polishing after which the surfaces were rinsed with deionised water and then degreased with acetone to remove any impurities. This procedure was done to ensure a smooth, clean, and mirror-like surface. The polished samples were examined under an optical and scanning electron microscope (SEM), to characterise the surface and to check for porosity prior to any type of corrosion testing.

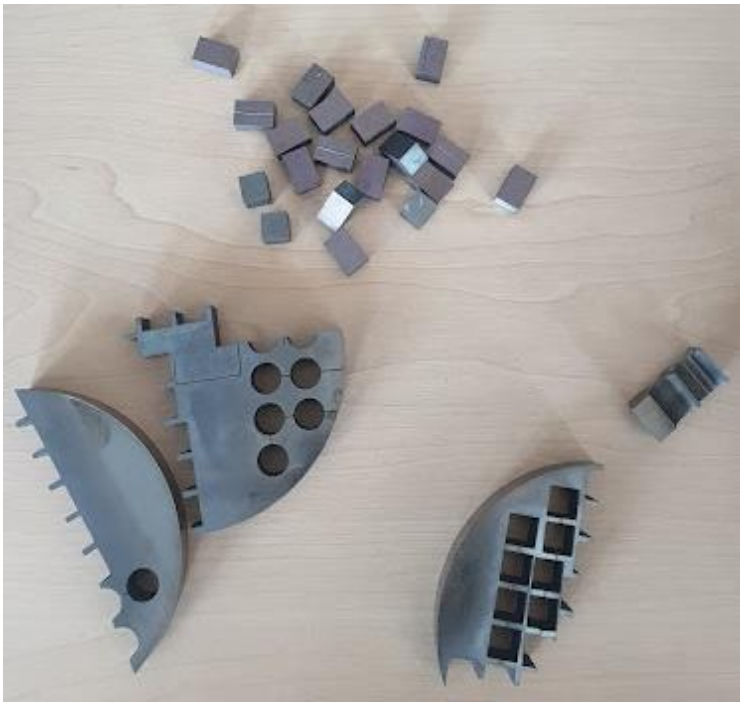


Figure 48: Titanium sample coupons

5.3 Titanium Samples for Weight Loss Tests

The cut samples could not be drilled with a hole in the middle to allow the samples to be freely suspended, however a string was tied around the samples to allow the sample to be suspended, freely floating, and fully submerged within the corrosive solutions. There were six solutions in total. Two solutions were HCl and NaCl without inhibitor, two other solutions were HCl and NaCl with $La(acac)_3$ inhibitor, and the final two solutions were HCl and NaCl with $Ce(acac)_3$.

5.4 Titanium in NaCl Experiments

5.4.1 NaCl Solutions Weight Loss Tests

Two sets of six different immersion solution tests were conducted for titanium. Duplicates of 0.6M NaCl without inhibitor, 0.6M NaCl with $La(acac)_3$ and 0.6M NaCl with $Ce(acac)_3$ were run, consistent with the case of aluminium (*section 4.4.1*). The immersion time was monitored for a period of six weeks and the mass of the samples were measured at an interval of two weeks.

Titanium showed extremely good resistance to sodium chloride solution, as there was little, or no weight loss observed during the weight loss experiments over the period of

six weeks (see table 9). This is due to its strong passivation layer, as well as the fact that titanium is very stable over a wide range of potentials (Zielinski & Sobieszczyk, 2008).

Table 9: Summary of weight loss measurements of titanium coupons in 0.6M NaCl solutions at 25^0*C.*

Solution	Start Mass (g)	Week 2 Mass (g)	Week 4 Mass (g)	Week 6 Mass (g)
NaCl	3.132	3.132	3.132	3.132
NaCl	3.132	3.132	3.132	3.132
NaCl + $La(acac)_3$	3.131	3.131	3.131	3.131
NaCl + $La(acac)_3$	3.132	3.132	3.132	3.132
NaCl + $Ce(acac)_3$	3.134	3.134	3.134	3.134
NaCl + $Ce(acac)_3$	3.131	3.131	3.131	3.131

In conjunction with the weight loss results (Table 9), the high level of corrosion resistance can also be appreciated by comparing the SEM micrographs of the Titanium reference sample (figure 49) and the sample immersed in 0.6 NaCl solution without inhibitor (figure 51), and which indicates no surface and structural differences. However, a slight difference in surface texture was observed after immersion in NaCl. The SEM secondary images for the reference sample in figure 50 and the NaCl weight loss sample in figure 52 also confirmed the similarity between the surface images in terms of topography structures. These similarities can also be seen in the SEM images with inhibitors (figure 53 and 54).

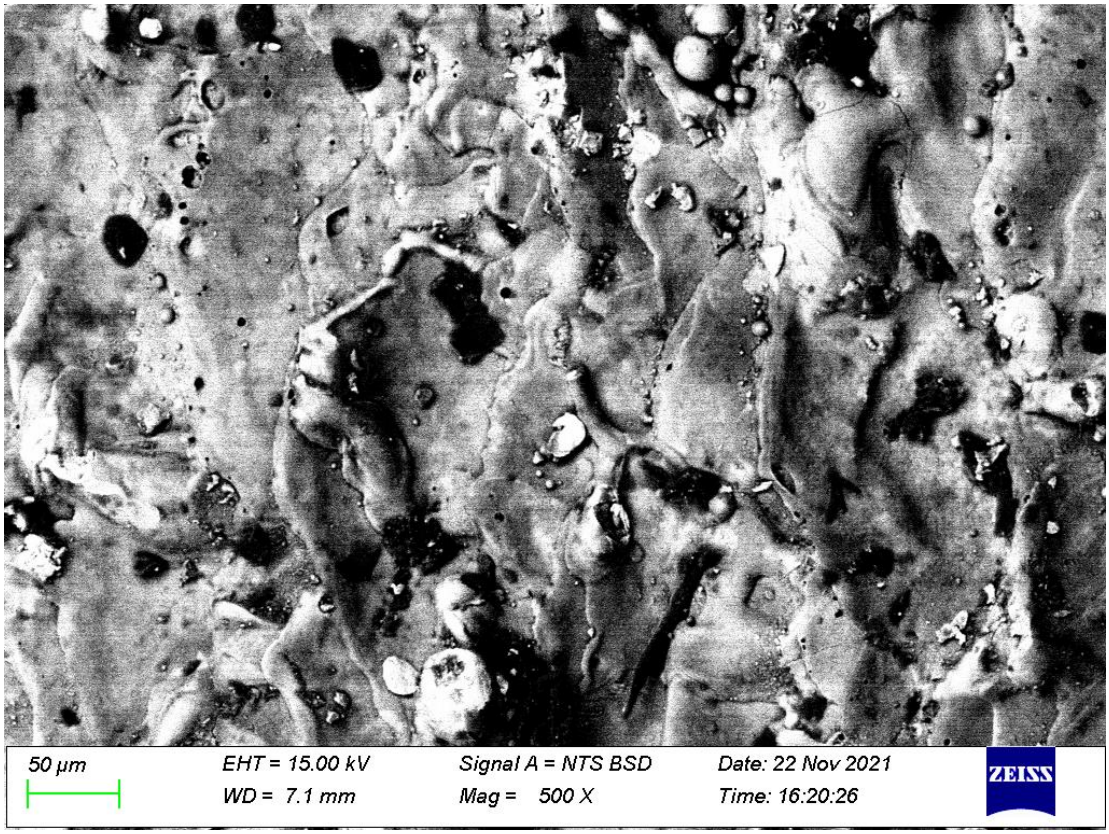


Figure 49: SEM image of Ti, without immersion for weight loss test (500 X).

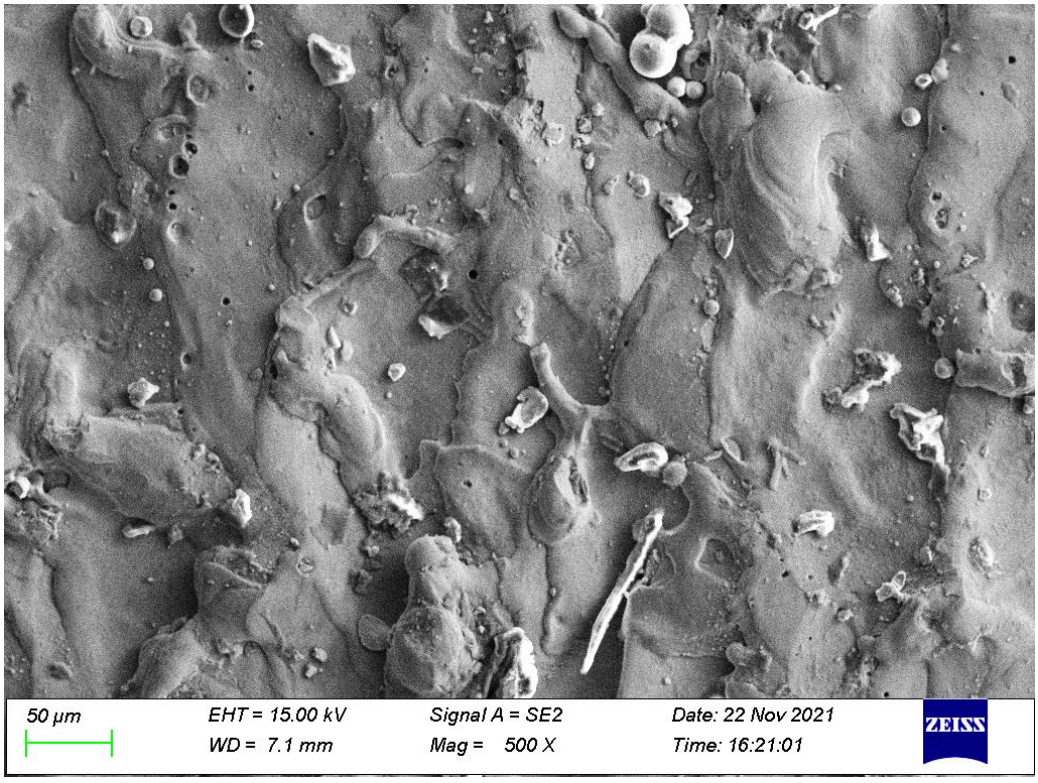


Figure 50: SEM secondary of Ti sample, without immersion for weight loss test (500 X).

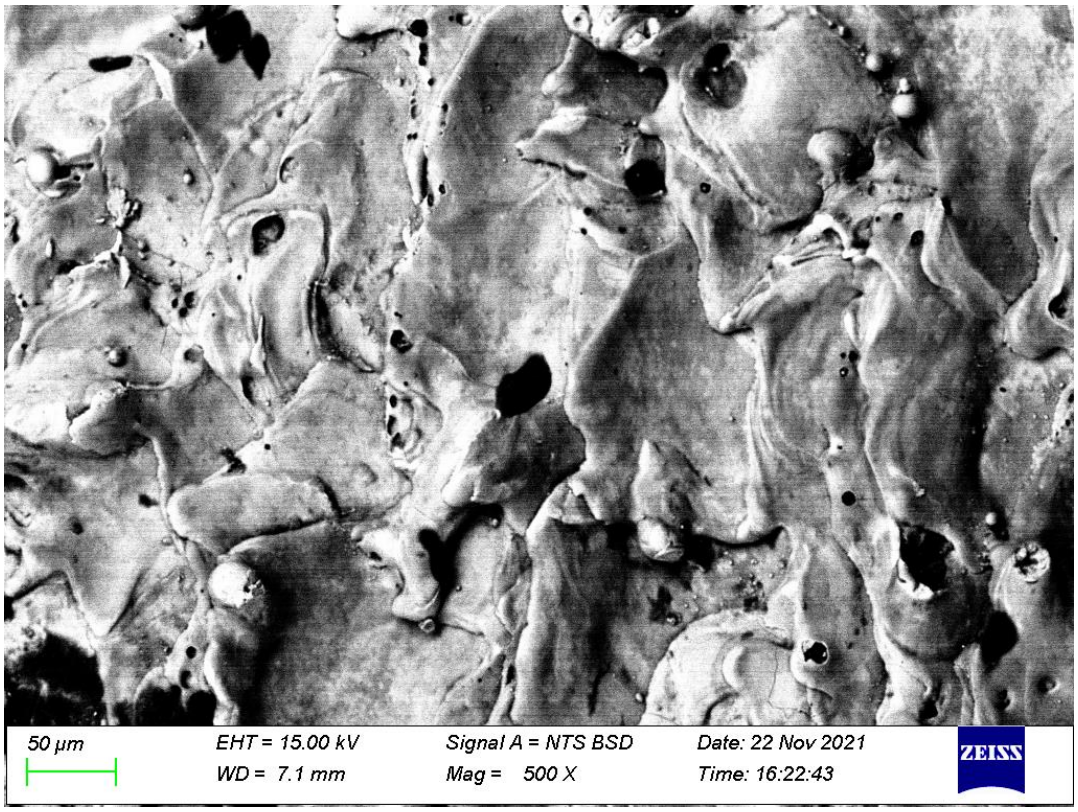


Figure 51: SEM image of Ti in 0.6M NaCl without inhibitor after six weeks weight loss test (500 X).

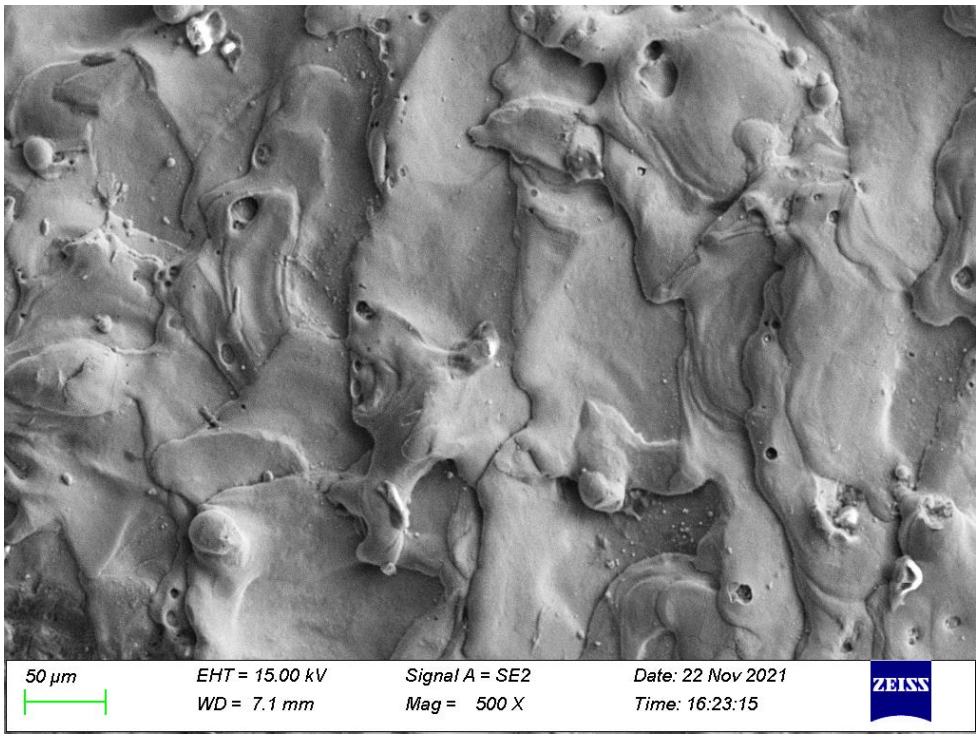


Figure 52: SEM secondary image of Ti in 0.6M NaCl without inhibitor after six weeks weight loss test (500 X).

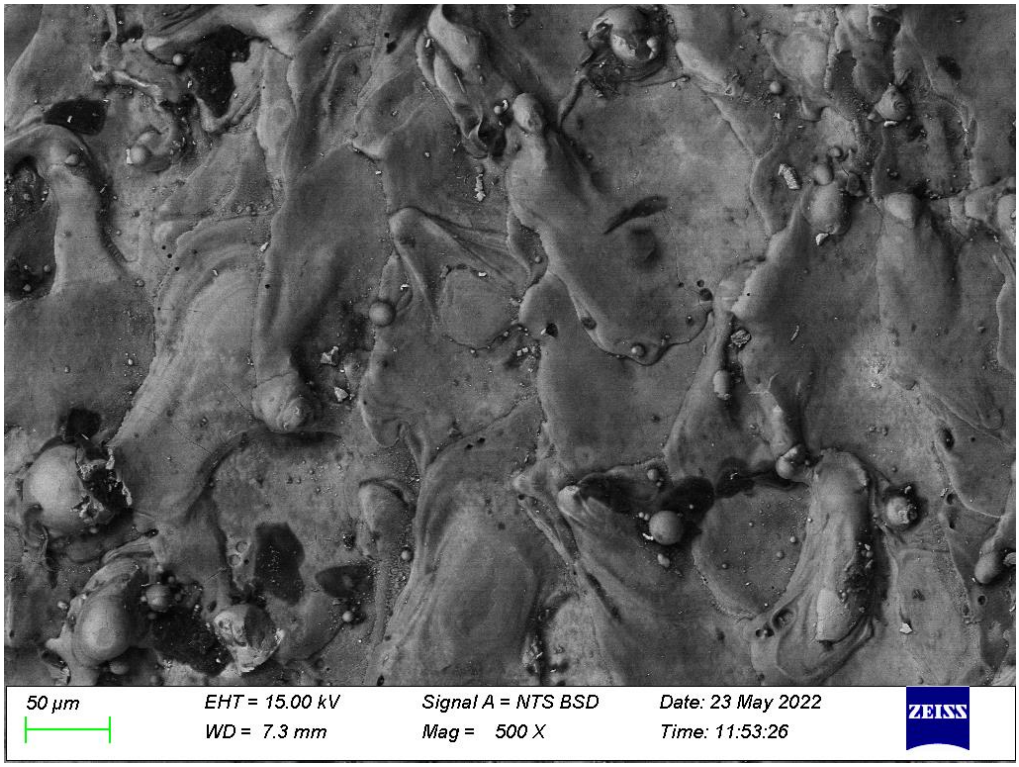


Figure 53: SEM of Ti immersed in 0.6M NaCl with $La(acac)_3$ for a six-week weight loss test (500 X).

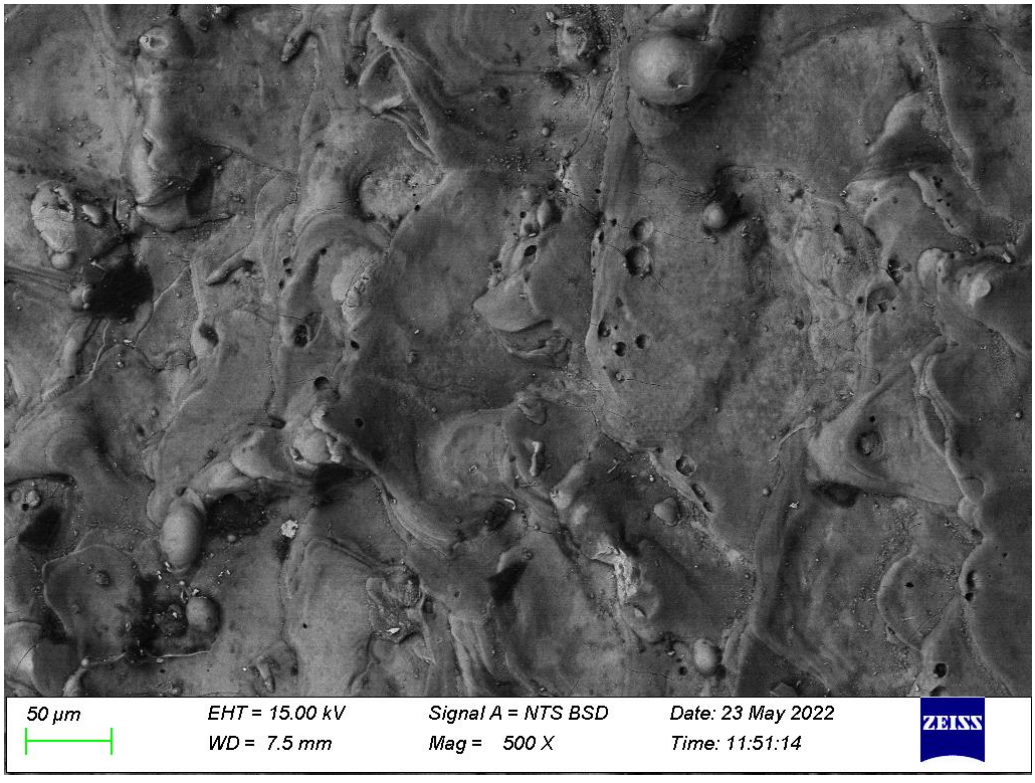


Figure 54: SEM of Ti immersed in 0.6M NaCl with $Ce(acac)_3$ for a six-week weight loss test (500 X).

5.4.2 NaCl Solutions Potentiodynamic Tests

Titanium coupons with an exposed surface of 0.16 cm^2 were placed in three different types of 0.6M NaCl solutions. One solution was without inhibitor and the others contained $La(acac)_3$ and $Ce(acac)_3$. The resulting potentiodynamic plots are shown in Figure 55.

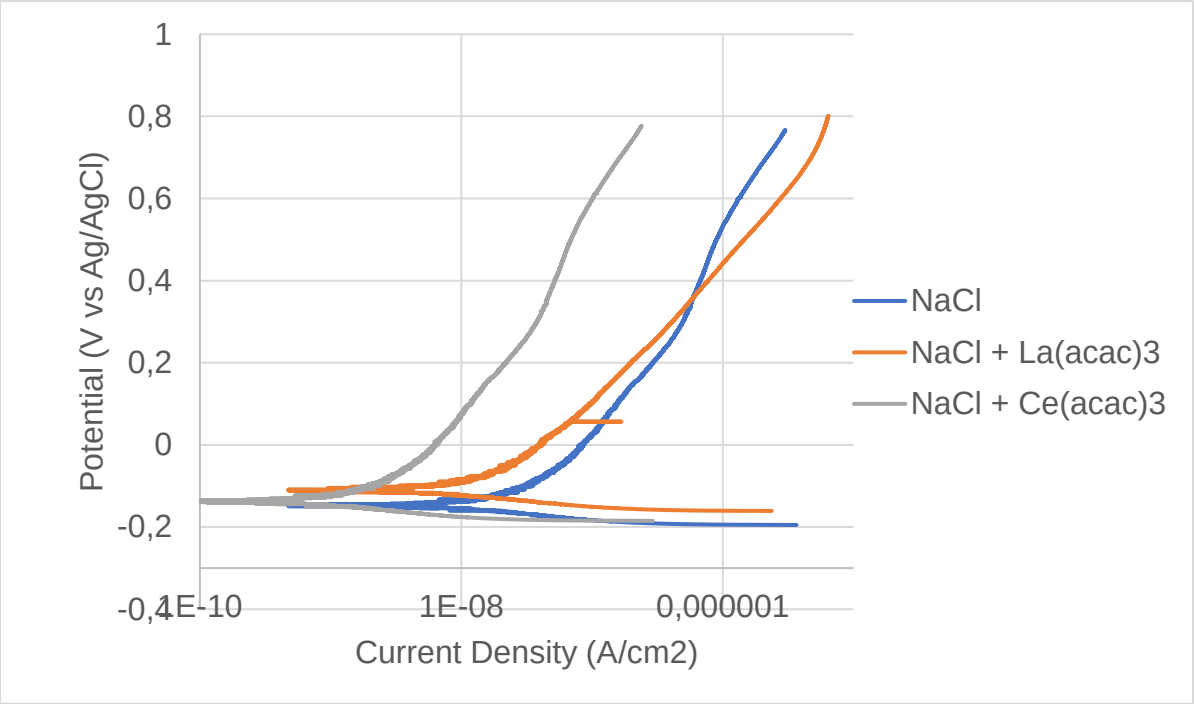


Figure 55: Potentiodynamic plot of Ti immersed in 0.6M NaCl at 25^0*C.*

The low current density values of order 10^{-8} (two orders of magnitude lower than that of Al in same solution, figure 25), observed in the potentiodynamic curve for titanium indicate very low corrosion rates and highlights the metal's, as well as inhibitors', corrosion resistance under these conditions. The curves with the inhibitors $La(acac)_3$ and $Ce(acac)_3$ display a further decrease in corrosion current and consequently a decrease in corrosion rate as compared to the alloy in the solution containing no inhibitor, as can be expected (Forsyth & Hinton, 2014).

The i_{corr} parameters were used to calculate the corrosion rates and inhibition efficiencies for the various solutions (table 10). The corrosion rate in the presence of the two corrosion inhibitors are at least an order of magnitude smaller than in their

absence, which confirms the trend observed in the mass loss tests. The electrochemical evaluation shows that their final efficiencies are similar, as $La(acac)_3$ and $Ce(acac)_3$ curves showed very little positive E_{corr} offset of 38 mV and 8mV respectively, as well as a slight decrease in I_{corr} values relative to the NaCl curve. These small anodic shifts in potential and slight decrease in current could indicate that both inhibitors act as mixed inhibitors with cathodic inclination in this system (Khaled & Amin, 2009). It is also important to note that relative to the aluminium system, the offset and differences in Ecorr and Icorr for titanium is smaller which highlights the stronger corrosion resistance of titanium relative to aluminium for the same system (Shoesmith & Noel, 2010).

The corrosion rate values were in turn used to obtain the inhibitor efficiency of the solutions, which were 89.2% and 76.7% for $La(acac)_3$ and $Ce(acac)_3$ respectively. This is in the range of other works cited in literature where efficiencies ranged from 89% to 98% (Rabab, et al., 2011).

Table 10: Summary of potentiodynamic test for Ti in 0.6M NaCl solutions at 25^0*C.*

	$-E_{corr}$ (mV)	I_{corr} ($\mu A/cm^2$)	CR (mm/yr)	Ba	Bc	IE (%)
NaCl	149	2.24E-03	1.20E-04	180	4	
$La(acac)_3$	111	1.6E-03	1.30E-05	480	10	89.2%
$Ce(acac)_3$	141	1.6E-03	2.80E-05	880	5	76.7%

5.4.3 SEM Analysis of NaCl Potentiodynamic Samples

5.4.3.1 SEM of Titanium Control Sample

The titanium reference sample SEM and EDX showed the metal coupon surface with spots highlighting the intermetallic components of the alloy (figure 56 & 59). Figure 58 confirms the presence of Ti, V and Al in the alloy.

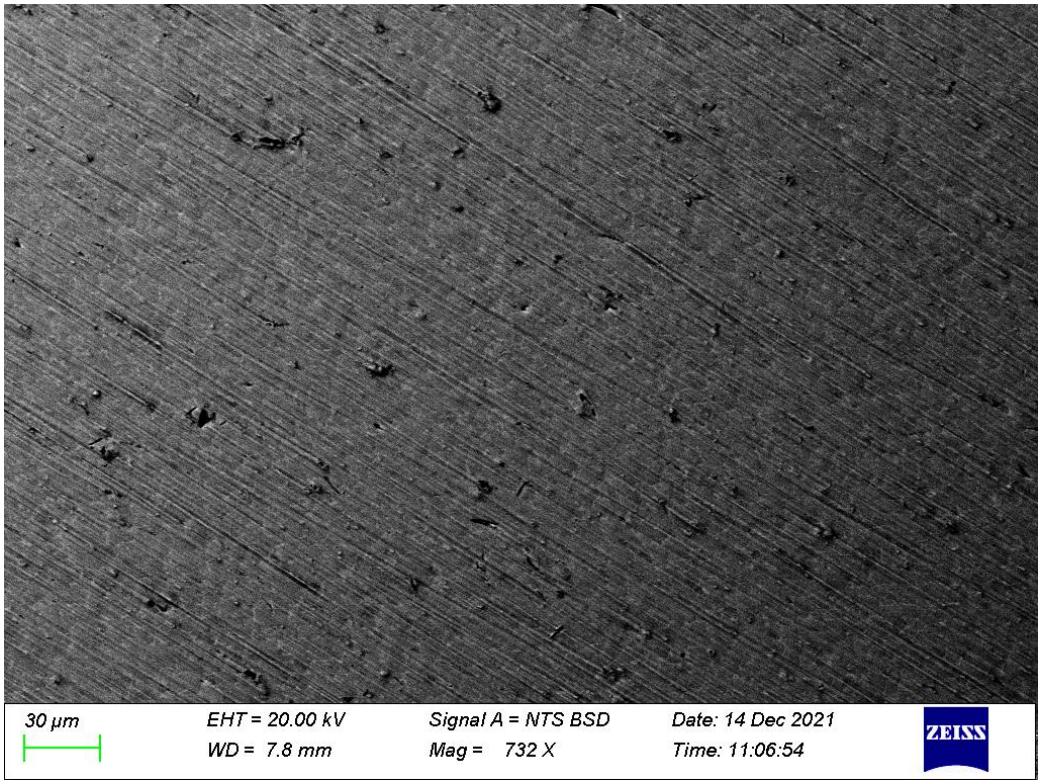


Figure 56: SEM image of Ti reference sample without potentiodynamic test (732 X).

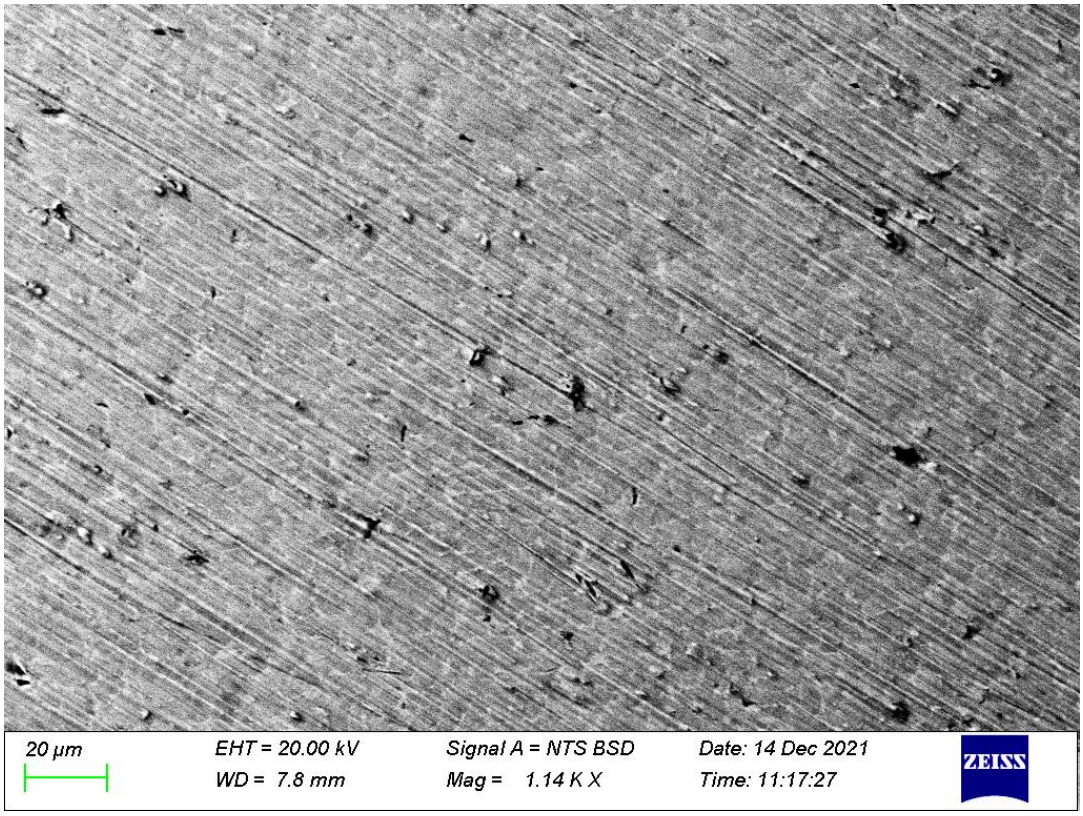


Figure 57: SEM image of Ti reference sample without potentiodynamic test (1140 X).

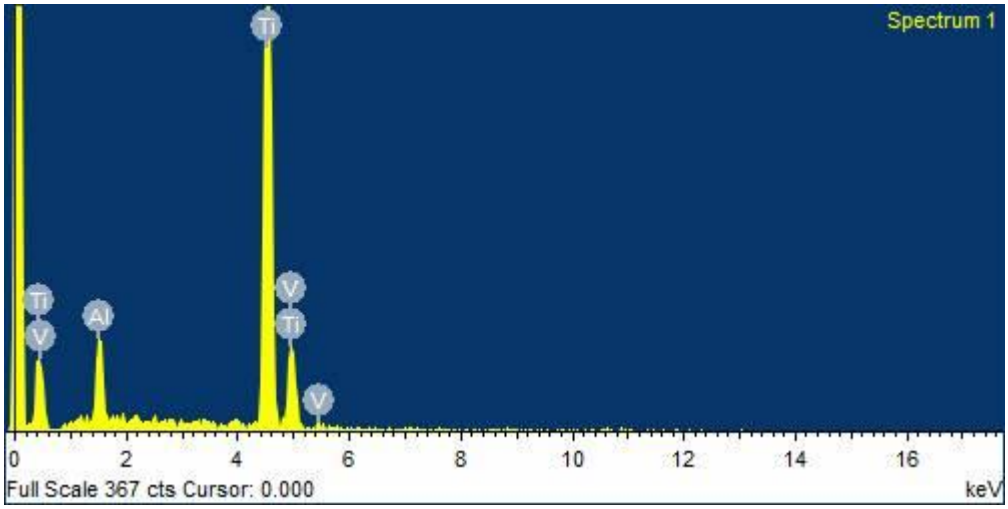


Figure 58: EDX of Ti reference sample without potentiodynamic test.

5.4.3.2 SEM of Titanium Sample in NaCl Without Inhibitor

In addition to the observations from the weight loss and potentiodynamic tests, the comparison between the SEM reference (figure 57,58) and NaCl immersion (figure 59,60) image show very little disparity to the coupon surface elements. This highlights the inherent corrosion resistance ability of titanium.

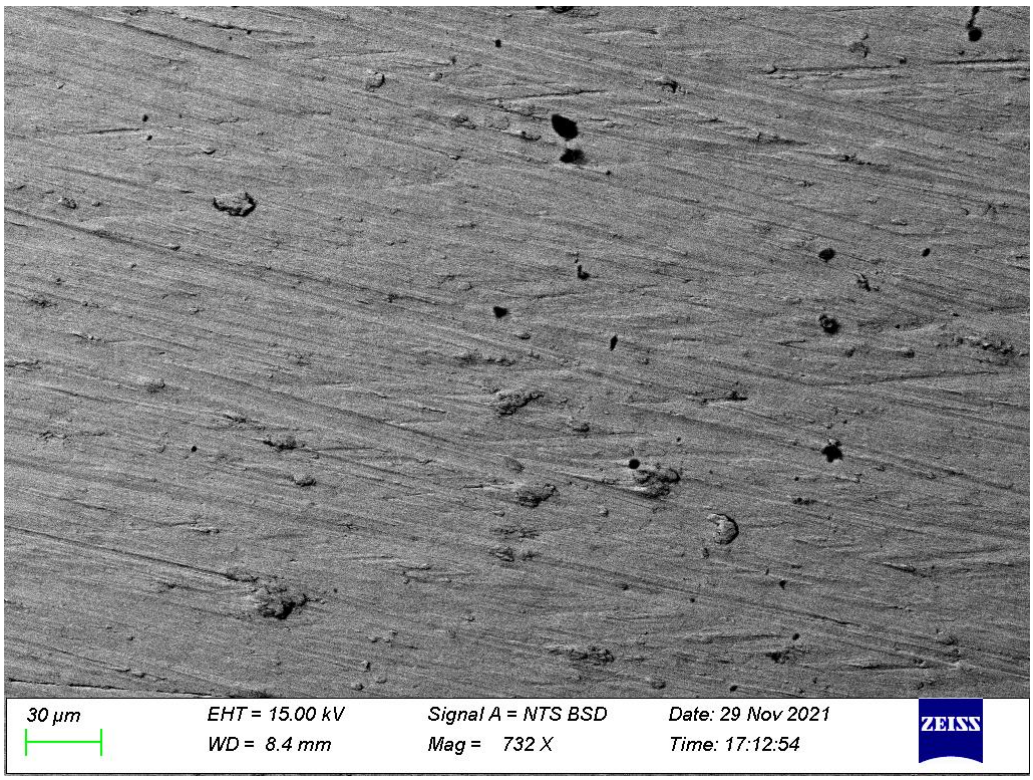


Figure 59: SEM of Ti surface after immersion in 0.6M NaCl without inhibitor, after potentiodynamic test at 25^0*C (732 X).*

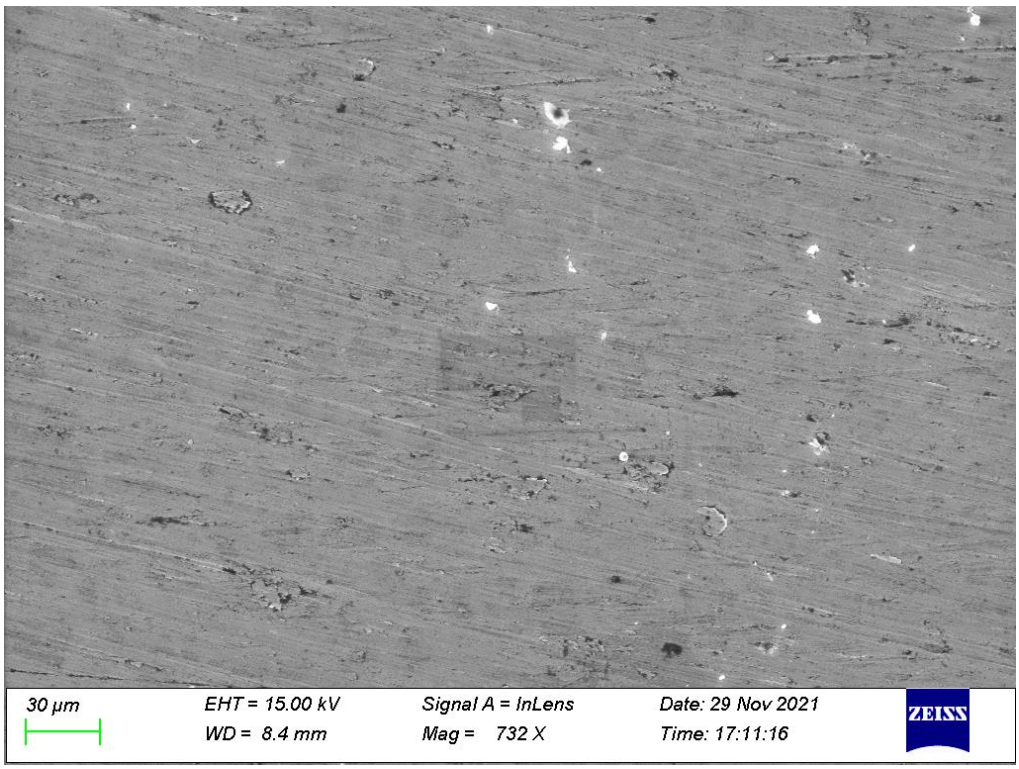


Figure 60: SEM image of Ti surface after immersion in 0.6M NaCl without inhibitor, after potentiodynamic test at 25^0*C (732 X).*

5.4.3.3 SEM of Titanium Sample in NaCl with Inhibitor

The SEM analysis of the Ti in NaCl without inhibitor and the SEM scans of Ti with inhibitors show similar surface features (figure 61,62 and 64,65). EDX analyses after immersion indicated no traces of any surface films formed during the polarisation of the alloy in the solutions with corrosion inhibitors.

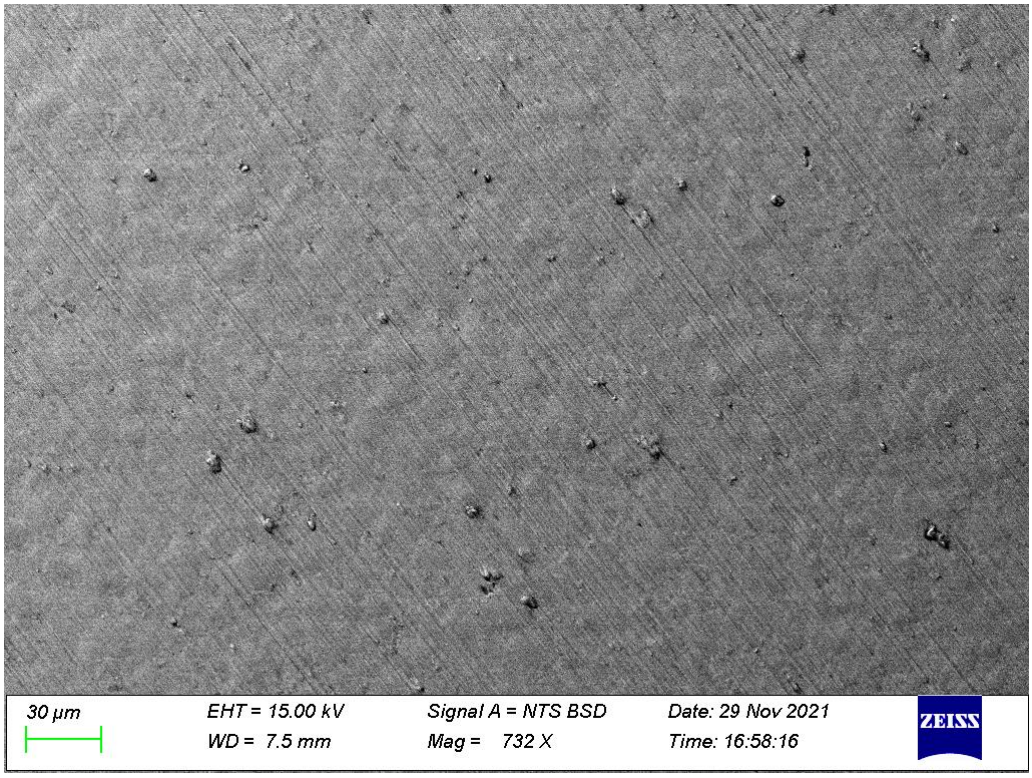


Figure 61: SEM of Ti surface after immersion in 0.6M NaCl with $La(acac)_3$, after potentiodynamic test at 25^0C (732 X).

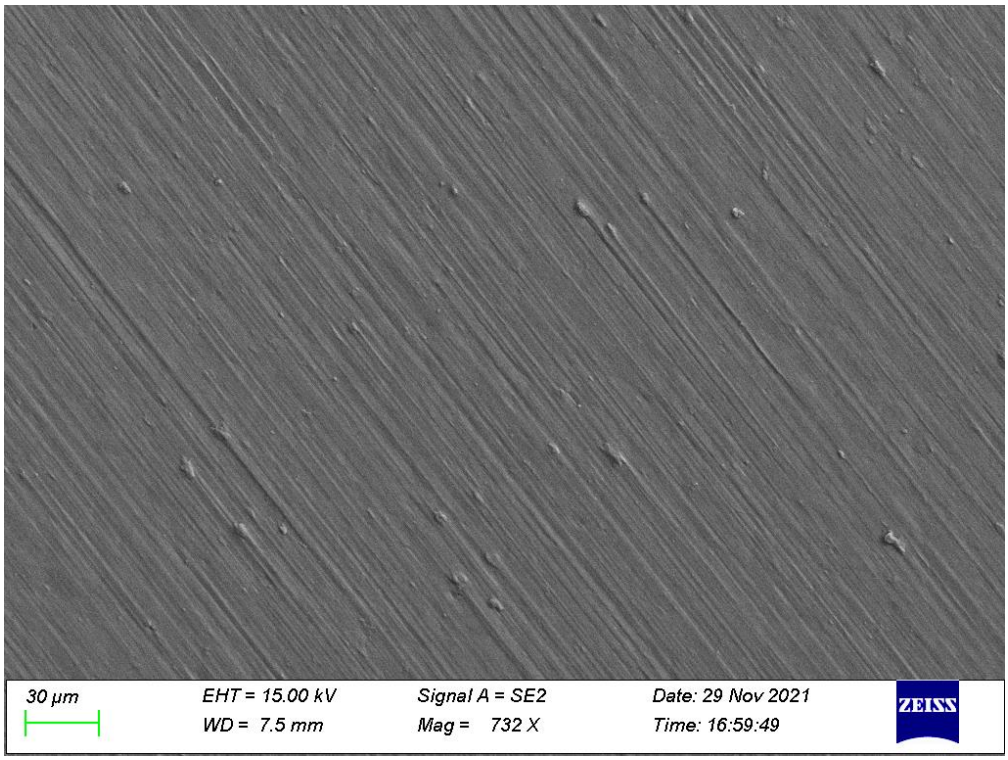


Figure 62: SEM secondary Ti surface after immersion in 0.6M NaCl with $La(acac)_3$, after potentiodynamic test at 25^0C (732 X).

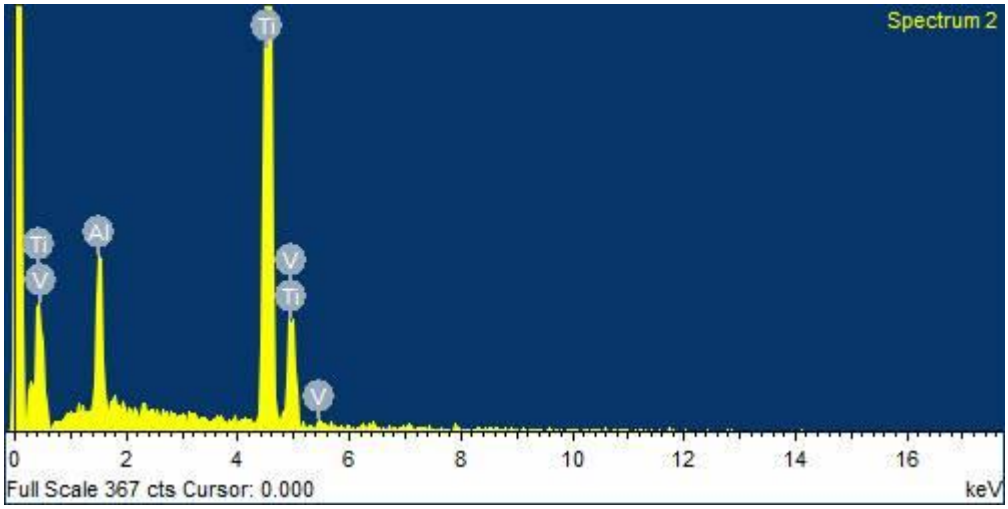


Figure 63: EDX of Ti surface after immersion in in 0.6M NaCl with $La(acac)_3$, after potentiodynamic test at 25^0*C.*

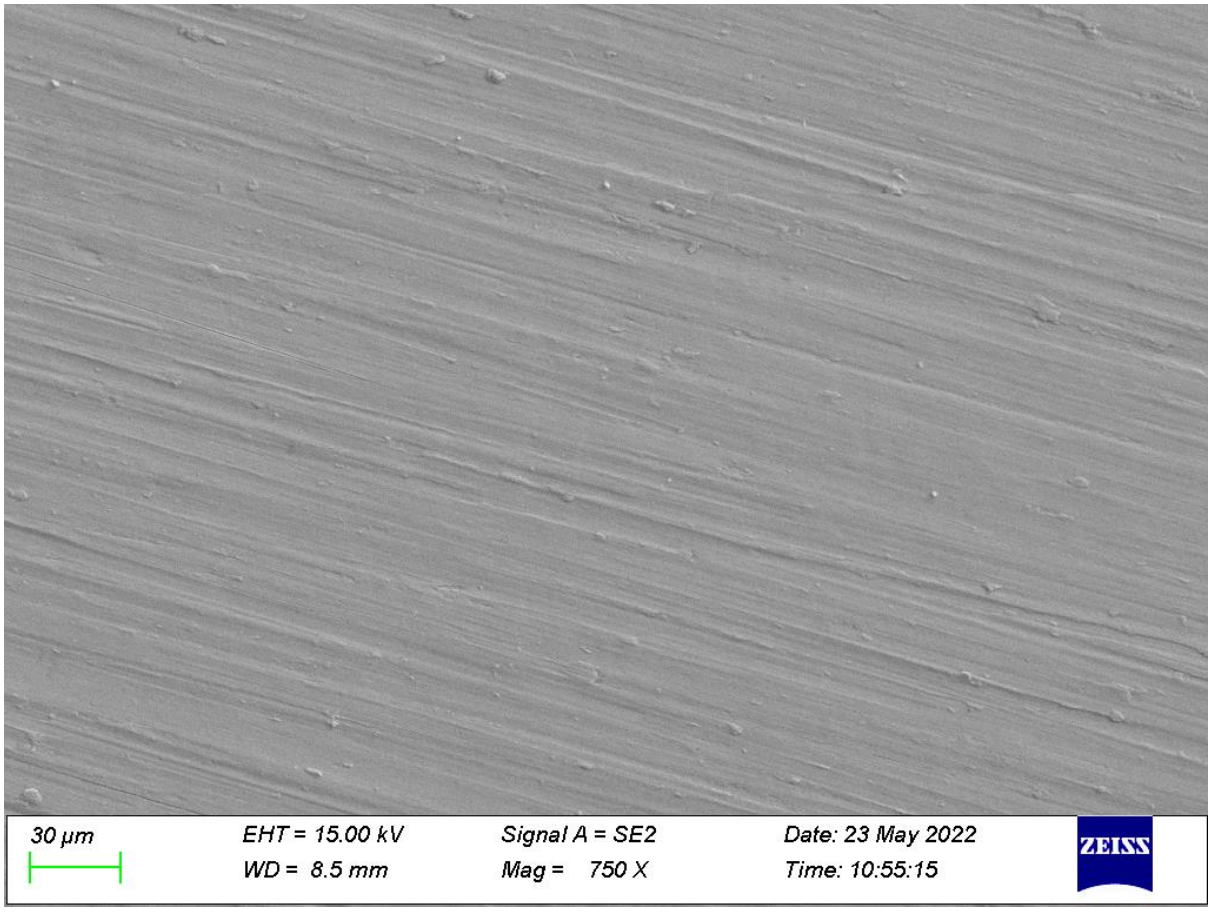


Figure 64: SEM secondary Ti surface after immersion in 0.6M NaCl with $Ce(acac)_3$, after potentiodynamic test at 25^0*C (750 X).*

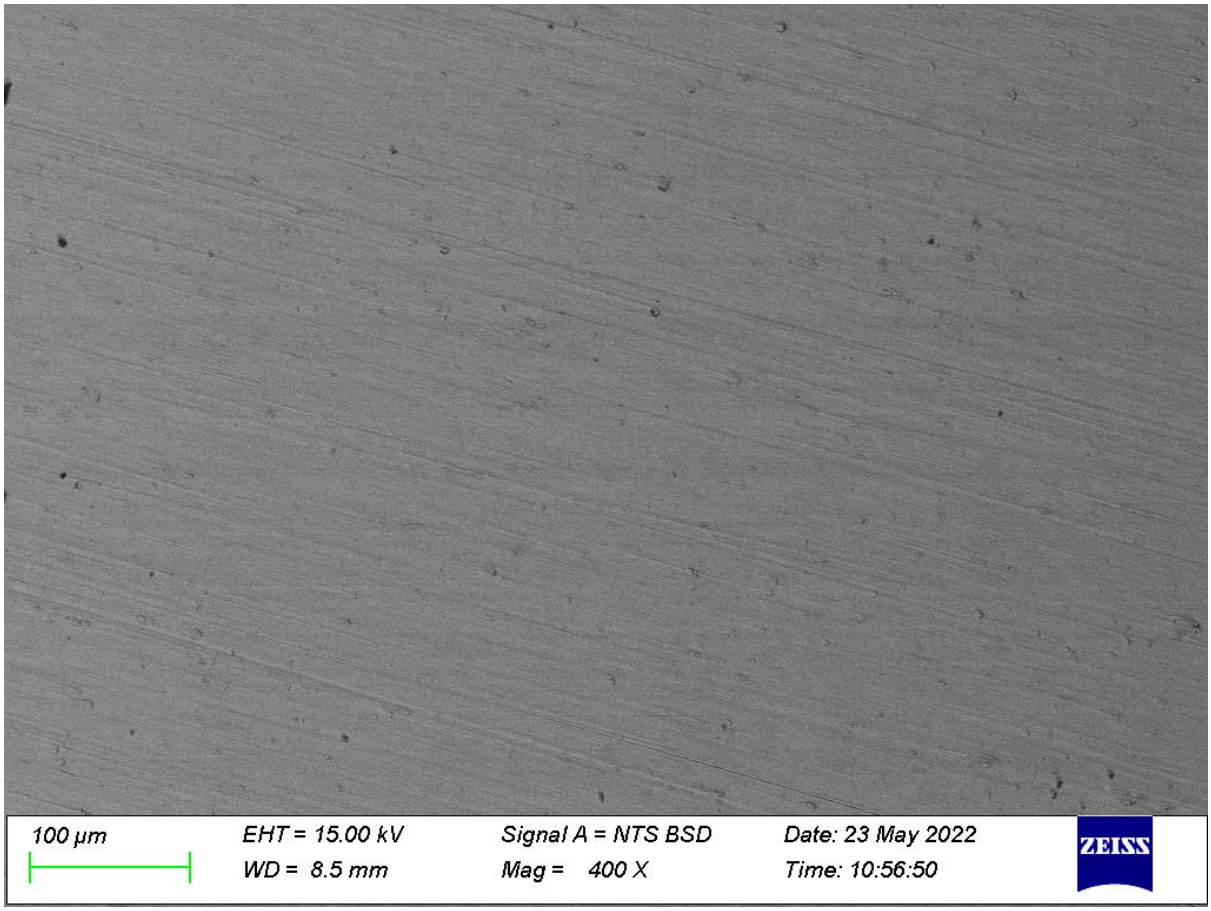


Figure 65: SEM secondary Ti surface after immersion in 0.6M NaCl with $Ce(acac)_3$, after potentiodynamic test at 25^0C (400 X).

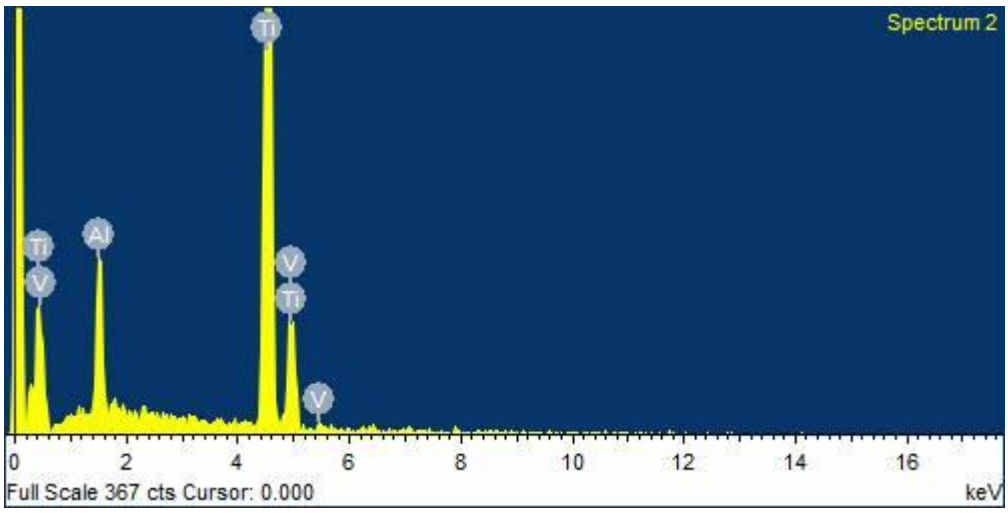


Figure 66: EDX of Ti surface after immersion in in 0.6M NaCl with $Ce(acac)_3$, after potentiodynamic test at 25^0C.

5.5 Titanium in HCl Experiments

5.5.1 HCl Solutions Weight Loss Tests

Two sets of six different immersion solution tests were conducted for titanium. Duplicates of 0.1M NaCl without inhibitor, 0.1M NaCl with $La(acac)_3$ and 0.1M NaCl with $Ce(acac)_3$ were run, consistent with the case of aluminium (*section 4.5.1*). The immersion time was monitored for a period of six weeks and the mass of the samples were measured at an interval of two weeks (table 11).

Table 11: Summary weight loss measurements of titanium coupons in 0.6M NaCl solutions at 25^0*C.*

Solution	Start Mass (g)	Week 2 Mass (g)	Week 4 Mass (g)	Week 6 Mass (g)
HCl	3.133	3.133	3.123	3.122
HCl	3.133	3.133	3.123	3.122
HCl + $La(acac)_3$	3.131	3.133	3.133	3.133
HCl + $La(acac)_3$	3.133	3.133	3.133	3.133
HCl + $Ce(acac)_3$	3.131	3.131	3.133	3.133
HCl + $Ce(acac)_3$	3.131	3.131	3.133	3.133

Titanium showed good resistance to the HCl solution in comparison to the system with aluminium in HCl, as the cumulative weight loss of titanium without inhibitor was 0.001g in six weeks. In contrast to this, that of aluminium was 0.197g after six weeks. This is due to its strong passivation layer, as well as the fact that titanium is very stable over a wide range of potentials (Zielinski & Sobieszczyk, 2008).

Table 12: Summary of corrosion rate of Ti results for chloride solutions without inhibitor

Solution	4 Weeks	6 Weeks
HCl - mm/yr	-	0.12

Despite the good resistance to corrosion of the titanium metal in 0.1M HCl corrosion, the corrosion rate after a period of four and six weeks was calculated to be 0.18mm/yr and 0.12 mm/yr respectively, which is similar to the range reported in other studies of titanium alloys in HCl (Junying, et al., 2017). The decrease in corrosion rate in the case of HCl without inhibitor (table 12), is due to the increasing resistance to mass transfer which is a factor of the passivation layer and some of corroded material which reduces the influx of the chloride species (French, et al., 1993).

The intensity of corrosion action between NaCl and HCl solutions can be appreciated by evaluating the SEM figure 67, which reveals a surface deposition of an apparent corrosion product. The secondary SEM image in figure 68, highlights the observation that the corrosion products on the surface are shallow and do not seem to penetrate the metal.

The SEM of the samples immersed with La(acac)3 and Ce(acac)3 showed little or no signs of corrosion surface damage, as can be seen in figures 69 & 70.

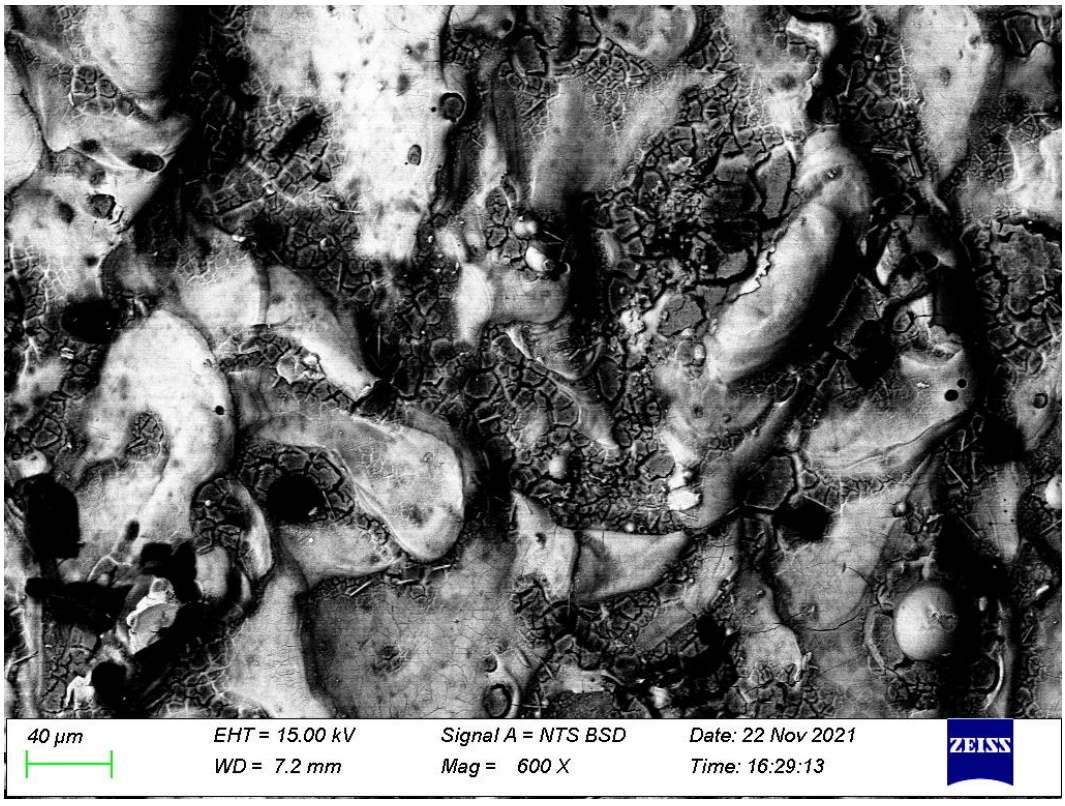


Figure 67: SEM image of Ti in 0.1M HCl without inhibitor after six weeks weight loss test (600 X).

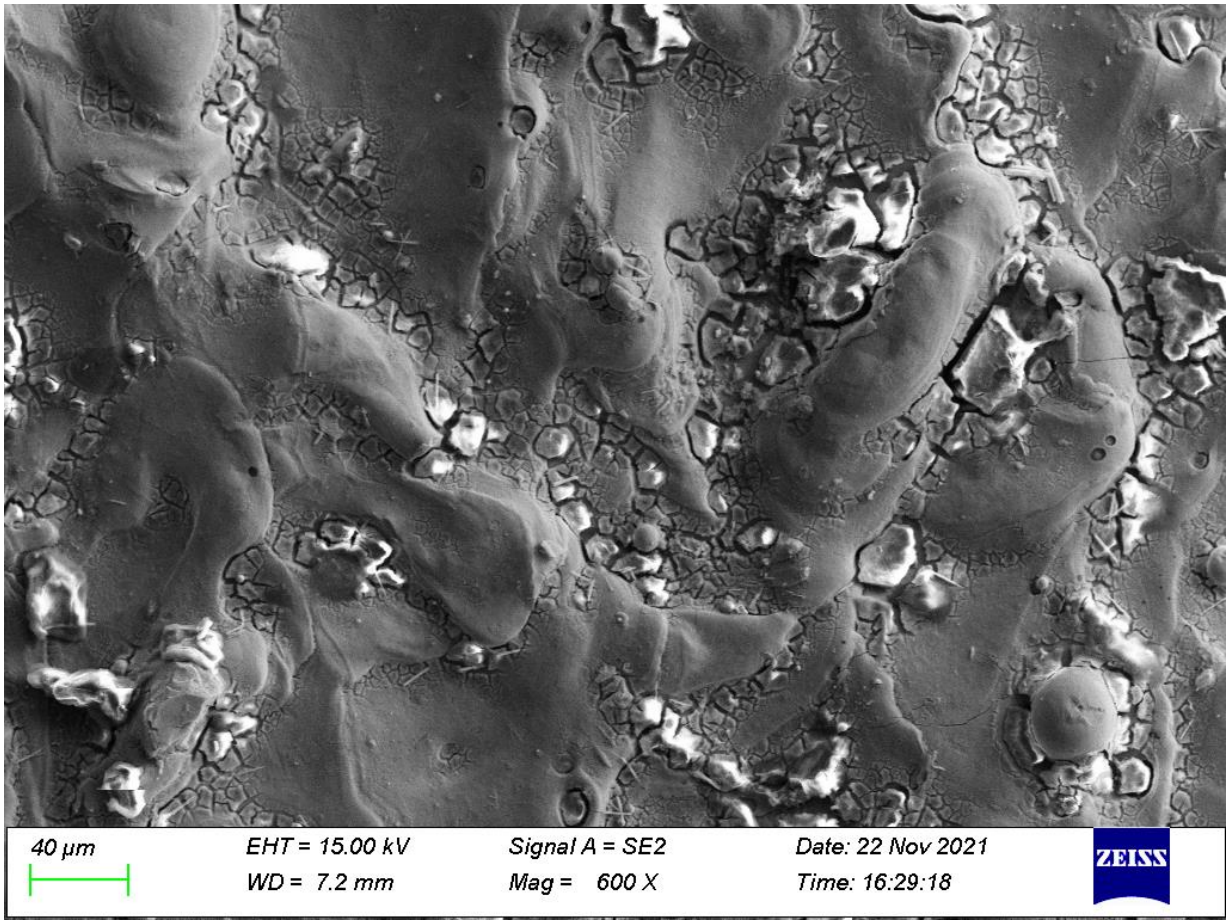


Figure 68: SEM secondary image of Ti in 0.1M HCl without inhibitor after six weeks weight loss test (600 X).

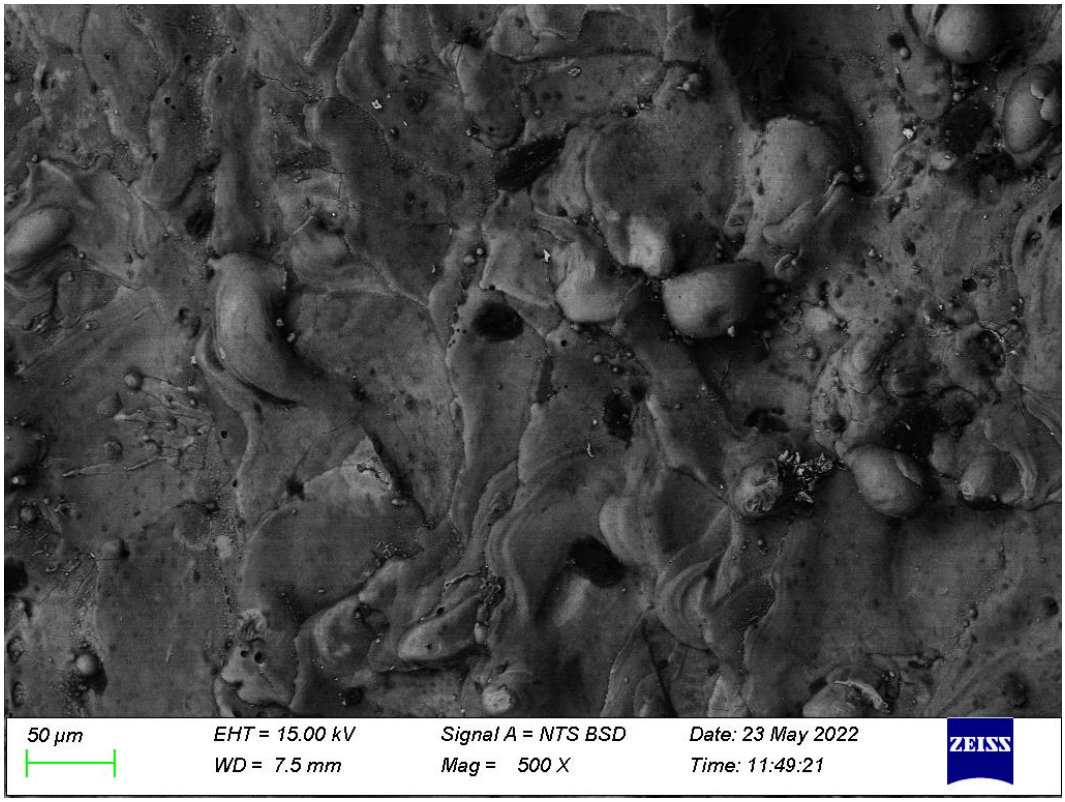


Figure 69: SEM image of Ti in 0.1M HCl with $La(acac)_3$ after six weeks weight loss test (500 X).

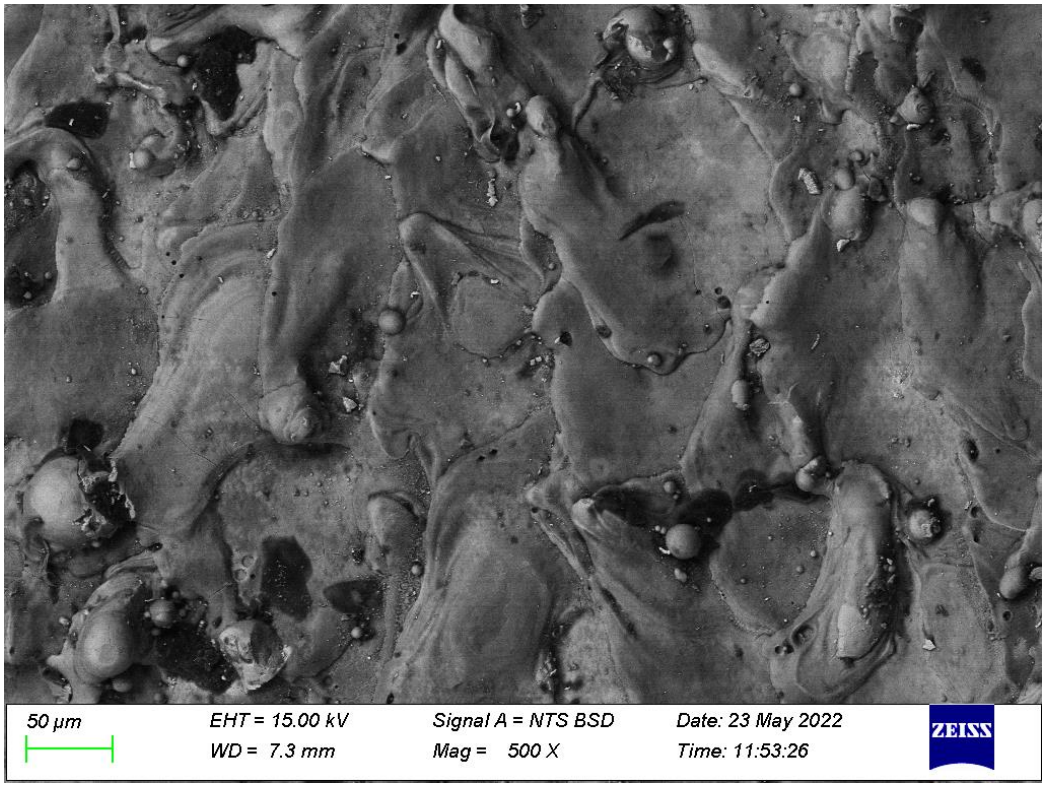


Figure 70: SEM image of Ti in 0.1M HCl with $Ce(acac)_3$ after six weeks weight loss test (500 X).

5.5.2 HCl Solutions Potentiodynamic Tests

Titanium coupons with an exposed surface area of 0.16 cm^2 were placed in three different types of 0.1M HCl solutions. One solution without inhibitor, and the others containing $La(acac)_3$ and $Ce(acac)_3$. The resulting potentiodynamic plots are seen in Figure 71.

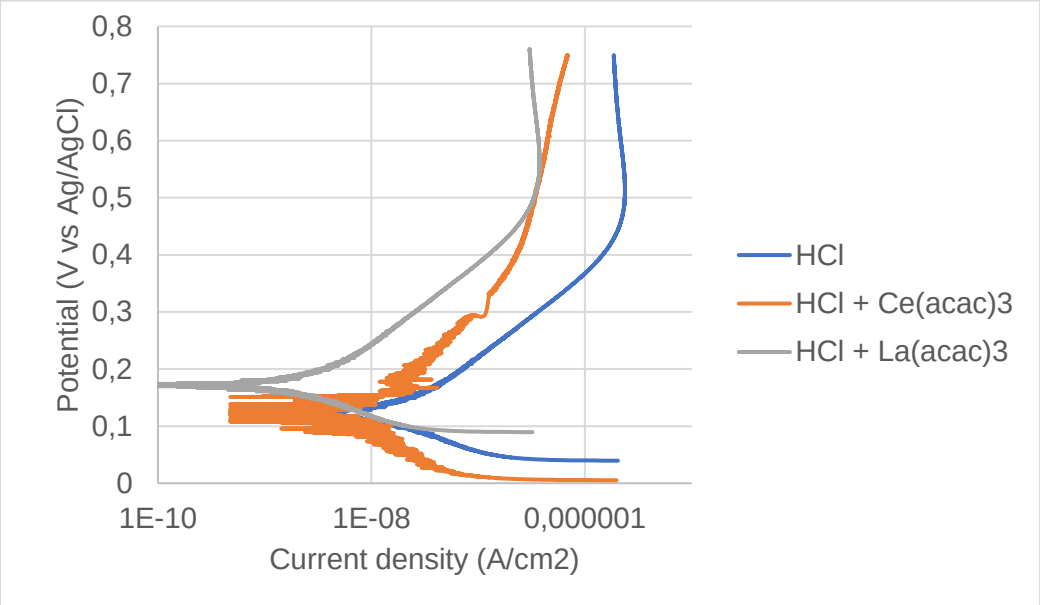


Figure 71: Potentiodynamic plot of Ti immersed in 0.1M HCl at 25^0C.

The low current density values of the order of 10^{-8} (two orders of magnitude lower than that of Al in same solution, figure 43), observed in the potentiodynamic curves for titanium, indicate relatively low corrosion rates and highlights the metal's as well as inhibitors' addition to increase the corrosion resistance under these conditions. The curves with the inhibitors $La(acac)_3$ and $Ce(acac)_3$ displays a decrease in corrosion current and consequently a decrease in corrosion rate, as can be expected (Forsyth & Hinton, 2014). The $La(acac)_3$ and $Ce(acac)_3$ curves showed very little positive E_{corr} offset of 40 mV and 0 mV respectively, as well as a slight decrease in I_{corr} values relative to the HCl curve. These small anodic shifts in potential and slight decrease in current indicate that both inhibitors could act as mixed inhibitors in this system (Khaled & Amin, 2009). The i_{corr} parameters were used to calculate the corrosion rates and inhibition efficiencies for the various solutions (table 13).

Table 13: Summary of potentiodynamic test for Ti in 0.1M HCl solutions at 25^0C.

	$-E_{corr}$ (mV)	I_{corr} (µA/cm^2)	Ba	Bc	CR (mm/yr)	IE (%)
HCl	110	2.24E-03	450	20	2.30E-04	---
$La(acac)_3$	150	1.6E-04	550	30	1.20E-05	94.8%
$Ce(acac)_3$	111	1.6E-03	475	64	4.50E-05	80.4%

The corrosion rate values were in turn used to obtain the inhibitor efficiency of the solutions, which were 94.8% and 80.4% for $La(acac)_3$ and $Ce(acac)_3$ respectively. This is in the range of other works cited in literature where efficiencies from 80% to 99% (Junying, et al., 2017).

5.5.3 SEM Analysis of HCl Potentiodynamic Samples

5.5.3.1 SEM of Titanium Sample in HCl Without Inhibitor

In addition to the observations from the weight loss and potentiodynamic tests, the comparison between the SEM reference (figure 49,50), NaCl immersion (figure 59,60) and HCl immersion (figure 72,73) image show very little disparity to the coupon surface features. This highlights the inherent corrosion resistance of titanium (Greenwood & Earnshaw, 2007).

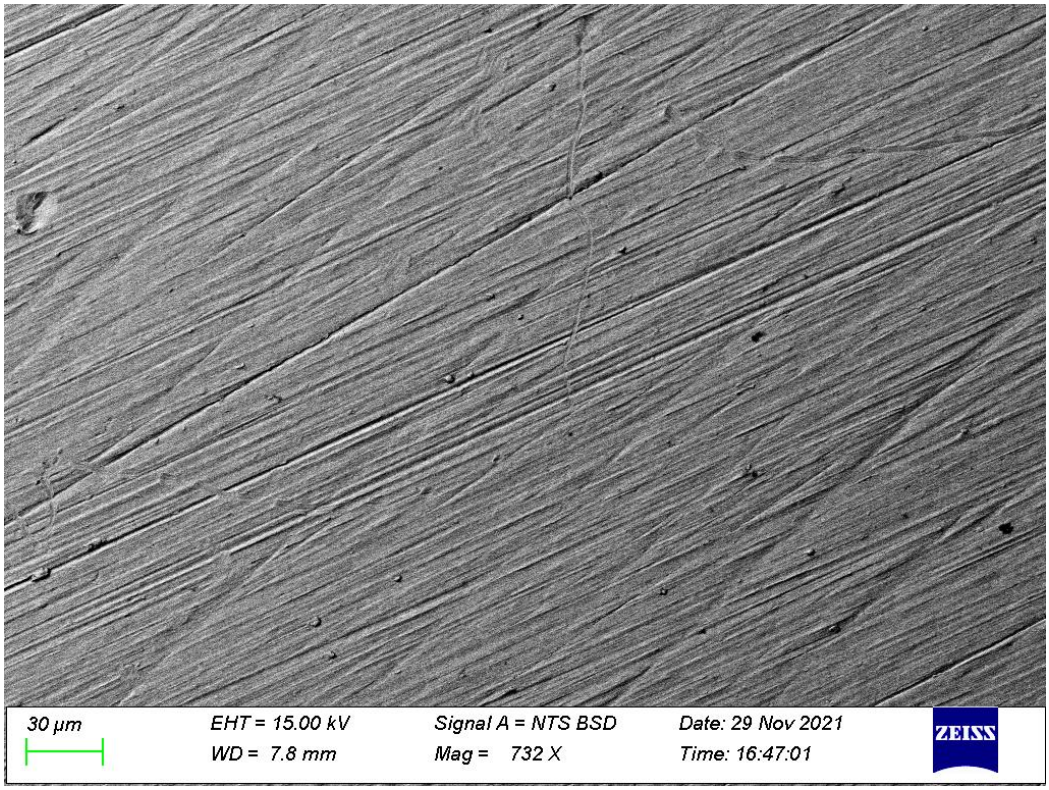


Figure 72: SEM of Ti surface after immersion in 0.1M HCl without inhibitor, after potentiodynamic test at 25^0*C (732 X).*

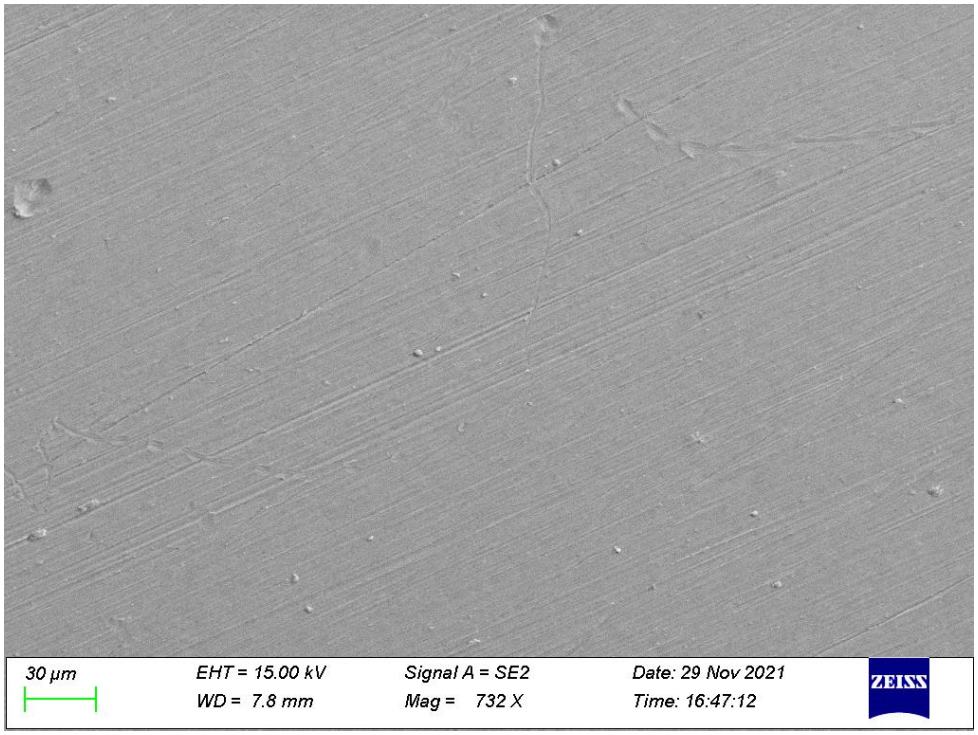


Figure 73: SEM secondary image of Ti surface after immersion in 0.1M HCl without inhibitor, after potentiodynamic test at 25^0*C (732 X).*

5.5.3.2 *SEM of Titanium Sample in HCl With Inhibitor*

Similar with the SEM analysis of the Ti in NaCl without inhibitor, NaCl with inhibitor and HCl without inhibitor, the SEM scans of Ti HCl with inhibitors show similarly and no huge differences in terms of surface features (figure 74 to 79).

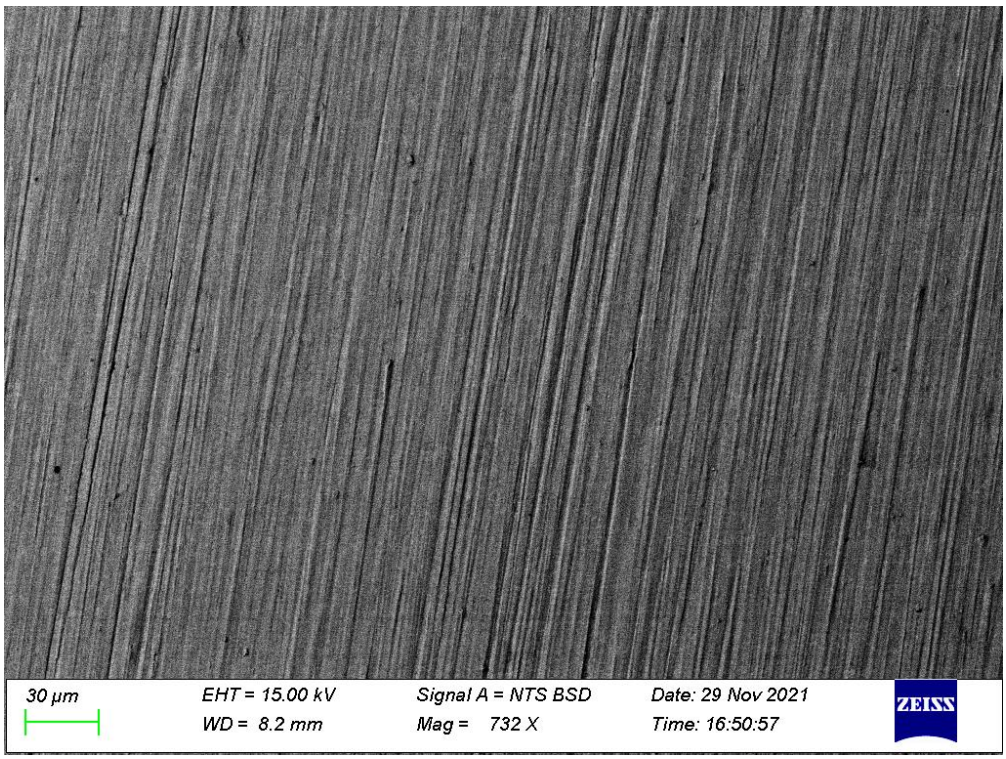


Figure 74: SEM of Ti surface after immersion in 0.1M HCl with La(acac)3, after potentiodynamic test at 25^0*C (732 X).*

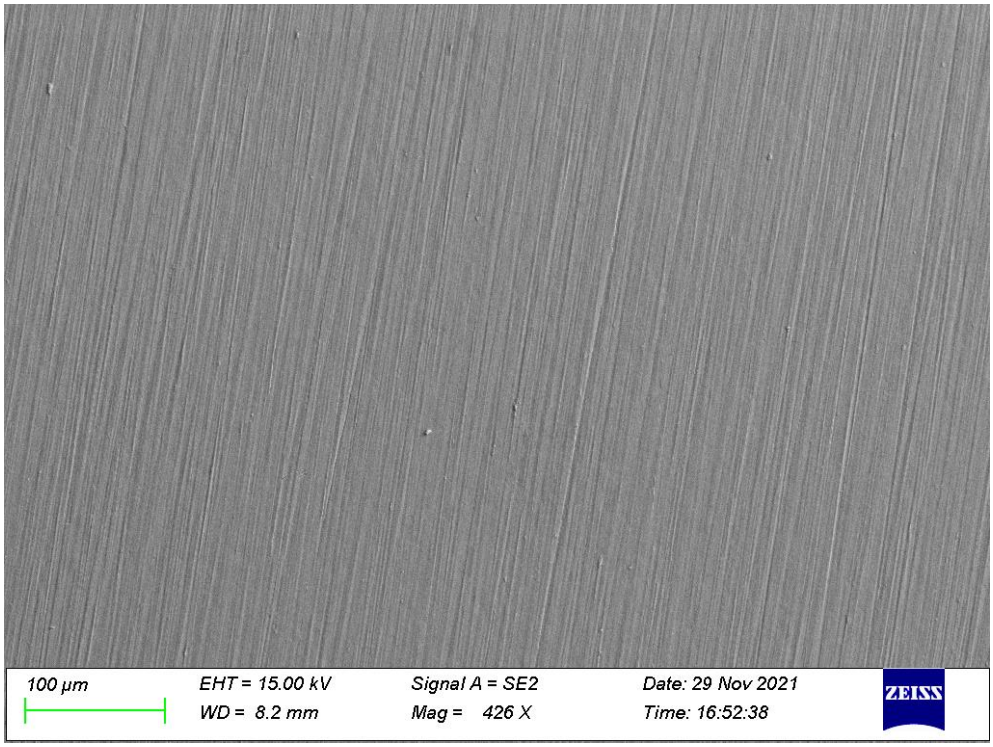


Figure 75: SEM secondary of Ti surface after immersion in 0.1M HCl with La(acac)3, after potentiodynamic test at 25^{0}C (426 X).

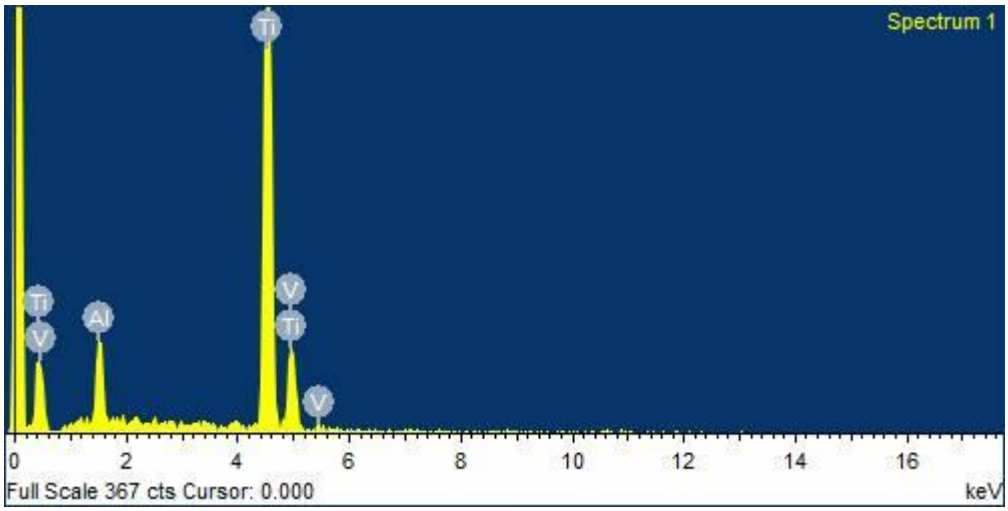


Figure 76: EDX of Ti surface after immersion in in 0.1M HCl with La(acac)$_3$, after potentiodynamic test at 25^{0}C.

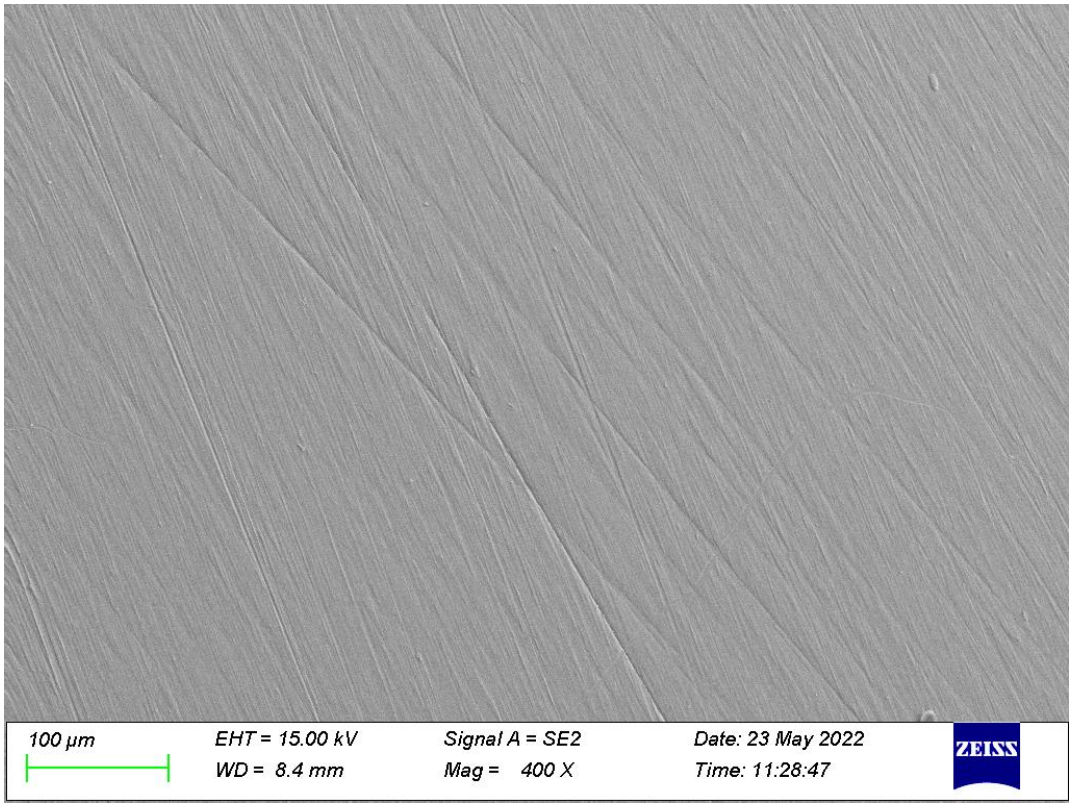


Figure 77: SEM of Ti surface after immersion in 0.1M HCl with Ce(acac)3, after potentiodynamic test at 25^0*C (400 X).*

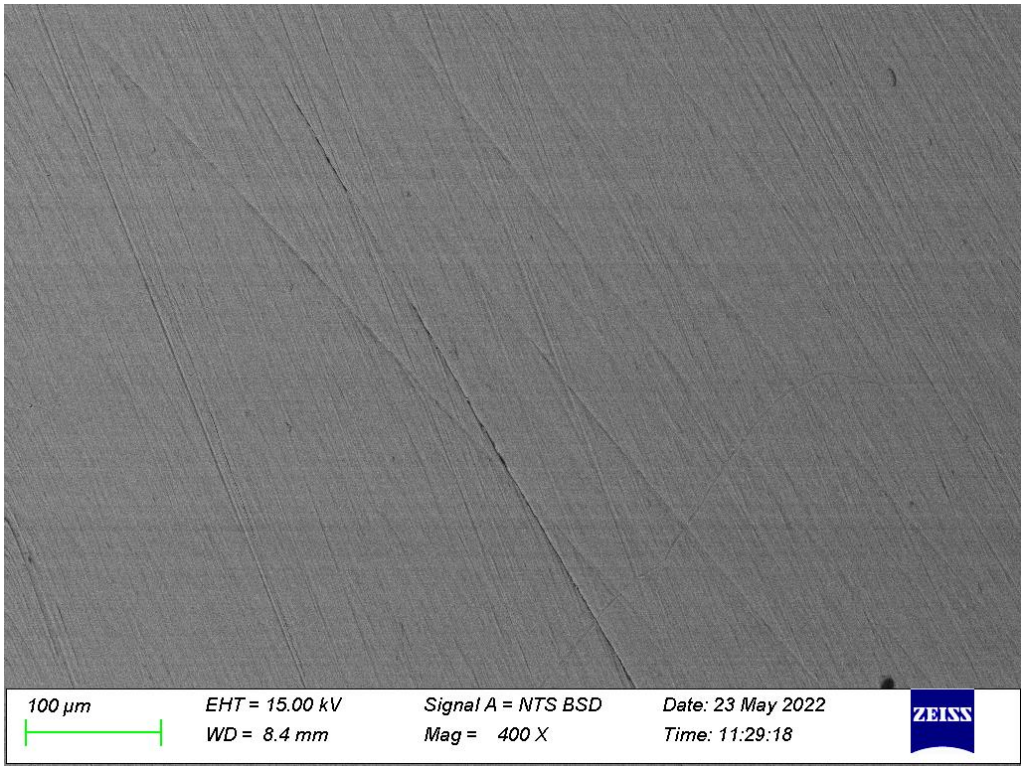


Figure 78: SEM of Ti surface after immersion in 0.1M HCl with Ce(acac)3, after potentiodynamic test at 25^0*C.*

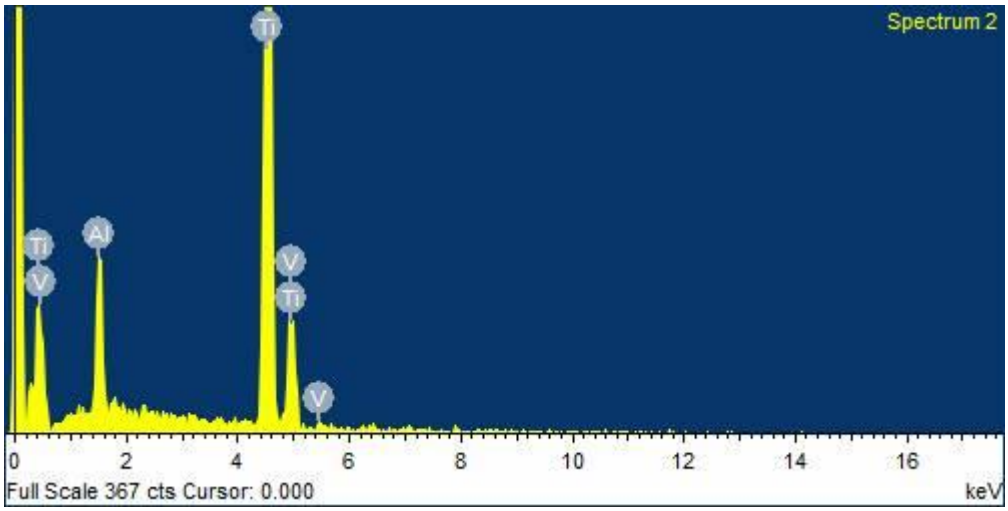


Figure 79: EDX of Ti surface after immersion in in 0.1M HCl with $Ce(acac)_3$*, after potentiodynamic test at* 25^0*C.*

Evident from the SEM and EDX analysis, it can be concluded that within a 0.1M HCl system, Titanium metal has an innately good corrosion resistance. In addition, the effect of both inhibitors proved effective in decreasing the corrosion rate of Ti as the results from the weight loss and potentiodynamic tests show.

CHAPTER 6: CONCLUSION AND RECOMMENDATION

6.1 Conclusion

The process of corrosion deteriorates the structural and mechanical integrity of a metal. This is evident in terms of the recorded weight loss over time, as well as visual and optical observation of the surface of the aluminium and titanium metals investigated.

In this study, it was confirmed that aluminium and titanium both show good resistance to corrosion attacks in chloride media as seen from the observation of the various tests. This is due to their ability to form a protective, passivating, self-regenerating metal oxide layer on their surfaces. However, titanium showed better corrosion resistance relative to aluminium by almost 2 orders of magnitude lower corrosion rates.

The inhibition effect of lanthanum and cerium acetylacetone were observed in the weight loss and potentiodynamic tests conducted. The inhibitors were observed to reduce the corrosion rate of both aluminium and titanium by one order of magnitude, relative to the respective solutions without inhibitors.

As evident from the potentiodynamic tests, lanthanum acetylacetone was observed to act as an anodic inhibitor due to its shifting of the E_{corr} towards higher and more positive (anodic) values in the system containing aluminium and NaCl, as well as in aluminium and HCl. Meanwhile, in the titanium experiments, lanthanum acetylacetone display indications of acting as a mixed inhibitor. Cerium acetylacetone did not show a significant shift in E_{corr} to be classified as either anodic or cathodic, hence it could be concluded that it acted more as a mixed inhibitor in all systems in this study. However, both lanthanum and cerium acetylacetone showed good inhibitor properties in chloride media, with lanthanum acetylacetone being the better inhibitor of the two.

The results obtained from the weight loss tests and potentiodynamic tests both highlighted the similar corrosion characteristics, consistent too with observations through the optical and scanning electron microscopic study of the samples, across all the various solutions.

6.2 Recommendation

It is recommended that this study be further conducted to analyse the specific corrosion inhibitor mechanisms of these inhibitors with a variation of inhibitor concentration, type, solution temperature, pH, as well as exploring more classes of beta-diketonate and REM salt combinations. This will give deeper understanding and better context into the efficiency and viability of the use of REM beta-diketonate in the field of corrosion inhibition in chloride systems.

APPENDICES

Appendix A:

Table 14: Weekly weight measurements (in grams) of Al coupons in NaCl solutions

NaCl							
Sample No/ No of weeks	**Wk 0**	**Wk 1**	**Wk 2**	**Wk 3**	**Wk 4**	**Wk 5**	**Wk 6**
1	0,468	0,465	0,461	0,457	0,454	0,452	0,45
2	0,454	0,45	0,446	0,444	0,439	0,435	0,432
3	0,425	0,42	0,417	0,415	0,412	0,41	0,405
4	0,457	0,454	0,451	0,445	0,441	0,437	0,434
5	0,462	0,457	0,454	0,452	0,447	0,445	0,443
$NaCl + La(acac)_3$							
7	0,461	0,461	0,46	0,46	0,459	0,459	0,458
8	0,466	0,462	0,461	0,461	0,46	0,46	0,459
9	0,466	0,464	0,463	0,463	0,462	0,462	0,461
10	0,444	0,444	0,443	0,443	0,442	0,442	0,442
11	0,457	0,457	0,457	0,457	0,456	0,456	0,456
$NaCl + Ce(acac)_3$							
10	0,475	0,474	0,473	0,472	0,47	0,468	0,467
11	0,46	0,46	0,459	0,458	0,456	0,455	0,454
12	0,455	0,454	0,453	0,451	0,448	0,446	0,443
13	0,451	0,451	0,449	0,448	0,447	0,445	0,444
14	0,47	0,47	0,469	0,469	0,468	0,467	0,467

Table 15: Weekly weight measurements (in grams) of Al coupons in HCl solutions

HCl							
Sample No/ No of weeks	**Wk 0**	**Wk 1**	**Wk 2**	**Wk 3**	**Wk 4**	**Wk 5**	**Wk 6**
16	0,461	0,411	0,388	0,366	0,331	0,301	0,269
17	0,482	0,431	0,412	0,382	0,342	0,322	0,281
18	0,436	0,387	0,365	0,345	0,316	0,296	0,236
19	0,456	0,404	0,384	0,346	0,317	0,288	0,268
20	0,449	0,405	0,381	0,342	0,319	0,279	0,245
HCl + $La(acac)_3$							
21	0,438	0,431	0,424	0,416	0,41	0,404	0,398
22	0,439	0,434	0,424	0,416	0,412	0,406	0,396
23	0,419	0,416	0,41	0,398	0,391	0,386	0,377
24	0,455	0,449	0,443	0,433	0,427	0,42	0,411
25	0,437	0,434	0,429	0,417	0,409	0,400	0,39
HCl + $Ce(acac)_3$							
26	0,47	0,467	0,464	0,456	0,446	0,436	0,427
27	0,438	0,434	0,43	0,42	0,411	0,402	0,394
28	0,43	0,425	0,421	0,414	0,406	0,395	0,385
29	0,445	0,441	0,437	0,423	0,415	0,406	0,398
30	0,408	0,404	0,401	0,389	0,383	0,371	0,362

Appendix B:

Table 16: Summary of Aluminium Corrosion Rate results for weight loss and potentiodynamic tests.

Aluminium	Average Corrosion Rate (mm/yr)	
	Weight loss	Potentiodynamic
NaCl	0.30	0.0512
NaCl + $La(acac)_3$	0.06	0.00201
NaCl + $Ce(acac)_3$	0.09	0.0052
HCl	2.50	0.296
HCl + $La(acac)_3$	0.60	0.0231
HCl + $Ce(acac)_3$	0.60	0.0562

Table 17: Summary of Titanium Corrosion Rate results for weight loss and potentiodynamic tests.

Titanium	Average Corrosion Rate (mm/yr)	
	Weight loss	Potentiodynamic
NaCl	0.1207	0.00012
NaCl + $La(acac)_3$	-	0.000013
NaCl + $Ce(acac)_3$	-	0.000028
HCl	0.1509	0.00023
HCl + $La(acac)_3$	-	0.000012
HCl + $Ce(acac)_3$	-	0.000045

Appendix C:

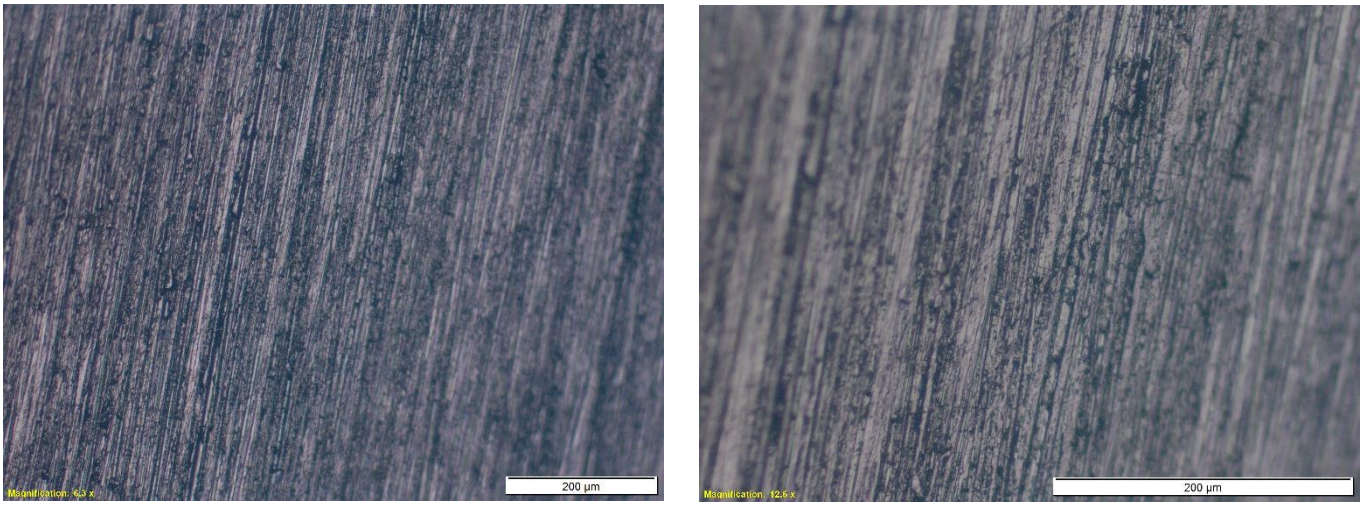


Figure 80: 10X (left) and 20X (right) optical micrograph of Al reference (potentiodynamic test).

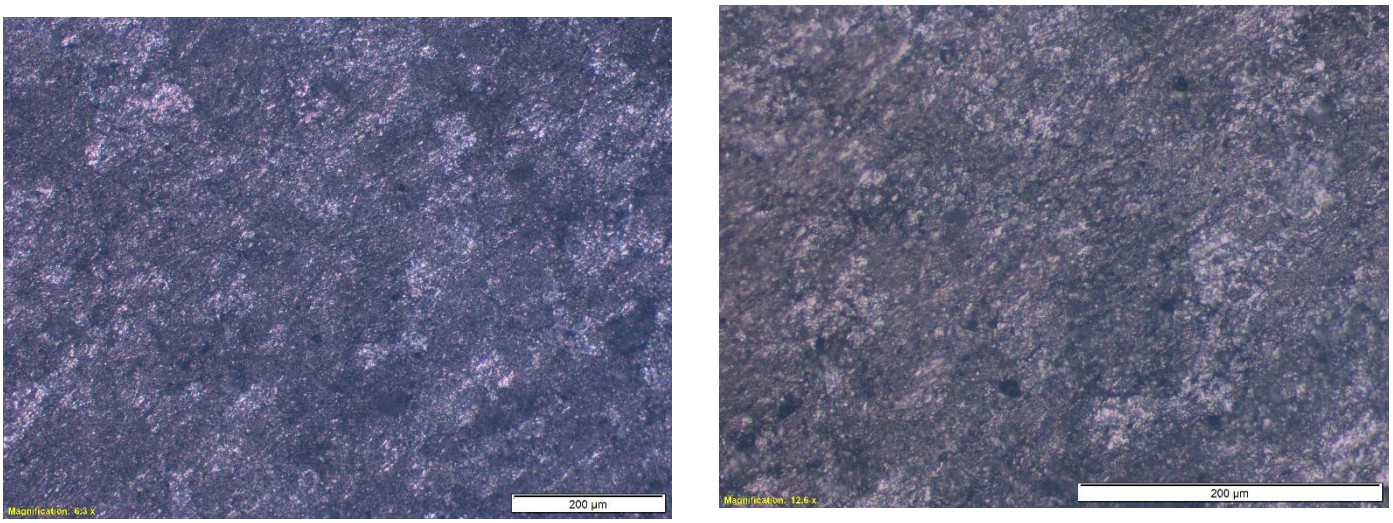


Figure 81: 10X (left) and 20X (right) optical micrograph of Al in 0.6M NaCl without inhibitor (potentiodynamic test).

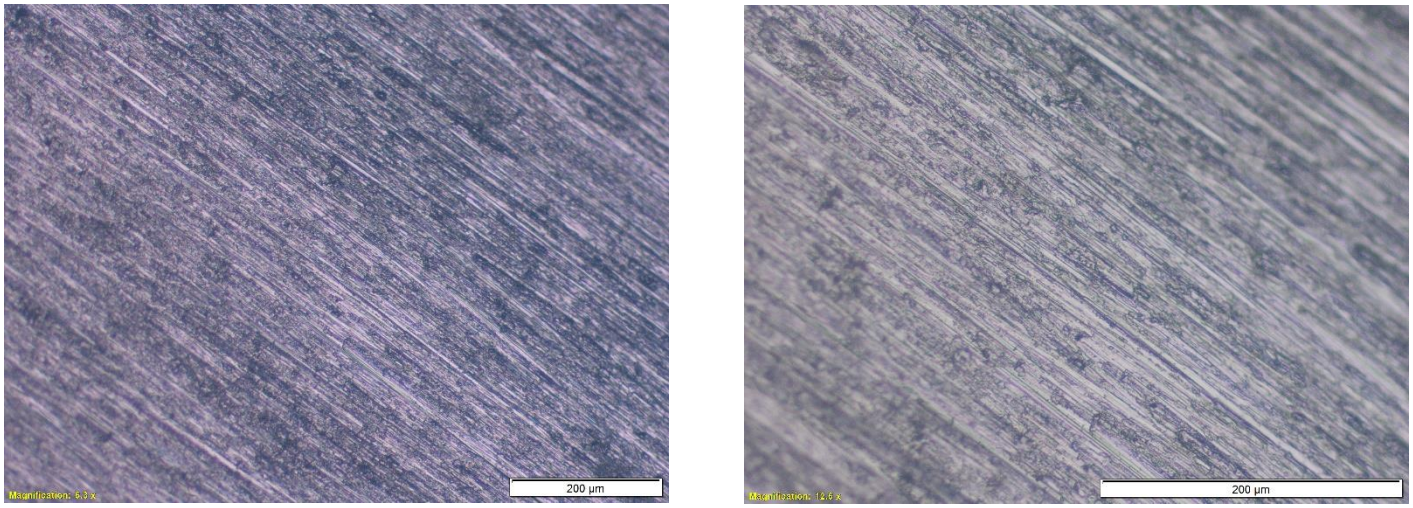


Figure 82: 10X (left) and 20X (right) optical micrograph of Al in 0.6M NaCl with $La(acac)_3$ (potentiodynamic test)

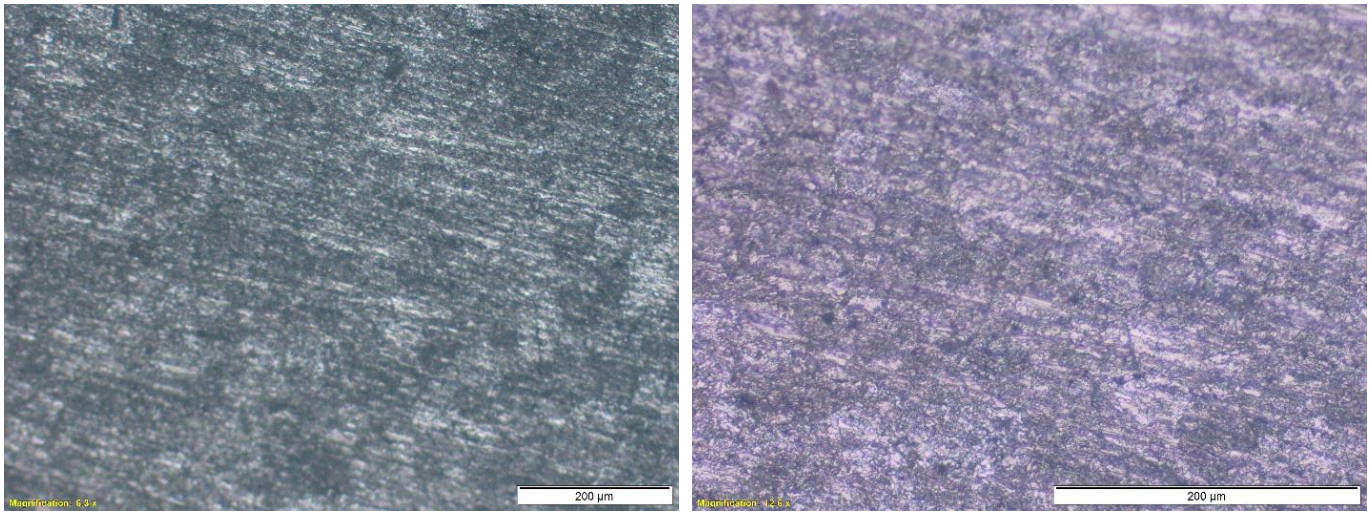


Figure 83: 10X (left) and 20X (right) optical micrograph of Al in 0.1M HCl without inhibitor (potentiodynamic test)

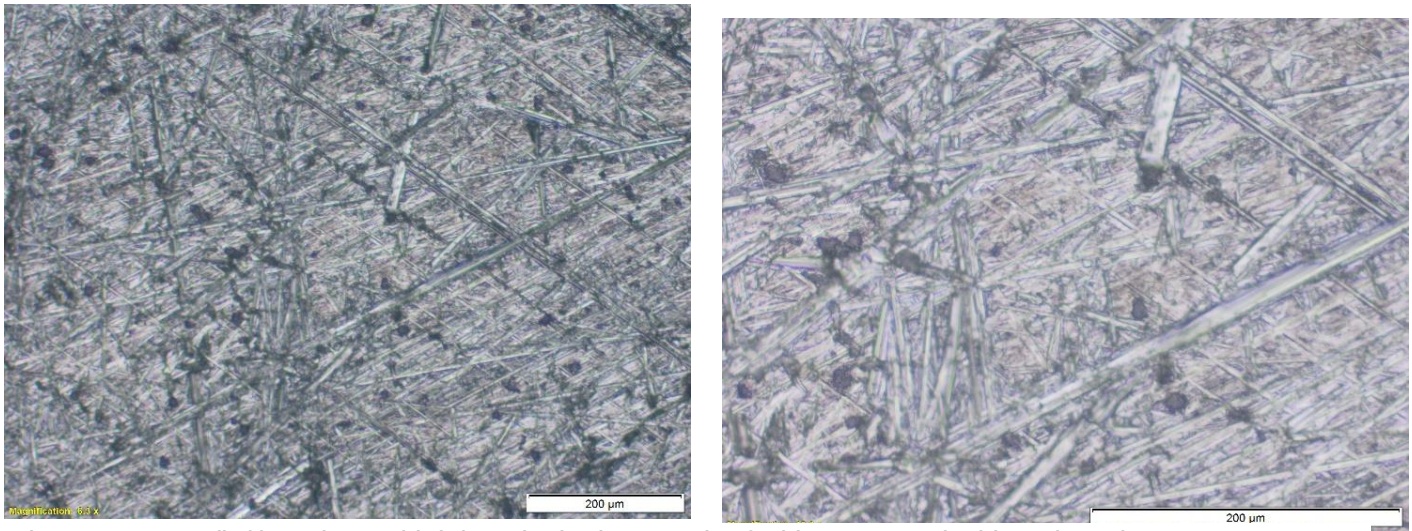


Figure 84: 10X (left) and 20X (right) optical micrograph of Al in 0.1M HCl with $La(acac)_3$ (potentiodynamic test)

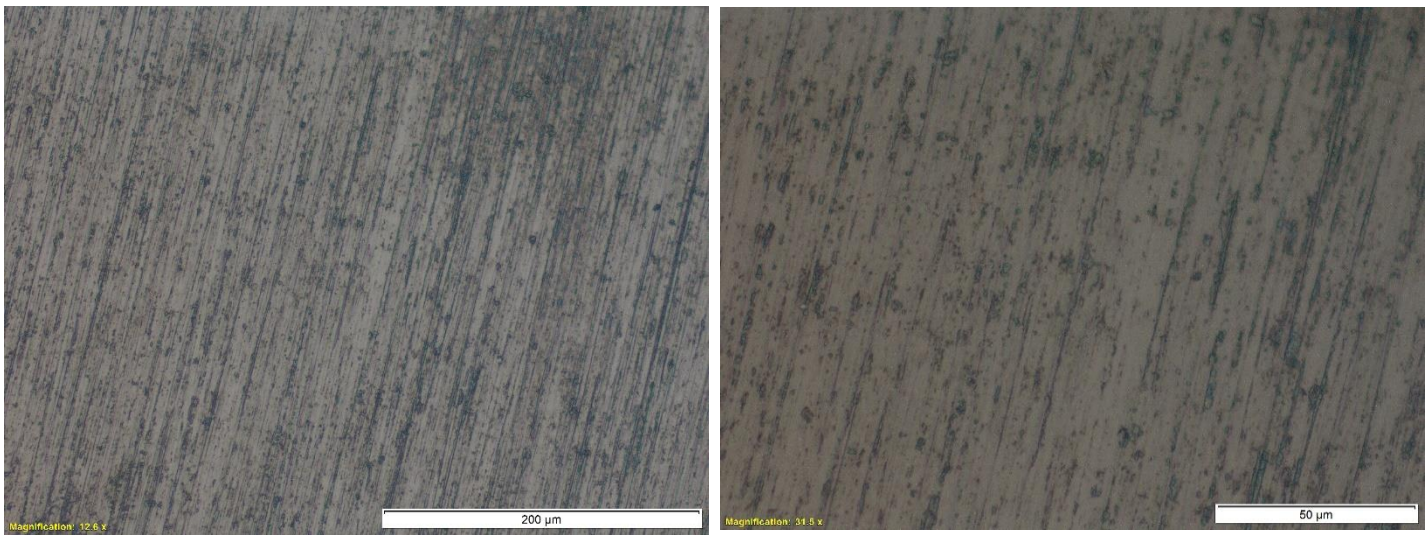


Figure 77: 20X (left) and 50X (right) optical micrograph of Ti reference (potentiodynamic test)

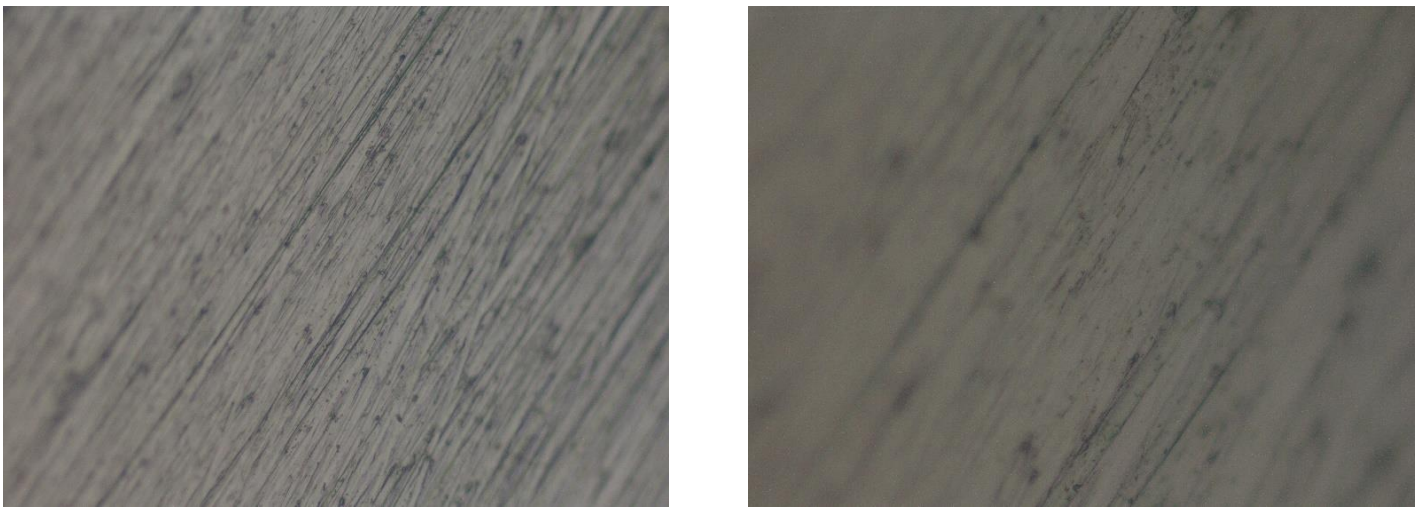


Figure 85: 20X (left) and 50X (right) optical micrograph of Ti in NaCl without inhibitor (potentiodynamic test)

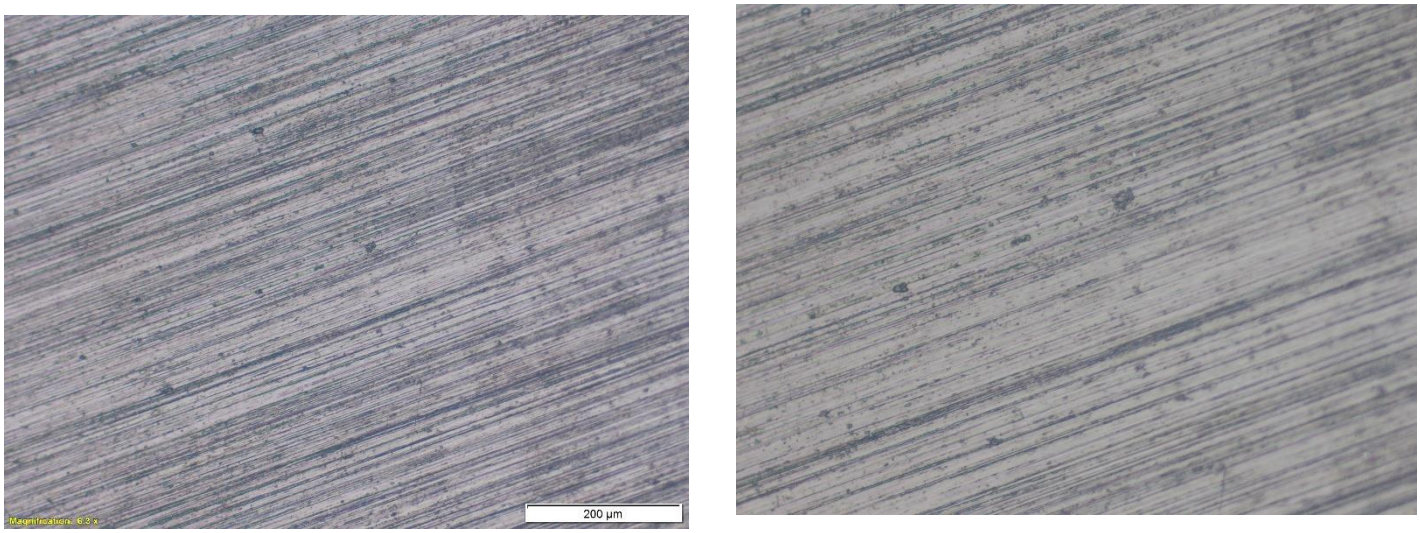


Figure 86: 10X (left) and 20X (right) Optical micrograph of Ti in HCl without inhibitor.

REFERENCES

Aejitha, S., Narmatha, M. & Palanisamy, G., 2018. Corrosion Inhibition and Adsorption Properties of Mild Steel in 1 M Hydrochloric Acid Medium by Expired Ambroxol Drug. *Journal of Bio- and Tribo- Corrosion.*

Alfantazi, A., Asselin, E. & Liu, J., 2016. *The Pitting Corrosion of Titanium in Aggressive Environments,* Houston: NACE Corrosion Congress.

Arnott, D., Hinton, B. & Ryan, N., 1987. Cationic film- forming inhibitors for the corrosion protection of AA 7075 aluminium alloy in chloride solutions. In: *Material Performance.* s.l.:s.n., pp. 42-47.

Arnott, D., Hinton, B. & Ryan, N., 1989. Cationic film-forming inhibitors for the protection of AA 7075 aluminium alloy against corrosion in aqueous chloride solution. In: *Corrosion.* s.l.:s.n., pp. 12-18.

Arnott, D. et al., 1985. Auger and XPS studies of cerium corrosion inhibition on 7075 aluminum alloy. In: *Applications of Surface Science.* s.l.:s.n., p. 236+251.

Baroux, B., 2014. *La corrosion des metaux. Passivite et corrosion localisee,* Paris: s.n.

Blashchuk, V., Onoprienko, L. & Chervonyi, M., 1988. *Corrosion Resistance of VT1-0 Titanium in Hydrochloric Acid Solutions,* s.l.: s.n.

Brown, B., Fujii, C. & Dahlberg, E., 1969. Methods for studying the solution chemistry within stress corrosion cracks. *Journal of the Electrochemical Society,* pp. 218-219.

Chatalov, A., 1952. *Effet du pH sur le comportement electrochimique des metaux et leur resistance a la corrosion,* s.l.: s.n.

Coupry, J. & Develay, R., 1971. *Alliages d'aluminium. Resistance a la fatigue d'eprouvettes presentant differentes protections de surface. Influence de quelques milieux corrosifs. Corrosion Traitements Protection et Finitions,* s.l.: s.n.

Cutler, J., 1981. Reactions between halogenated hydrocarbons and metals. *Journal of of Hazardous Materials,* pp. 99-108.

Drunen, J. V., Zhao, J. & Jerkiewicz, G., 2011. *Corrosion Behaviour of Surface - Modified Titanium in a simulated body fluid,* s.l.: s.n.

Duret-Thual, C., Oltra, R. & J, B., 1994. Erosion-corrosion, cavitation-corrosion et corrosion localisee. In: *Corrosion localise. Les Editions de Physique.* s.l.:s.n., pp. 321-352.

Esmailzadeh, S., Sariak, H. & Aliofkhazraei, M., 2018. Intepretation of Cyclic Polarization Test Results for Study of Corrosion Behaviour of Metals. *Protection of Metals and Physical Chemistry of Surfaces.*

Eyu, G., G., W., W., D. & J., M., 2016. Effect of Dissolved Oxygen and Immersion Time on the Corrosion Behaviour of Mild Steel in Bicarbonate/Chloride Solution. *Materials,* 9(9).

Fazel, M., Salimijazi, H., Golozar, M. & M, G. J., 2015. *A comparison of corrosion, tribocorrosion and electrochemical impedance properties of pure Ti and Ti6Al4V alloy treated by micro-arc oxidation process,* s.l.: s.n.

Forsberg, J., 1981. Complexes with diketones and polyketones. In: *Gmelin Handbuch der Anorganis chen Chemie.* Berlin: Springer, p. 65.

Forsyth, M. & Hinton, B., 2014. *Rare Earth-Based Corrosion Inhibitors.* Cambridge: Elsevier.

Fragoza-Mar, L. et al., 2012. Corrosion inhibitor activity of 1,3-diketone malonates for mild steel in aqueous hydrochloric acid solution.. *Corrosion Science,* Volume 61, pp. 171-184.

French, E., Martin, R. & Dougherty, J., 1993. Corrosion and Its Inhibition in Oil and Gas wells. *Reviews on Corrosion Science and Technology,* Volume II, pp. 1-25.

Ghanbari, A., Attar, M. & Mahdavian, M., 2009. Acetylacetonate complexes as new corrosion inhibitors in phosphoric acid media: Inhibition and synergism study.. *Progress In Colour, Colourants and Coatings,* Volume 2, pp. 115-122.

Gräfen, H., Horn, E.-M., Schlecker, H. & Schindler, H., 2002. *"Corrosion" Ullmann's Encyclopedia of Industrial Chemistry.* Weinheim: Wiley-VCH.

Greene, D. & Fontana, G., 1959. *A critical analysis of pitting corrosion,* s.l.: s.n.

Greenwood, N. & Earnshaw, A., 2007. Titanium, Zirconium and Hafnium. In: *Chemistry of the elements.* Oxford: s.n., pp. 954-975.

Hackerman, N. & Snaveley, S., 1984. Inhibitors. In: *Corrosion Basics.* Houston: NACE International, pp. 127-146.

Hugel, G., 1960. Corrosion Inhibitors—Study of their Activity Mechanism. In: *1st European Symposium on Corrosion Inhibitors.* Ferrara: s.n.

Ivusic, F., Lahordny-Sarc, O., Curkovic, H. & Alar, V., 2015. Synergistic inhibition of carbon steel corrosion in seawater by cerium chloride and sodium gluconate. *Corrosion Science,* Volume 98, pp. 88-97.

Janse van Rensburg, D., Cornish, L. & Van Der Merwe, J., 2019. Corrosion Map of South Africa's Macro Atmosphere. *South African Journal of Science,* Issue 115, pp. 7-8.

Junying, H. et al., 2017. Corrosion Inhibition of Titanium in Hydrochloric Acid containing Na2MoO4. *International Journal of Electrochemical Science,* Volume 12, p. 8878 – 8891.

Kalman, E., 1994. *Routes to the development of low toxicity corrosion inhibitors for use in neutral solutions,* London: The institute of Materials.

Kelly, R., 2001. *Critical factors and challenges in crevice corrosion, Research Tropical Symposium Localized Corrosion.* s.l., NACE International.

Khaled, K. & Amin, M., 2009. Electrochemical and molecular dynamics simulation studies on the corrosion inhibition of aluminum in molar hydrochloric acid using some imidazole derivatives. *Journal of Applied Electrochemistry,* Issue 39, p. 2553–2568.

Khamaj, J., 2016. Cyclic polarization analysis of corrosion behavior of ceramic coating on 6061 Al/SiCp composite for marine applications. *Protection of Metals and Physical Chemistry of Surfaces,* Issue 52, pp. 886-893.

Lawal, O., Potgieter, J., Billing, C. & Whitefield, D., 2022. The Influence of REE β-Diketone Complexes on the Corrosion Behaviour of Mild Steel and 304 SS in 3.5% NaCl Solution. *Minerals,* 416(12).

Levy, M. & Sklover, G., 1969. *Anodic Polarization of Titanium and Titanium Alloys in Hydrochloric Acid,* Massachusetts: Army Materials and Mechanics Research Center.

lian, Y. et al., 2017. A state-of-the-art review on passivation and biofouling of Ti and its alloys in marine environments. *Journal of Materials Science & Technology.*

Mansfeld, F., Wang, Y. & Lin, S., 1995. *Symposium on Critical Factors in Localised Corrosion II.* s.l., s.n.

McCafferty, E., 2009. Introduction to Corrosion Science. In: New York: Springer, pp. 357-402.

Monticelli, C., 2018. Corrosion Inhibitors. In: *Encyclopaedia of Interfacial Chemistry.* s.l.:s.n.

Munir, M., M, P. & W, W., 2016. Potentiodynamic Corrosion Testing. *Journal of Visualized Experiments.*

Mustafa, A. et al., 2022. Inhibition of mild steel corrosion in hydrochloric acid environment by 1-amino-2-mercapto-5-(4-(pyrrol-1-yl)phenyl)-1,3,4-triazole. *South African Journal of Chemical Engineering ,* Issue 39, pp. 42 - 51.

Nakagawa, M., Matsuya, S., Shiraishi, T. & Ohta, M., 1999. Effect of Fluoride Concentration and pH on Corrosion . In: *Behavior of Titanium for Dental Use. .* s.l.:s.n., pp. 1568-1572.

Ningshen, S. et al., 2011. *Oxygen Ion Irradiation Effect on Corrosion Behaviour of Titanium in Nitric Acid Medium,* s.l.: s.n.

Oakes, B., 1981. Historical review inhibitors mechanisms. In: *Corrosion.* s.l.:NACE Corrosion Congress.

Patrie, J., 1952. Les phenomenes de passivation de l'aluminium immerge en milieu nitrique. In: *Revue de l'Aluminium.* s.l.:s.n.

Phul, B., 2003. Evaluating uniform corrosion. In: *Corrosion Testing and Evaluation.* s.l.:ASM International, pp. 542-544.

Pourbaix, M., 1957. Lecons sur la corrosion electrochimique. In: *Rapports Techniques du Cebelcor.* s.l.:s.n.

Pourbaix, M., 1979. *Atlas of Electrochemical Equilibria in Aqueous Solution.* 2nd ed. Houston: National Association of Corrosion Engineers.

Pourbaix, M., 1990. Thermodynamics and Corrosion. In: *Corrosion.* s.l.:s.n., pp. 963-988.

Pourbaix, M. & Deltombe, E., 1958. The electrochemical behavior of aluminum, potential pH diagram of the system AI-H2O at 25 oC. In: *Corrosion.* s.l.:s.n., pp. 16-20.

Rabab, M. et al., 2011. Corrosion and Inhibition of Ti-6Al-4V Alloy in NaCl Solution. *International Journal of Electrochemical Science,* Volume 6, pp. 5499 - 5509.

Reboul, M., 2005. Corrosion des alliages d'aluminium. In: *Techniques de l'Ingenieur.* s.l.:s.n.

Salnikow, K. & Zhitkovich, A., 2008. *Genetic and Epigenetic Mechanisms in Metal Carcinogenesis and Cocarcinogenesis: Nickel, Arsenic, and Chromium,* s.l.: s.n.

Sastri, V., 2011. *Green Corrosion Inhibitors: Theory and Practice.* s.l.:Wiley.

Shoesmith, D. & Noel, J., 2010. Corrosion of Titanium and its Alloy. In: Oxford: s.n., pp. 2042-2052.

Sotoudeh, K., Nguyen, T., Foley, R. & Brown, B., 1981. The chemical nature of aluminium corrosion. In: *Corrosion of aluminium surfaces by aluminium salts.* s.l.:s.n., pp. 358-362.

Toba, K. & Kawano, K., 2014. *Corrosion of Carbon Steel and Alloys in Ammonium Chloride Salt,* Houston: NACE International Corrosion Conference Series.

Usman, A., Adams, F. & Okoro, L., 2016. Weight Loss Corrosion Study of Some Metals in Acid Medium. *Journal of Advances in Chemistry,* 11(2), pp. 3434-3440.

Veronica, A. et al., 2015. *Corrosion Behavior Analysis of Plasma-assisted PVD Coated Ti-6Al-4V Alloy in 2M NaOH,* Sao Paolo: s.n.

Xianghong, L., Shuduan, D., Hui, F. & Guannan, M., 2010. Synergistic inhibition effect of rare earth cerium(IV) ion and sodium oleate on the corrosion of cold rolled steel in phosphoric acid solution. *Corrosion Science,* 52(4), pp. 1167-1178.

Yasakau, K. A., Zheludkevich, M., Lamaka, S. & Ferreira, M. G., 2006. Mechanism of corrosion inhibition of AA2024 by rare-earth compounds. *The Journal of Physical Chemistry B,* Issue 110, pp. 5515-5528.

Yasakau, K., Zheludkevich, M. L. & Ferreira, M., 2008. Lanthanide Salts as Corrosion Inhibitors for AA5083: Mechanism and Efficiency of Corrosion Inhibition. *Journal of Electrochemical Society,* 155(5).

Zielinski, A. & Sobieszczyk, S., 2008. *Corrosion of Titanium Biomaterials, mechanisms, effects and modelisation,* s.l.: s.n.